UNIVERSITY OF GENOVA

PHD PROGRAM IN BIOENGINEERING AND ROBOTICS

Cycle XXXI

A novel Three-Dimensional Micro-Electrode Array for *in-vitro* electrophysiological applications

Author:
Nicolò Colistra

Supervisor:
prof. Sergio Martinoia

Thesis submitted for the degree of *Doctor of Philosophy*

Giorgio Cannata Head of the PhD program

Thesis Jury:

Prof. Michele Giugliano, *University of Antwerp*

Dott. Leandro Lorenzelli, *Bruno Kessler Foundation*

Dibris

Department of Informatics, Bioengineering, Robotics and Systems Engineering

Dedicated to my parents and my brothers

Declaration

I hereby declare that except where specific reference is made to the work of others, the contents of this dissertation are original and have not been submitted in whole or in part for consideration for any other degree or qualification in this, or any other university. This dissertation is my own work and contains nothing which is the outcome of work done in collaboration with others, except as specified in the text and Acknowledgements. This dissertation contains fewer than 65,000 words including appendices, bibliography, footnotes, tables and equations and has fewer than 150 figures.

Nicolò Colistra
December 2018

Acknowledgments

First and foremost I would like to sincerely thank my supervisor Prof. Sergio Martinoia for the opportunities he offered me during these years and for all the support he has been able to give me along the way.

I would like to thank Brunella Tedesco for her precious advice and Giorgio Carlini for his priceless technical support. Thanks Ilaria, for your precious friendship and for your backing over these hard years.

Special thank goes to Dr. Maria Rosa Scalise for her precious support and friendliness during both the PhD and master degree.

The final and biggest thanks go to my parents, my brothers, my grandparents, my uncle, and my aunt: without your presence and your unconditional love, I simply would never found the strength to pursue my dreams and follow my path. You gave me more than you think, and much more than I can ever explain within these few lines.

Abstract

Microelectrode arrays (MEAs) represent a powerful and popular tool to study *in vitro* neuronal networks and acute brain slices. The research standard for MEAs is planar or 2D-MEAs, which have been in existence for over 30 years and used for extracellular recording and stimulation from cultured neuronal cells and tissue slices. However, planar MEAs suffer from rapid data attenuation in the z-direction when stimulating/recording from 3D *in-vitro* neuronal cultures or brain slices. The existing proposed 3D *in-vitro* neuronal models allow to record the electrophysiological activity of the 3D network only from the bottom layer (i.e. the one directly coupled to the planar MEAs). Thus, to further develop and optimize such 3D neuronal network systems and to study and understand how the 3D neuronal network dynamics changes in different layers of the 3D structure, new three-dimensional microelectrodes arrays (3D-MEAs) are required.

Early attempts in this field resulted in interesting integrated approaches toward protruding or spiked 3D-MEAs. Although these first prototypes could be successfully employed with brain slices, the limited heights of the electrodes (up to max 70 µm) and the peculiar shape of the recording areas made them not an ideal solution for 3D neuronal cultures. Moreover, a convenient and versatile method for the fabrication of multilevel 3D microelectrode arrays has yet to be obtained, due to the usually complicated and expensive designs and a lack of a full compatibility with standard MEAs both in terms of materials and recording area dimensions.

To overcome the afore-mentioned challenges, in this work, I present the design, microfabrication, and characterization of a new 3D-MEA composed of pillar-shaped gold 3D structures with heights of more than 100 µm that can be used, in principle, on every kind of MEA, both custom-made and commercial. I successfully demonstrate the capability and ability of such 3D-MEA to record electrophysiological spontaneous activity from 3D engineered *in-vitro* neuronal networks and both 4-AP-induced epileptiform-like and electrically-evoked activity from mouse acute brain slices. I also demonstrate how the developed 3D-MEA allows better recording and stimulating conditions while interfacing with acute brain slices as compared to planar electrode arrays and previously reported 3D MEA technologies.

Table of contents

List of figures

Chapter 1

Introduction

1.1 Motivation and Goals

In the last years, several studies have been devoted to the introduction of new *in-vitro* experimental paradigms constituted by 3D engineered neuronal networks coupled to planar or two-dimensional microelectrode arrays (2D-MEAs) (Frega et al. 2014, Tedesco et al. 2018). The potential advantages of 3D engineered constructs are evident as they can be used as a more accurate investigational *in-vitro* platform than standard 2D network systems. 3D neuronal networks coupled to planar MEAs, represent a powerful *in-vitro* model capable of better emulating *in-vivo* physiology. The use of MEAs devices allows to better explore and understand the functional properties of biomimetic 3D neuronal networks.

However, the existing proposed 3D *in-vitro* neuronal systems lack of appropriate micro-transducers arrays that can be coupled to such models to record the electrophysiological activity of the 3D networks from different locations in the 3D space. 2D-MEAs allow to record the electrophysiological activity of the 3D neuronal structure only from the bottom layer (i.e. the one directly coupled to the planar MEAs).

Overall, 2D-MEAs suffer from several drawbacks while interfacing with 3D *in-vitro* neuronal constructs like 3D neuronal cultures or acute brain slices.

Indeed, signals from cells that occur at a certain height above the planar structure can be lost since the electrodes are not in proximity to these cells. The increased neuron-microelectrode distance results in an attenuation of the recorded electrophysiological signal from the active cells (leading to poor signal-to-noise ratios (SNRs)), and thus, in a reduction of the efficiency of the measurements conditions.

Therefore, there is a tremendous need to design and fabricate new 3D recording/stimulation devices able to record spontaneous or/and stimulus-evoked electrophysiological activity of 3D neuronal structures from different locations in the 3D space. The design and development of innovative and truly three-dimensional microelectrode arrays (3D-MEAs) would open new perspectives for *in-vitro* neurophysiological studies and would allow to study and characterize a complete 3D-3D *in-vitro* neuronal model.

In the past 15 years, several groups addressed the technological challenge of providing electrophysiological tools capable of fully exploit the potentials of 3D neuronal cultures and brain slices. Early attempts in this field resulted in interesting integrated approaches toward protruding or spiked 3D-MEAs. Although these first prototypes could be successfully employed with brain slices, the limited heights of the electrodes (up to max 70 µm) and the peculiar shape of the recording areas made them not an ideal solution for 3D neuronal cultures.

These specific approaches, however, are not suitable for long term monitoring of dissociated neuronal cultures, being more suitable for acute measurements. Despite these interesting attempts to address the problem, a convenient and versatile method for the fabrication of multilevel 3D microelectrode arrays has yet to be obtained, due to the usually complicated and expensive designs and a lack of a full compatibility with standard MEAs both in terms of materials and recording area dimensions.

To this aim, this dissertation mainly addresses the design, development, and characterization of a novel pillar-shaped gold 3D-MEA, where multi-level 3D electrodes with heights of more than 100 µm can be used, in principle, on every kind of MEA, both custom-made and commercial. The characterization of the developed 3D-MEA is first performed from an electrical point of view to carry out impedance measurements of such 3D device. Then, tests in *in-vitro* environment with 3D engineered neuronal networks and mouse acute brain slices are performed to experimentally validate the fabricated 3D-

MEA. Associated goals address the study and characterization of new experimental paradigms composed of 3D engineered neuronal networks coupled to both 2D- and 3D-MEAs.

1.2 Thesis Organization

In this dissertation, I present an innovative three-dimensional microelectrode array (3D-MEA) for *in-vitro* electrophysiological applications.

This chapter serves as a motivation for the need of 3D-MEAs for multi-site stimulation and recording from 3D *in-vitro* neuronal structures (i.e. acute brain slices or 3D neuronal cultures).

Chapter 2 provides the state-of-art of MEA technology for *in-vitro* neuronal interfacing. First, an overview of various planar or 2D-MEAs that have been developed by various researchers worldwide in the last 35 years is provided. Then, a description of the *in-vitro* applications of such 2D-MEA devices is reported. In particular, a brief introduction about 2D *in-vitro* neuronal models is first shown, followed by an overview of the main works dealing with 3D engineered *in-vitro* neuronal models developed in the last ten years. Subsequently, the study and characterization of a new *in-vitro* experimental paradigm composed of 3D chitosan engineered neuronal network coupled to planar MEA is reported in details. In the last section of chapter 2 (see § 2.2), the state-of-art of integrated microfabrication approaches used for the development of *in-vitro* 3D-MEAs is presented. Finally, a detailed study and characterization of a complete 3D-3D *in-vitro* neuronal model composed of 3D engineered neuronal network coupled to a new 3D-MEA device are provided.

Chapter 3 presents the novel and true three-dimensional microelectrode array (3D-MEA) designed and developed in this dissertation – pillar-shaped gold 3D-MEA.

Firstly, design and microfabrication of such 3D-MEA devices are reported in details. Then, an electrical characterization based on electrochemical impedance spectroscopy is performed to carry out impedance measurements of the electrodes of the fabricated 3D-MEAs. Experimental validation of the developed 3D-MEA devices is shown by performing *in-vitro* tests with 3D engineered neuronal cultures and mouse acute brain slices**.** Preliminary electrophysiological characterization of such 3D pillar-shaped gold MEAs with 3D engineered *in-vitro* neuronal networks is successfully carried out. Moreover, the capability of these new 3D-MEAs to record both 4-AP-induced epileptiform-like and electrically-evoked activity from mouse acute brain slices is successfully demonstrated. Advantages of the fabricated 3D pillar-shaped gold MEAs with respect to standard planar MEAs and previously reported 3D-MEA technologies for

use with *in-vitro* acute brain slices are also showed and explained.
Chapter 4 presents conclusions to this dissertation and prospects for future research in this interesting area.

References

Frega M., Tedesco M., Massobrio P., Pesce M., and Martinoia S. (2014). Network dynamics of 3D engineered neuronal cultures: a new experimental model for in-vitro electrophysiology. *Scientific Reports 4*, a. n.: 5489.

Tedesco M.T., Di Lisa D., Massobrio P., Colistra N., Pesce M., Catelani T., Dellacasa E., Raiteri R., Martinoia S., Pastorino L. (2018). Soft chitosan microbeads scaffold for 3D functional neuronal networks. *Biomaterials,* vol. 156, pp. 159-171.

Chapter 2

MEA TECHNOLOGY FOR *IN-VITRO* NEURONAL INTERFACING

In this chapter, I first report the state-of-art of planar MEAs developed by researchers worldwide in the last 35 years. Then, I present the *in-vitro* applications of such 2D-MEAs, providing a brief introduction about 2D neuronal models and an overview of the main works dealing with 3D engineered neuronal systems developed in the last ten years. Subsequently, a detailed study and characterization of a new 3D *in-vitro* experimental paradigm constituted by 3D chitosan engineered neuronal network coupled to planar MEA are provided. In addition, I present a simple method for building interconnected 3D *in-vitro* neuronal networks coupled to MEA substrates and the study and characterization of such an *in-vitro* 3D model are also reported.

Finally, the state-of-art of 3D-MEAs for *in-vitro* electrophysiological applications is provided. In addition, I present and characterize a complete 3D-3D *in-vitro* neuronal model composed of 3D engineered neuronal network coupled to a new 3D-MEA.

2.1 Two Dimensional Micro-Electrode Arrays (2D-MEAs)

Microelectrode arrays (MEAs) provide important information about single neurons and functional organization of neural networks and tissue slices. Due to the size of the cells involved which are in the micron-scale, an attractive technique for manufacturing MEAs is microfabrication, which has been used to make planar or 2D devices (Rajaraman et al. 2007).

Several microfabricated 2D arrays have been reported in the last 35 years for extracellular stimulation and recording from cultured neuronal cells and brain slices. The first work related to 2D microelectrodes fabrication was described by Thomas and collaborators in 1972 (Thomas et al. 1972). They constructed a platinized gold microelectrodes (two rows of 15 electrodes each, spaced 100 μm apart) embedded onto a glass substrate and passivated by photoresist. This device allowed to record field potentials from spontaneous contracting sheets of cultured chick cardiomyocytes, but it was not able to record activity from each single cell.

Another early approach toward development of MEAs was on non-conventional substrates and was reported by May and coworkers in 1979 (May et al. 1979). They demonstrated the fabrication of a 2D-MEA on a sapphire substrate with tantalum metal traces and platinum electrodes. They used tantalum due to the excellent properties of a self-passivating layer of tantalum pentoxide that preserves the quality of the metal electrodes and traces for long-term *in-vivo* stimulation and recording.

Another early study was performed by Guenter Gross and his collaborators, who reported the fabrication of 2D-MEAs for *in-vitro* cultures in 1977 and 1979 (Gross et al. 1977, Gross et al. 1979). They fabricated MEAs combining photolithography and laser-etch techniques to achieve a high-density array and *in-vitro* recordings of electrical activity of more than 30 neurons that were dissociated from snail ganglia.

The first successful recording from dissociated neuronal cells using 2D-MEA was reported by Pine in 1980. He performed single recording from a network of rat superior cervical ganglion neurons, cultured for up to three weeks over an MEA with 32 gold electrodes, platinized and insulated with silicon dioxide (Pine 1980).

In collaboration with the Prof. Yu-Chong Tai, the Pine group reported integrated microfabrication approaches for an all silicon structure consisting of etched wells whose size was slightly smaller than the hippocampal neuronal cell (around 16 μm) integrated with platinum electrodes and silicon nitride insulation (Tatic-Lucic 1994; Maher 1999). The idea was to trap the body of a single neuron in a well and an array of such well electrodes to culture *in-vitro* neuronal networks. Figure 2.1 reports an SEM image of such an MEA device.

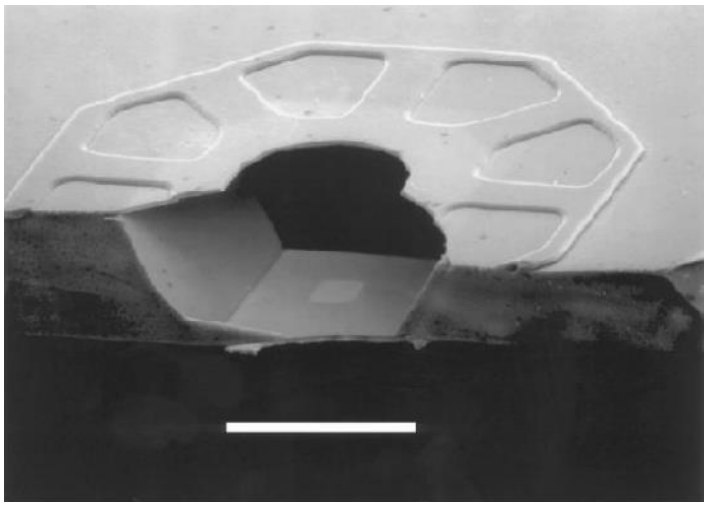

Figure 2.1. Single well approach to capturing a neuron on a planar MEA. The scale bar in the image is 20μm. (From Maher 1999).

Another pioneer of the MEA technology is Professor Bruce Wheeler at the University of Illinois (Urbana-Champaign, IL, USA) who has reported 2D-MEA fabrication techniques from his group since 1986. In a first work (Novak et al. 1986), they proposed planar MEAs devices constituted by rigid structures fabricated directly on glass substrates. The microelectrodes were made of gold and included deposits of platinum black. Such developed MEAs were used to perform electrophysiological recordings of spiking activity from abdominal ganglion of marine mollusk.

The Natural and Medical Sciences Institute (NMI) at the University of Tubingen (Reutlingen, Germany) has made a great contribution to the MEA development since the early 1990s (Nisch et al. 1994, Janders et al. 1996, Stett et al. 2003). In their work, Nisch and collaborators reported the fabrication of MEAs on glass substrates with either titanium nitrite or iridium as the electrode material using standard lift-off processes. The metal traces on the glass substrates were defined using another lift-off process with gold.

These electrode materials have been selected to achieve a high specific capacitance of the electrodes enabled by a higher surface area. Such a process has been commercialized by Multi Channel Systems (MCS, Reutlingen, Germany) along with interfacing circuits and systems. Figure 2.2 depicts optical and SEM images of these types of MEAs.

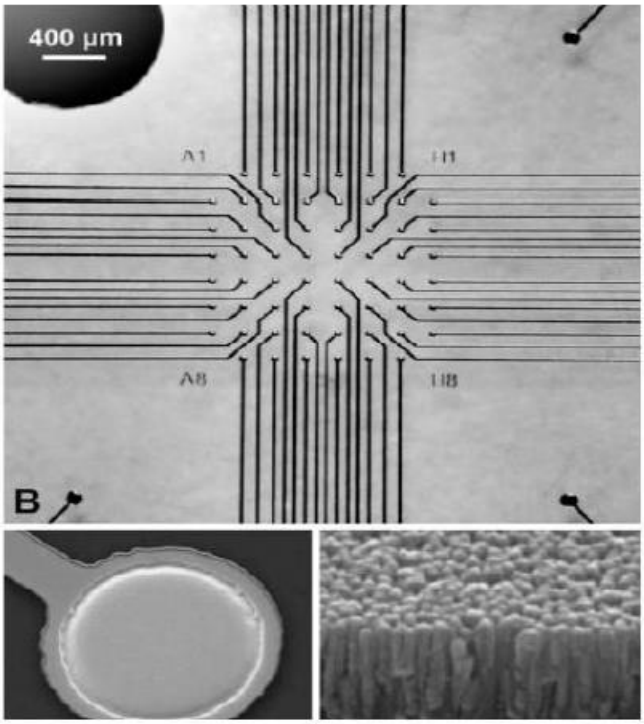

Figure 2.2. Optical (top) and SEM images (bottom) of 2D-MEAs from NMI. (From Stett et al. 2003).

At the beginning of the 1990s, the progress in CMOS technology encouraged researchers to investigate the integration of MEAs onto CMOS chips. The pioneers in this field were Gregory Kovacs' group at Stanford University (Palo Alto, CA) and Andreas Hierlemann's group at ETH Zurich (Zurich, Switzerland).
They reported various high-density arrays of planar microelectrodes by using post-processing techniques to fabricate the electrodes after the CMOS electronics were structured using commercially available processes (Borkholder et al. 1998, DeBusschere et al. 2001, Franks et al. 2003, Heer et al. 2006).
Many of these developed CMOS-based MEAs have been mainly used as sensors for detection of chemical and biological toxins. Moreover, they have also been utilized for screening of pharmacological compounds.

The use of CMOS-based devices can overcome some limitations of passive MEAs, as performing measurements at a high spatial and temporal resolution.

To this aim, several studies have been devoted to the introduction of CMOS-based high-density MEA platforms. In 2009, Berdondini and collaborators developed and tested a Pl high-density (HD)-MEAs constituted of 4 clusters of 15 high-density microelectrodes each (Figure 2.3 (A) and (B)) (Berdondini, et al. 2009).

The advantage of this configuration relies on the possibility of investigating interconnected sub-populations of neuronal cell. Such HD-MEAs offer the advantage to increase the spatial resolution with respect to the standard and commercial devices, but they are limited in terms of amount of electrodes. The increase in number of recording sites of some order of magnitude is necessary to study signal propagation along neuronal networks.

To this aim, in another work, Berdondini and coworkers developed an innovative CMOS technology-based solid-state Active Pixel Sensor (APS) array, constituted of 4096 pixels (Figure 2.3 (C)) enabling the study of micro- and macro-circuitry in *in-vitro* neuronal preparations (Berdondini, Imfeld et al. 2009). Such a fabricated APS-MEA included a 64x64 microelectrodes array device, which provided extracellular electrophysiological activity recordings with high spatial (21 mm of electrode separation) and temporal resolution (from 0.13 ms for 4096 microelectrodes down to 8 µs for 64 microelectrodes). Applied to *in-vitro* neuronal preparations, they demonstrated how this approach enables neuronal signals to be acquired for investigating neuronal activity from single cells and microcircuits to large-scale neuronal networks.

In another approach, Frey and co-authors (Frey et al. 2007) provided a reconfigurable electrode/readout-channel routing able to select an arbitrary subset of electrodes to perform electrophysiological recording and stimulation from dissociated neuronal networks. The developed system was composed of 11011 metal electrodes and 126 channels, each of which comprised recording and stimulation electronics.

Muller and collaborators recently developed a high-resolution CMOS-MEA platform to study neurons at subcellular, cellular, and network levels (Muller et al. 2015). In this study, they presented a CMOS-based device, capable to simultaneously record the electrical activity of over a thousand cells in *in-vitro* neuronal networks (Figure 2.3 (D)). The device provided a sufficiently high spatiotemporal resolution to enable, at the same time, access to neuronal preparations on subcellular, cellular, and network level. The key feature was a rapidly reconfigurable array of 26400 microelectrodes arranged at a low pitch (17.5 µm) within a large overall sensing area (3.85 x 2.10 mm^2). An arbitrary subset of the electrodes can be simultaneously connected to 1024 low-noise readout channels as well as 32 stimulation units. Each electrode or electrode subset can be used to electrically stimulate or record the signals of virtually any neuron on the array.

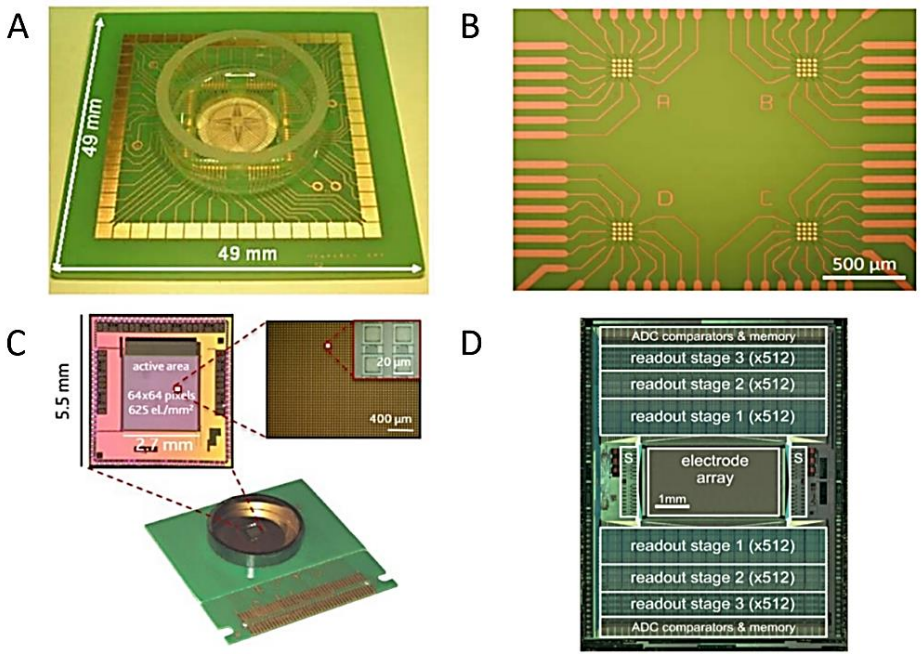

Figure 2.3. High-density devices. (A) High-density 60-channel planar MEA (From Berdondini, Massobrio et al. 2009). (B) Image showing the 4 clusters of 15 high-density microelectrodes each of the MEA chip reported in A (From Berdondini, Massobrio et al. 2009). (C) CMOS technology-based solid-state Active Pixel Sensor (APS) array (From Berdondini, Imfeld et al. 2009). (D) Micrograph of a CMOS-based device (10.1 x 7.6 mm^2). The 1024 readout channels are arranged at the top and bottom of the 3.85 x 2.10 mm^2 microelectrode array. The 32 stimulation units (S) are located on the left and right side of the array (From Muller et al 2015).

Nowadays, the MEA technology includes arrays of 60-256 microelectrodes with sizes of 10, 20 or 30 μm and interelectrode distances of 100, 200, or 500 μm.

Current MEAs consist of microfabricated electrodes embedded in a biocompatible insulation substrate (e.g., polyamide or silicon nitride/oxide) which prevents short circuits with the electrolyte bath, forming a sort of wired Petri dish. The electrodes are typically made of Au, Indium-Tin-Oxide (ITO), Titanium Nitride (TiN), or black platinum. They must also be biocompatible, long-term lasting, and preferably should have low impedance (less than 500 KΩ at 1 kHz) for low thermal noise (www.multichannelsystems.com, Reutlingen, Germany).

MEAs are realized in a clean-room environment and are mainly fabricated by means of thin-film technology and standard photolithography processes.

In Figure 2.4, four different types of MEA devices provided by Multi-Channel System (Reutlingen, Germany) and currently on the market are shown.

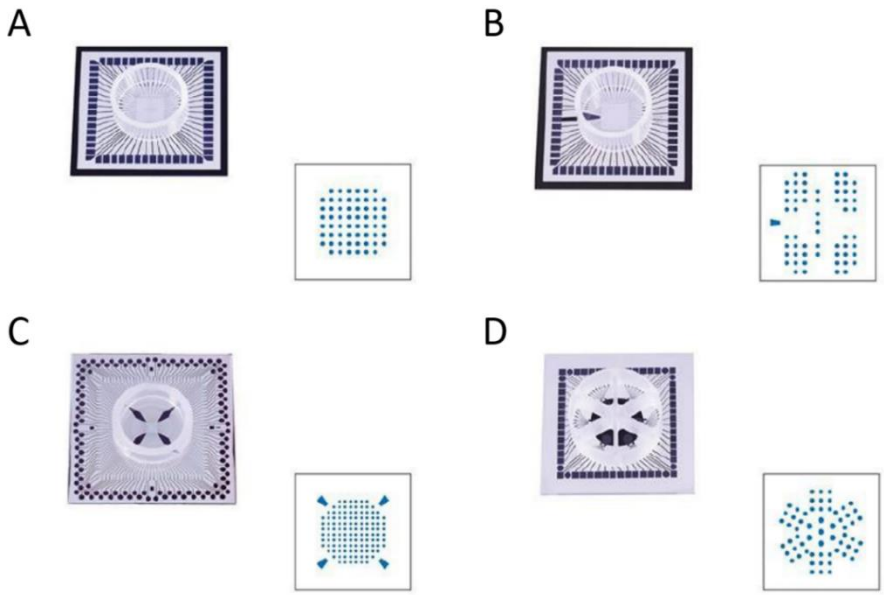

Figure 2.4. MEA devices and electrodes layouts (From www.multichannelsystems.com, Reutlingen, Germany). (A) Standard 60MEA: 60 electrodes, electrode grid 8x8, electrode spacing 100 μm and electrode diameter 10 μm. (B) 60-4QMEA: 60 electrodes, electrode grid 4x (1x4 + 1x5 + 1x4) + center line 1x7, electrode spacing 200 μm inside the quadrants, 1000 μm between the quadrants, electrode diameter 30 μm. (C) 120MEA: 124 electrodes, electrode grid 12x12, electrode spacing 200 μm, electrode diameter 30 μm. (D) 60-6WellsMEA: 54 electrodes, electrode grid 3x3 in each area, electrode spacing 200 μm, electrode diameter 30 μm.

2.1.1 2D *in-vitro* Neuronal Models

2D neuronal populations coupled to planar Micro-Electrode-Arrays (MEAs) represent a well-established experimental *in-vitro* platform to study neurobiology, network electrophysiology, and basic injury-disease mechanisms.

Dissociated neuronal cultures can be used as an experimental paradigm for studying the neuronal network dynamics and for understanding some fundamental principles of brain coding, learning, and memory (Marom et al. 2002). In this type of preparation, neuronal cells self-organize during development creating networks, which show complex spatio-temporal patterns of activity (Wagenaar et al. 2006, Rolston et al. 2007).

Indeed, neuronal networks are complex systems, which exhibit patterns of spatial and temporal correlations resulting from functional interactions within such networks. The level of network organization and connectivity modulates the expressed network dynamics (i.e., electrophysiological spontaneous activity) which can be recorded by means of arrays of microelectrodes and processed offline. MEAs coupled to neuronal networks represent a powerful tool for multi-site stimulation and recording of the electrophysiological activity, allowing to study and analyze the dynamics of the neuronal system.

Up to now, many studies have been devoted to the use of 2D-MEAs coupled to 2D dissociated neuronal populations (Eytan et al. 2006, Chiappalone et al. 2006, Brewer et al 2009, Gandolfo et al 2010, Cullen et al. 2011).

It is demonstrated that both 2D hippocampal and cortical neuronal networks show electrophysiological spontaneous activity in the mature phase of their development (i.e., after 3-4 weeks *in-vitro*) characterized by oscillating dynamics and high synchronous bursting activity involving most of the active channels in the MEA (Chiappalone et al. 2006, Brewer et al. 2009). Especially, the percentage of random spikes is very low and the electrophysiological activity is dominated by network bursting activity patterns (Chiappalone et al. 2006; Gandolfo et al. 2010).

In this dissertation, I performed some experiments using hippocampal and cortical neuronal networks during the mature phase of development.

Figure 2.5 shows two raster plots (i.e. activity recorded from 60 channels) of a 2D hippocampal culture (Figure 2.5 (A)) and a 2D cortical culture (Figure 2.5 (B)) during the third week *in vitro*. Thanks to this plot, it is possible to observe the electrophysiological activity of the network recorded from all the electrodes during 100 s. As anticipated, we can observe the quasi-synchronous activity and network dynamics composed mainly of network bursts. There are synchronized events, which involve most of the recording channels interspersed by a period of time in which almost no activity is recorded.

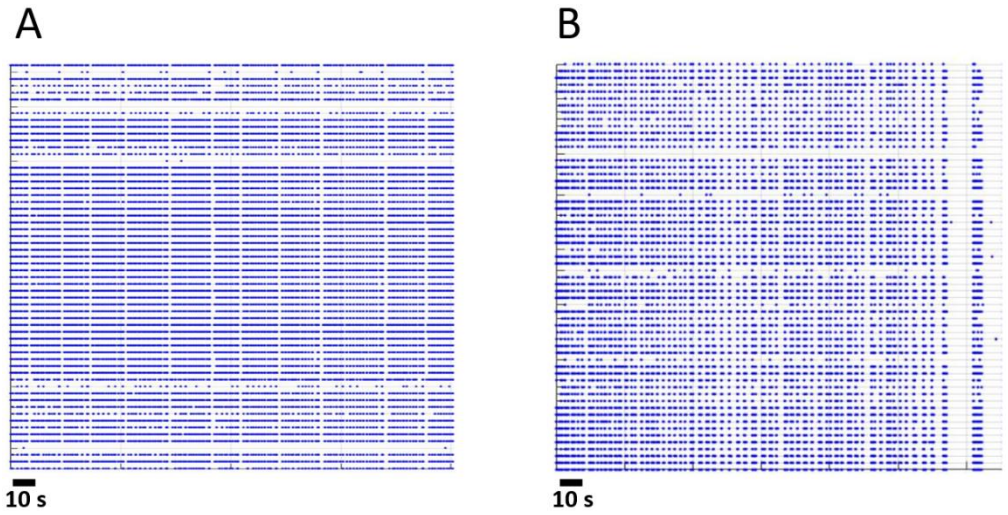

Figure 2.5. (A) Raster plot showing 100 s of hippocampal neuronal network spontaneous activity recorded from 60 planar MEA channels. (B) Raster plot showing 100 s of cortical neuronal network spontaneous activity recorded from 60 planar MEA channels.

Besides clear advantages related to controllability and observability, such 2D *in-vitro* neuronal model systems have major limitations, as they might be inherently unable to exhibit characteristics of *in-vivo* systems.

In order to approach and mimic the natural assemblies in the brain, designing of specific network architectures, which force neurons to follow a pre-defined structure, is required. This can be achieved by using patterning techniques to spatially control the neuronal network growth. Neuronal populations cultured on a monolayer (patterned networks) can give insights into the communication between cells and network dynamics versus topology.

Latest studies reports micro-patterning and micromachining techniques to define network architectures by arranging cell bodies and cell processes onto the microelectrodes (Macis et al. 2007, Marconi et al. 2012).

Especially, Macis and coworkers developed a system to define patterned and interconnected sub-populations of neuronal cultures on planar MEA devices (Macic et al. 2007). The developed system was constituted by an automated micro-drop delivery platform, which allowed to design and realize spatially distributed neuronal sub-populations by depositing sub-nanoliter volumes of adhesion molecules on which neurons grow and develop (Macic et al. 2007). Electrophysiological tests demonstrated that functionally interconnected clusters can be obtained and experimental results (both spontaneous and stimulus-evoked activity recordings) attested the feasibility of the proposed approach.

In another work, Marconi and collaborators achieved patterning and growth of neuronal cultures by coupling the microcontact printing of an adhesion promoter with the use of an agarose repulsive layer (Marconi et al. 2012). They also investigated, by patch-clamp and MEA electrophysiology, the emerging functional properties of these grid-confined networks. They found that the basic properties of synaptic transmission, the overall network development, and the emerging overall network activity were not altered with respect to control random cultures. Figure 2.6 shows a close-up view of patterned hippocampal neuronal networks on a grid mesh and on a node. It is possible to observe that the synaptic connections are mainly formed at the nodes of the grid pattern.

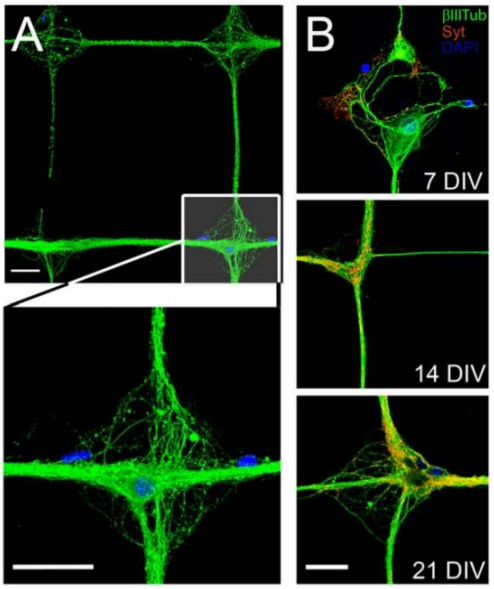

Figure 2.6. (A) Close-up of a 21 DIV culture on a grid mesh (top) and on a node (bottom). A well established and organized wiring is visible with neuronal cell bodies predominantly localized at the nodes. (B) Synaptotagmin (Syt) staining performed at 7, 14 and 21 DIV reveals the formation of synaptic contacts concentrated on the neuronal cell bodies and proximal dendrites at the nodes. (From Marconi et al. 2012).

In 2D *in-vitro* neuronal models, the network structure is constrained by the presence of a rigid planar substrate. The morphology of neurons is rather flat and the interaction with glial cells and extracellular matrix are limited by the planar substrate on which cells are grown. In this kind of preparation, soma are unrealistically flattened and the axons-dendrites outgrowth cannot occur in all directions (Cullen et al. 2011). Although these neuronal network systems are somehow widely accepted, one of the major issues has often been related to the poor dynamics exhibited by such networks often dominated by high-synchronized bursting activity, encompassing most of the neurons in the network (Wagenaar et al. 2005).

Thus, it is clear that a 2D neuronal model for studying the characteristic of the *in-vivo* system is too reduced. There is a tremendous need to develop new culture systems that more closely model the complexity of nervous tissue (Irons et al. 2008). Given the intricate relationships between structure and dynamics, it is needed to scale up from 2D neuronal network model to 3D neuronal network model. The development and implementation of a true 3D engineered *in-vitro* neuronal model could certainly be seen as a complementary-alternative and an interesting tool for neurophysiological investigations.

2.1.2 3D Engineered *in-vitro* Neuronal Models

Over the past decade, researchers and scientists have exploited tissue engineering to recreate *in-vitro* 3D neuronal networks by using different approaches based on the use of materials such as polymers, hydrogel, solid porous matrices or functionalized microbeads.

In 2008, Irons and coworkers reported a first significant study on the development of 3D engineered *in-vitro* neuronal network systems. They engineered novel active 3D neural constructs composed of neurons and astrocytes within a bioactive extracellular matrix-based scaffold (Irons et al. 2008). Neurons within these constructs exhibited extensive 3D neurite outgrowth, expressed mature neuron-specific cytoskeletal proteins and remained viable for several weeks.

In a similar work, Cullen and collaborators developed 3D engineered *in-vitro* neuronal networks by using cultures on or within biological matrices or hydrogel based-scaffolds (Cullen et al. 2011). They applied these engineered neural tissue surrogates as *in vitro* investigational platforms to study and manipulate neurobiological responses within 3D microenvironments.

In contrast to the aforementioned works, Pautot and co-authors proposed a step-by-step method based on the concept that dissociated cultured neurons are able to grow on functionalized micrometric silica beads. These microbeads provide a growth surface large enough for neuronal cell bodies to adhere and grow, mature, extend, and define synaptic contacts with other neurons. This method is simple and exploits the spontaneous assembly properties of mono-dispersed beads to form 3D layered hexagonal arrays encompassing growing and developing neurons and neuronal processes (Pautot et al. 2008).

In the latest approaches, researchers have explored and exploited the use of synthetic polymers or/and nanostructured scaffolds for the reconstruction of 3D *in-vitro* neuronal circuits (Bosi et al. 2015, Kim et al. 2017).

In 2015, Bosi and coworkers proposed a novel biocompatible, polydimethylsiloxane (PDMS) based-scaffold that can be reliably tailored in its mechanical micro- and nano-properties and allowed the development of 3D hippocampal cultures where the soma and processes of neurons and neuroglia are exposed to the third dimension (Bosi et al. 2015). They further nanostructured the scaffold by means of multi-walled carbon nanotubes (MWCNTs) exploiting their great properties (size, high electrical conductivity, large

surface area) in order to boost synaptic activity and to favor their interactions with distal dendrites, promoting the emergence of improved tissue functions.

In another study, Kim and collaborators investigated the neurite pathfinding on electrospun microfibers with various fiber densities, diameters, and microbead islands, and demonstrated the development of 3D connected artificial neuronal network within a Polystyrene nanofiber-microbead-based porous scaffold (Kim et al. 2017).

They found that enhanced porosity and vertical fiber orientation permitted cell body inclusion within the scaffold and substantial neurite outgrowth in a vertical direction. Moreover, they demonstrated that the neurite outgrowth was guided by the overall microfiber orientation, but the increase in fiber density induced the neurite path alteration, thus, the reduction in neurite linearity.

In the studies previously reported, several approaches have been proposed for the development and implementation of 3D *in-vitro* neuronal systems, but no attempt of functional multisite electrophysiological measurements of 3D neuronal networks has been presented. Design and implementation of 3D engineered neuronal networks with embedded sensors and recording/stimulating microelectrodes would certainly open new opportunities for investigation in the neuroscientific domain.

3D neuronal networks coupled to micro-transducer arrays would represent a new and powerful *in-vitro* model capable of better emulating the *in-vivo* physiology.

A first noteworthy work about the spontaneous and electrically evoked electrophysiological activity in 3D hippocampal neuronal cultures coupled to substrate with embedded planar MEAs was described by Frega and coworkers in 2014 (Frega et al. 2014).

They proposed an innovative *in-vitro* experimental paradigm constituted by 3D engineered networks coupled to planar MEAs.

The 3D neuronal constructs were implemented by using glass microbeads (Pautot et al. 2008) to design engineered *in-vitro* systems where the thickness of the preparation, cell density, and network connectivity are partly controlled to resemble brain tissue while enabling, at the same time, optical observation, environmental control and multisite electrical recording-stimulation. In Figure 2.7 (A) is shown the innovative method used to construct 3D engineered neuronal networks coupled to 2D-MEAs.

In order to prove *in-vivo* like cell morphology and demonstrate the reliability of implementing a 3D network, they gathered structural information on fixed 3D hippocampal cultures by indirect immunofluorescence techniques (Figure 2.7 (B), (C) and (D)).

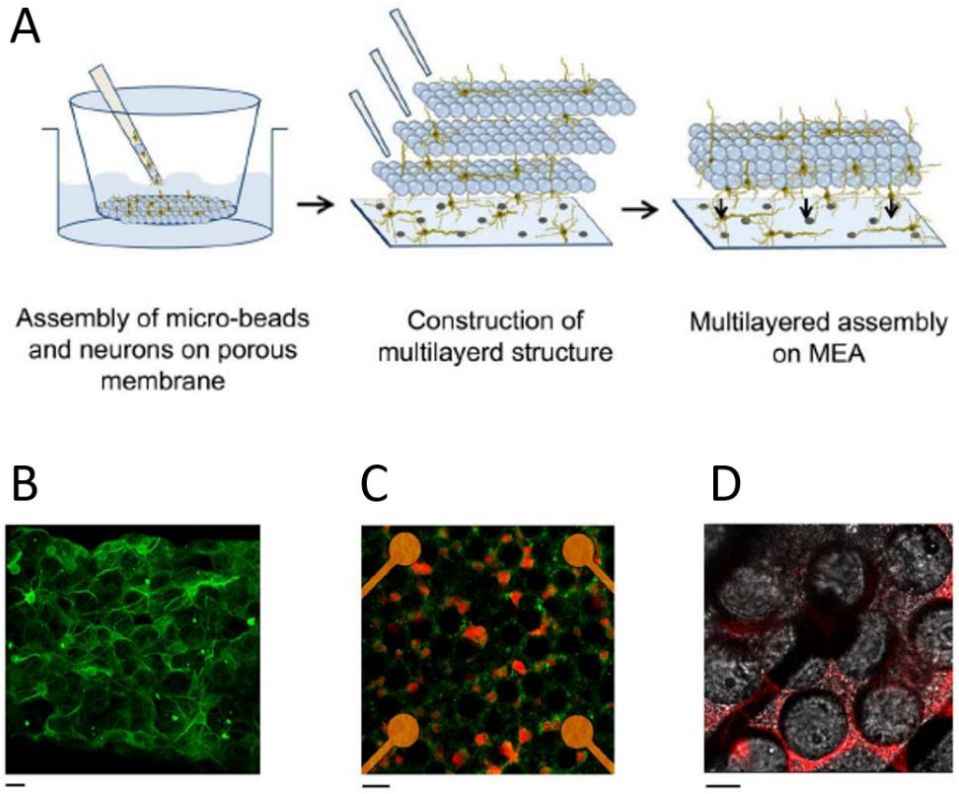

Figure 2.7. (A). Main steps for building a 3D neural network. (B). 3D rendering of 261.4 µm z-stack of the hippocampal network on MEA device showing a high density of neuronal processes, exposed to dendritic marker MAP-2. Scale bar: 40 µm. (C). 3D culture on MEAs, labeled with MAP-2 and NeuN. Scale bar: 40 µm. (D). The first layer of microbeads directly coupled to the top of a single microelectrode. Scale bar: 20 µm. (From Frega et al. 2014).

Moreover, they characterized the activity of the 3D hippocampal networks by comparing the expressed dynamics with traditional 2D neuronal networks grown over MEAs. They found that 2D neuronal networks show only a strong synchronous bursting activity with the absence of significant random spiking activity, which involve most of the recording channels interspersed by a period of time in which almost no activity is recorded.

Differently, they demonstrated that 3D neuronal networks coupled to planar MEAs exhibit a wider range of activity patterns with less global synchrony and more pronounced spiking at single channel-neuron level.

Figures 2.8 (A) and (B) report the electrophysiological spontaneous activity recorded by means of planar MEAs from one representative 2D and 3D hippocampal neuronal network, highlighting the wider range of activity patterns constituted of both network burst and random spike regions for 3D networks with respect to the 2D counterpart.

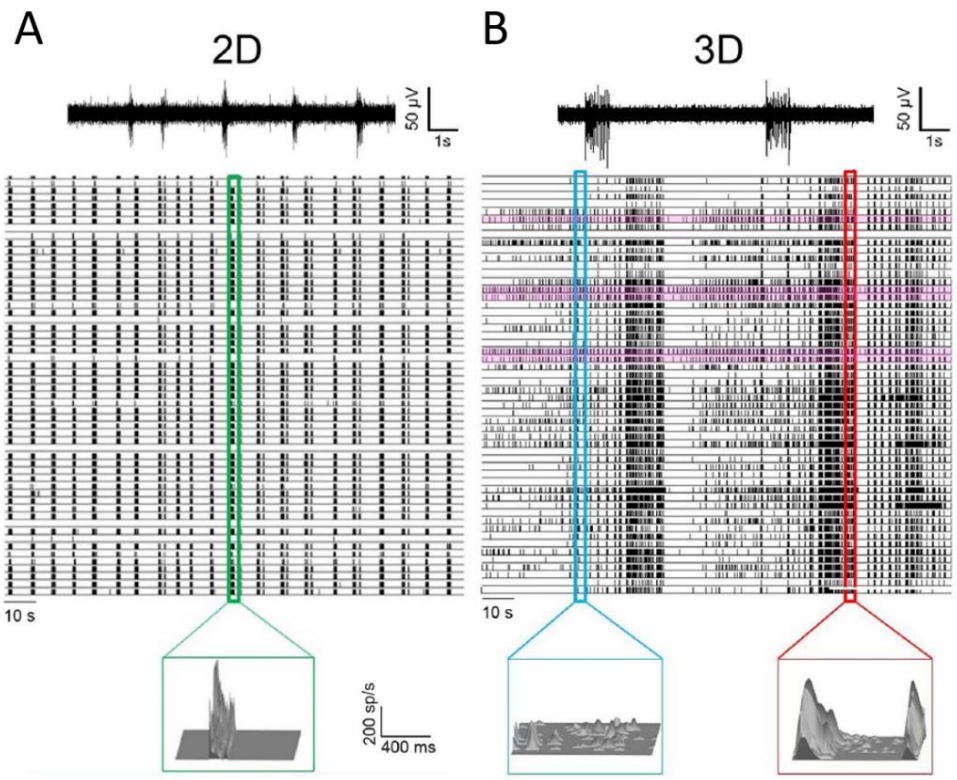

Figure 2.8. Electrophysiological activity of a representative neuronal network, (A). 2D and (B). 3D. From top to bottom: example of 10 s of raw data recorded from one microelectrode; raster plots showing 300 s of spontaneous activity. For the highlighted areas, the Instantaneous Firing Rate (IFR) profile is shown. For the 3D network, the blue and red boxes highlight random spiking and network bursting activity regions, respectively. For the 2D network, only network bursting regions can be detected (green box). (From Frega et al. 2014).

2.1.2.1 Development of Chitosan derived Scaffold for 3D Engineered Neuronal Cultures

As previously stated, 2D neuronal populations coupled to Micro-Electrode-Arrays (MEAs) constitute a well-established experimental *in-vitro* platform to study neurobiology, network electrophysiology, and basic injury-disease mechanisms.

Besides clear advantages related to controllability and observability, such 2D neuronal model systems have major limitations, as they might be inherently unable to exhibit characteristics of *in-vivo* systems.

Under this perspective, the development of a 3D engineered *in-vitro* neuronal model can certainly be seen as a complementary-alternative and interesting tool for neurophysiological investigations. As previously reported, in the last ten years, several studies have been devoted to the introduction of 3D engineered *in-vitro* neuronal systems (Irons et al. 2008, Pautot et al. 2008, Cullen et al. 2011, Frega et al. 2014, Bosi et al. 2015, Kim et al. 2017).

In this section, I report the study and characterization of a new *in-vitro* experimental model constituted by 3D engineered neuronal networks coupled to planar MEAs. The potential advantages of 3D engineered constructs are evident as they can be used as a more accurate investigational *in-vitro* platform than standard 2D network models (Frega et al. 2014). Indeed, 3D neuronal networks coupled to MEAs, represent a powerful *in-vitro* model capable of better emulating *in-vivo* physiology.

In this work, Dr. Laura Pastorino and her group at the University of Genoa (Genoa, Italy) proposed an innovative approach for designing 3D engineered *in-vitro* neuronal cultures. They compared different methods for the development of 3D *in-vitro* neuronal models with respect to a previous work, where the scaffold of 3D networks was realized by means of glass microbeads (Frega et al. 2014). They developed and implemented the 3D neuronal constructs by using layers of chitosan microbeads in the view of mimicking the extracellular matrix environment.

Chitosan is characterized by the greatest surface of amine content and, at the same time, by the lowest equilibrium of water content which contributes to the high viability of cells in culture. This polysaccharide is able to exert a positive effect on the cellular adhesion and to promote a quick neuritic growth (Tedesco et al. 2018).

Specifically, two types of chitosan were adopted for the preparation of the 3D constructs: neutralized chitosan and cross-linked chitosan with tripolyphosphate (CS/TPP). TPP was used for the preparation of chitosan microparticles due to its basic property to promote the adhesion of neurons on the beads surface.

Once the chitosan microbeads were prepared, microparticles were assembled with hippocampal neurons following the same procedure implemented by Frega and collaborators in their work (Frega et al. 2014). The so obtained 3D chitosan engineered hippocampal neuronal network was then coupled to a planar MEA to record the electrophysiological activity of the network.

My contribution to this work was the network dynamics characterization of such two types of chitosan-derived microbeads. I specifically analyzed the expressed dynamics of 3D neutralized chitosan hippocampal neuronal network and 3D cross-linked CS/TPP hippocampal neuronal network comparing their spontaneous activity with the ones of two specific control systems: (i) 3D hippocampal neuronal network grown onto glass microbeads and (ii) standard 2D network, both coupled to MEAs.

In Figures 2.9 (A) and (B) are reported confocal images of such 3D hippocampal neuronal culture at DIV 24 *in-vitro*, assembled on neutralized chitosan microbeads and on cross-linked CS/TPP microbeads, respectively. In addition, a confocal image of a 3D hippocampal neuronal network grown onto cross-linked CS/TPP microbeads-based scaffold at DIV20 *in-vitro* coupled to planar MEA is also shown in Figure 2.9 (C). The final configuration of the 3D engineered *in-vitro* neuronal model made up of planar MEA, chitosan microbeads-neurons layers is reported in Figure 2.9 (D).

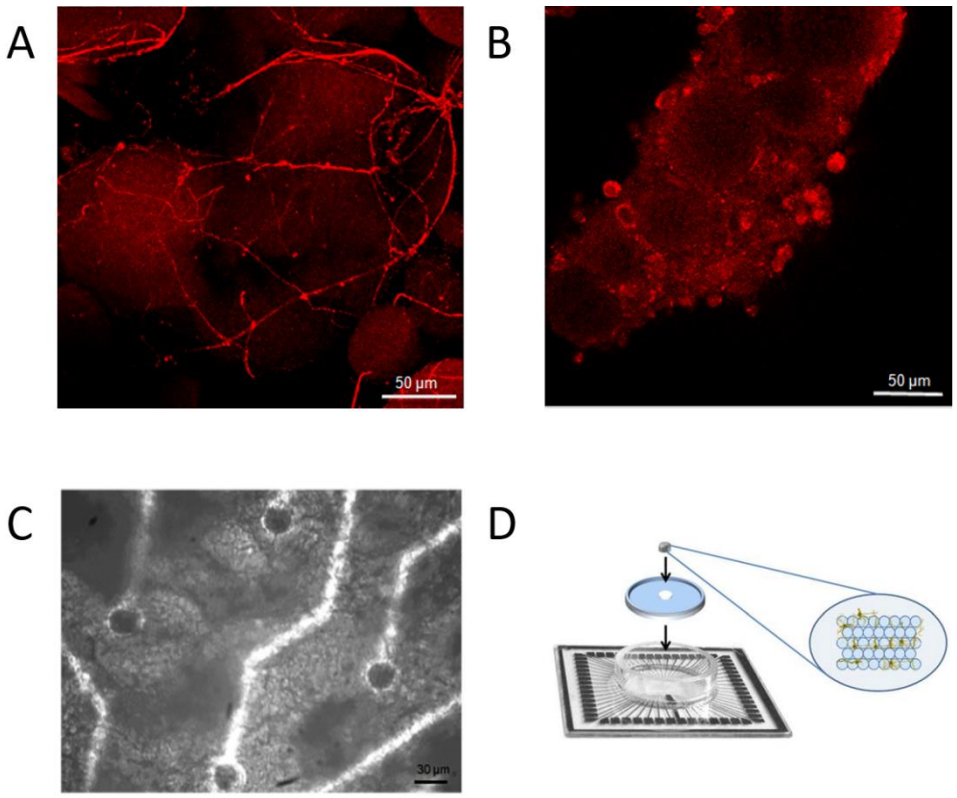

Figure 2.9. Confocal image of DIV24 hippocampal neuronal culture *in-vitro*, assembled (A) on neutralized chitosan microbeads and (B) on cross-linked chitosan tripolyphosphate (CS/TPP) microbeads immunolabeled with anti-tubulin ßIII-Alexa Fluor 546 conjugated. (C) Confocal image of 3D hippocampal neuronal network assembled on cross-linked CS/TPP microbeads at DIV20 *in-vitro* coupled to planar MEAs. (D) Cartoon illustrating the final configuration of the developed 3D engineered neuronal system: multi-layers of chitosan microbeads and neurons confined by a PDMS structure onto the active area of the MEA device.

The electrophysiological activity of 3D and 2D hippocampal neuronal networks (18-21 DIV) was recorded for 30 minutes in all (n=4) the performed experiments by means of 2D-MEAs made up of 60 planar microelectrodes (TiN/SiN, 30 µm electrode diameter, 200 µm spaced) arranged over an 8 X 8 square grid (except the four electrodes at the corners), supplied by Multi Channel Systems (MCS, Reutlingen, Germany).

Then, data and statistical analysis were performed. In particular, I performed data analysis off-line by using a custom software package named SPYCODE (Bologna et al. 2010) developed in MATLAB (The Mathworks, Natick, MA, USA). SPYCODE provides a working environment able to perform efficient data management and processing since it incorporates a very rich repertoire of standard and advanced signal analysis tools for analyzing neuronal networks activity.

I performed spike detection by using the Precise Timing Spike Detection (PTSD) algorithm (Maccione et al. 2009). The PTSD provides a good trade-off between performance and computational costs. The algorithm requires three parameters: a differential threshold set to 8 times the standard deviation of the baseline noise independently for each channel, a peak lifetime period (set at 2 ms) and a refractory period (set at 1 ms). I also performed burst detection according to the method described in Pasquale and collaborators (Pasquale et al. 2010). A burst consists of a fast sequence of spikes with a duration equal to the sum of the inter-spike intervals (ISIs) within the burst itself and separated by an interval (inter-burst interval, IBI) relatively long compared to the burst duration. The algorithm is based on the computation of the logarithmic inter-spike interval histogram in which inter-burst activity (i.e., between bursts and/ or outside bursts) and intra-burst activity (i.e., within burst) for each recording channel can be easily identified, and then, a threshold for detecting spikes belonging to the same burst is automatically defined. The same approach used for the detection of spike bursts was applied for the detection of network burst. A network burst is identified if it involves at least 80% of the network active channels (Bologna et al. 2010).
Regarding the statistical analysis, data were expressed as mean ± standard error of the mean. Statistical analysis was performed using MATLAB. Since data do not follow a normal distribution (evaluated by the Kolmogorov-Smirnov normality test), I performed a non-parametric Mann-Whitney U-test. Significance levels were set at $p < 0.001$.

As previously stated, to characterize the spontaneous electrophysiological activity of 3D neutralized chitosan hippocampal neuronal network and 3D cross-linked CS/TPP hippocampal neuronal network, I specifically compared the expressed dynamics with the one of two gold-standard reference models: 3D hippocampal neuronal network grown onto glass microbeads-based scaffold and 2D hippocampal neuronal network, both coupled to planar MEAs.

Figure 2.10 (A) shows a raster plot of the spontaneous activity of a representative experiment performed on a 2D hippocampal neuronal culture during the third week *in vitro*. Thanks to this plot, it is possible to observe the electrophysiological activity of the network recorded from all the electrodes during 5 minutes.

As reported in the literature (Gandolfo et al. 2010), we can observe the quasi-synchronous activity and network dynamics composed mainly of network bursts. There are synchronized events, which involve most of the recording channels interspersed by a period of time in which almost no activity is recorded. 2D hippocampal assemblies are characterized by high synchronous bursting activity and a very few random spiking activity.

Similarly, Figures 2.10 (B), (C) and (D) show a raster plot of the spontaneous activity of a representative experiment performed on a 3D neuronal network grown onto glass microbeads-based scaffold, on a 3D neutralized chitosan and on a 3D cross-linked CS/TPP microbeads-based scaffold at DIV21 *in-vitro*, respectively. It can be noticed that the signature of the three types of 3D neuronal network configuration presents a wider repertoire of activities with reduced global synchrony and more pronounced spiking activity at the single channel level.

From a preliminary qualitative observation, we can see that in all the three types of the 3D neuronal network there are periods in which the network holds a more synchronous activity, with the presence of network bursts. The duration of the network bursts is more variable: there is the presence of network bursts with a duration that seems similar to what observed in the 2D networks, but there are also network bursts longer than the ones observed in 2D.

The 3D neuronal networks exhibit also a significant random spiking and non-synchronous bursting activity. Thus, the 3D networks exhibit a wide range of activity patterns, with the presence of short and long network bursts, random spiking activity and synchronized bursts.

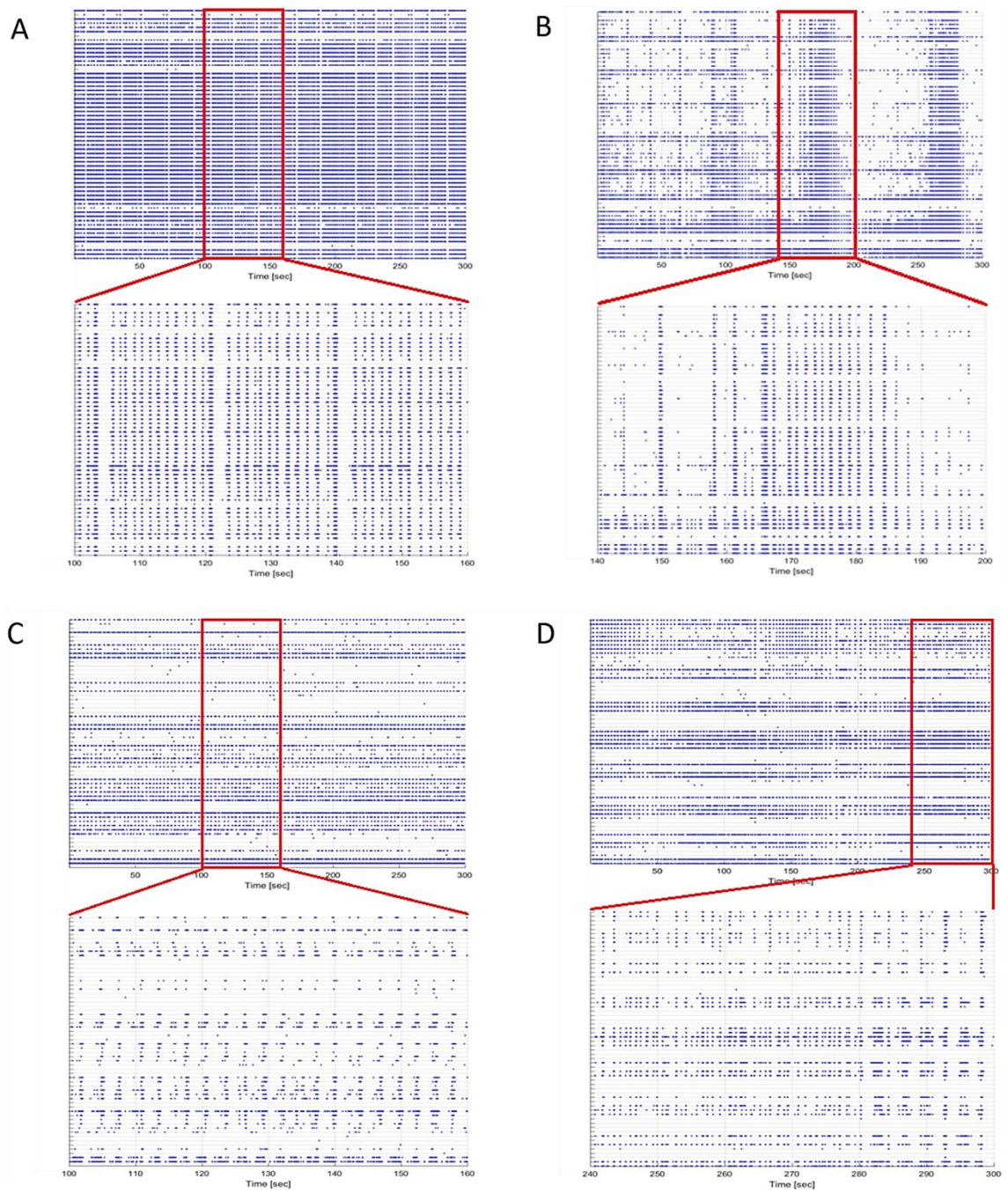

Figure 2.10. Comparison between the network dynamics exhibited by 2D (A), 3D grown onto glass microbeads (B), 3D neutralized chitosan (C) and 3D cross-linked CS/TPP (D) hippocampal neuronal cultures. At each time scale, 3D assemblies display a variety of signatures of activity (i.e., short and long network bursts, random spiking activity, synchronized bursts), while 2D ones display a more pronounced stereotyped activity with only high synchronized bursts.

I further quantify the network dynamics properties of the 3D and 2D neuronal cultures by means of first-order statistics like mean firing rate (MFR), percentage of random spike (PRS), mean bursting rate (MBR), burst duration (BD), network burst duration (NBD), mean network bursting rate (MNBR) (Figure 2.11).

I observed that 2D networks exhibit a low percentage of random spikes (10.4 ± 3.8%) with a high frequency of firing (12.9 ± 7.1 spikes/s), differently the three types of 3D neuronal network show a higher level of random spikes with a lower frequency of firing (Figures 2.11 (A) and (B)). This underlines the fact that in the 3D neuronal cultures the signature of the dynamics is mainly characterized by a more pronounced spiking activity at a single channel-neuron level than 2D ones. In particular, the 3D neutralized chitosan network presents a significant higher level of random spikes (40.7 ± 1.5%) with very low frequency of spikes (2.3 ± 1 spikes/s).

In order to quantify the bursting activity at the single channel level, the frequency and the duration of the bursts were evaluated in all the performed experiments (Figure 2.11 (C) and (D), respectively). 2D networks present a strong synchronous bursting activity with a higher bursting rate (21.5 ± 9.8 burst/min) than the three types of 3D neuronal networks. Especially, the mean bursting rate and duration are not significantly different between the 2D and 3D cross-linked CS/TPP hippocampal neuronal networks. In addition, 3D neutralized chitosan network exhibits a burst duration (311.7 ± 54.3 ms) higher than other cultures.

Finally, I computed the network mean bursting rate and duration evaluated over the entire dataset (Figure 2.11 (E) and (F), respectively). I observed that the 3D neutralized chitosan network shows few network bursts (12.4 ± 5.2 NB/min) with a high duration (978.5 ± 310.5 ms).

In summary, 2D networks exhibit a spontaneous activity that is composed mainly by burst pattern. In fact, as it is shown before, the random spiking activity is very low and the mean bursting rate is higher than 3D one. This behavior stresses the fact that 2D neuronal networks represent a close *in vitro* systems that, missing the natural input-output pathways of the in vivo brain, have to find a stable state with properly formed synapses. On the contrary, 3D neuronal networks present a high level of random spiking activity. This feature suggests that there are stimuli that arrive from the upper layers (i.e. external stimuli) that modulate the electrophysiological activity of the network.

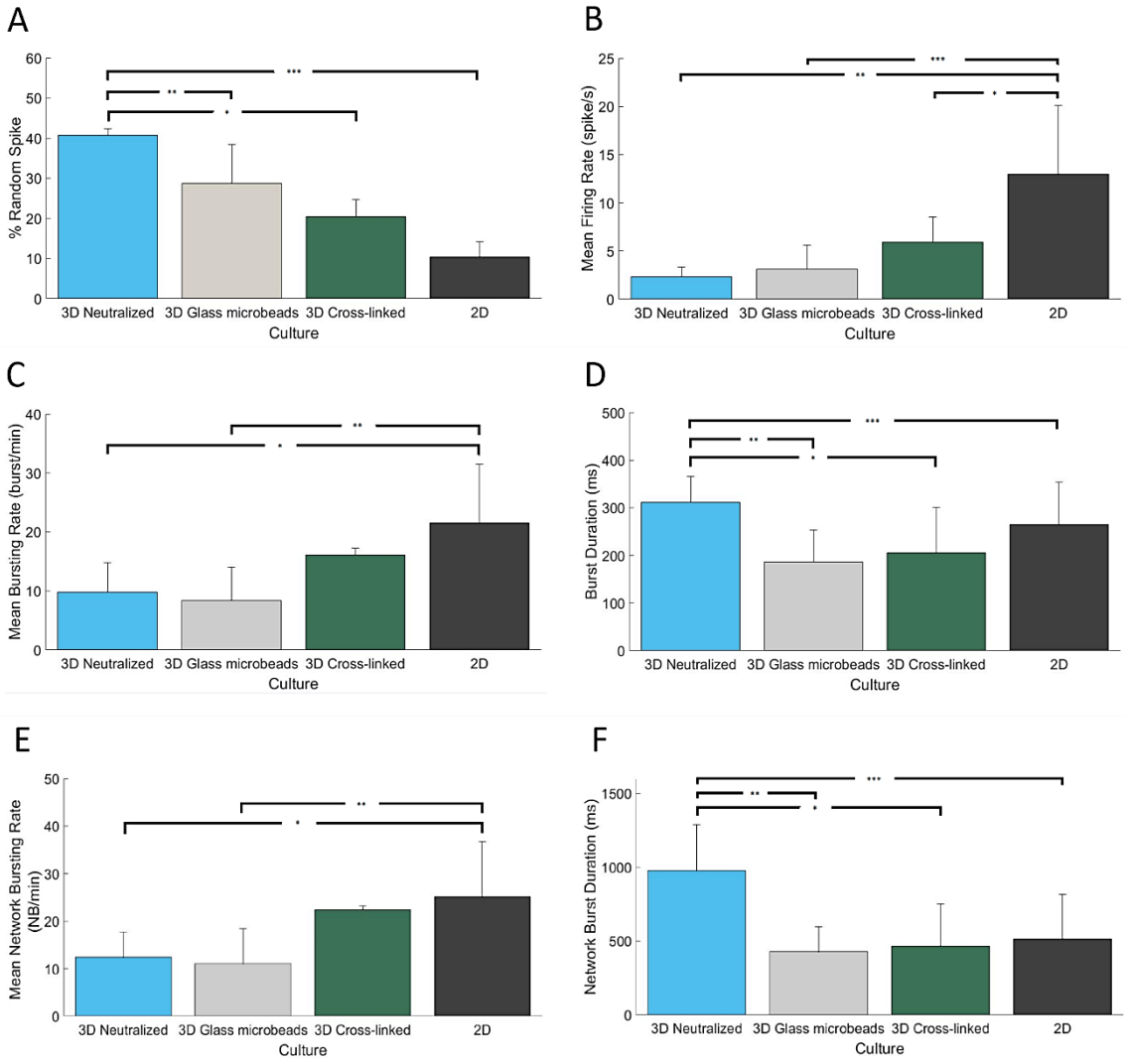

Figure 2.11. Spontaneous activity characterization. (A). Percentage of random spikes ($* \ Pvalue$=$2*10^{-7}$, $** Pvalue$=$6*10^{-6}$, $*** \ Pvalue$=$4*10^{-7}$, Mann-Whitney U-test). (B). Mean Firing Rate ($* \ Pvalue$=$6*10^{-6}$,$** \ Pvalue$=$6*10^{-8}$, $*** Pvalue$=$6*10^{-10}$, Mann-Whitney U-test). (C). Mean Bursting Rate ($* \ Pvalue$=$7*10^{-5}$, $** \ Pvalue$=$7*10^{-8}$, Mann-Whitney U-test). (D). Burst Duration ($* \ Pvalue$=10^{-4}, $** Pvalue$=$9*10^{-7}$, $*** Pvalue$=$3*10^{-2}$, Mann-Whitney U-test). (E). Mean Network Bursting Rate ($* \ Pvalue$=$5*10^{-3}$, $** \ Pvalue$=$9*10^{-5}$, Mann-Whitney U-test). (F). Network Burst Duration ($* \ Pvalue$=10^{-5}, $** Pvalue$=$7*10^{-7}$, $*** Pvalue$=$7*10^{-6}$, Mann-Whitney U-test). Parameters were evaluated over the entire dataset. Asterisks above the plots indicate statistically significant differences.

I further studied and characterized the spontaneous activity of 2D and 3D neuronal cultures by evaluating the signal propagation through the networks in order to demonstrate whether the layers of the 3D structures are effectively connected. Especially, I evaluated the signal sources, signal latencies and distance/latency correlation in each type of neuronal network taking into account. In 2D neuronal networks, the propagation of the signal is continuous. In this type of structure, the signal starts from one source and propagates rapidly and in a continuous way in the network. We are in the presence of a simple, stereotyped, organized and reliable system that without external inputs continues to repeat the same pattern of activity (Frega et al. 2014).

Instead, in the 3D neuronal networks, the signal starts from one source and propagates in a discontinuous way to the other parts of the network. In this type of configuration, we are in the presence of a complex and not reliable system that with external inputs (i.e. from the upper layers) continues to change the pattern of activity (Frega et al. 2014). In case of 2D neuronal network, in order to verify if the system exhibits a simple and stereotyped dynamic, I evaluated the sites from which the signal (i.e. network bursts) started during 30 minutes of recording of a representative experiment.

I evaluated the sources of the signal as the sites where bursts were initiated in at least 5% of all network bursts (Streit et al. 2001, Tscherter et al. 2001).

By looking at Figure 2.12 (A), it is possible to observe that there are a lot of network bursts but only two sources are present with high occurrence. In order to verify if in this system there is reliability of the sources, I also evaluated the signal sources in four different recording phases (5 minutes for each phase). The result is presented in Figure 2.12 (B). It is clear that sources are always the same in different experimental phases. The electrodes 12 and 28 are sources in all the four experimental phases taken into account. Thus, the system is organized and there is reliability of the sources.

The same evaluation approach has been repeated for the three types of 3D neuronal cultures taking into account. In Figure 2.12 (C) is reported the number of occurrence of the sites where bursts initiated for 3D hippocampal neuronal network grown on glass microbeads. It is possible to observe that there are few network bursts but a lot of sources that appear with low occurrence. In order to know if in this system there is reliability of the sources, I evaluated the signal sources in four different recording phases (5 minutes for each phase).

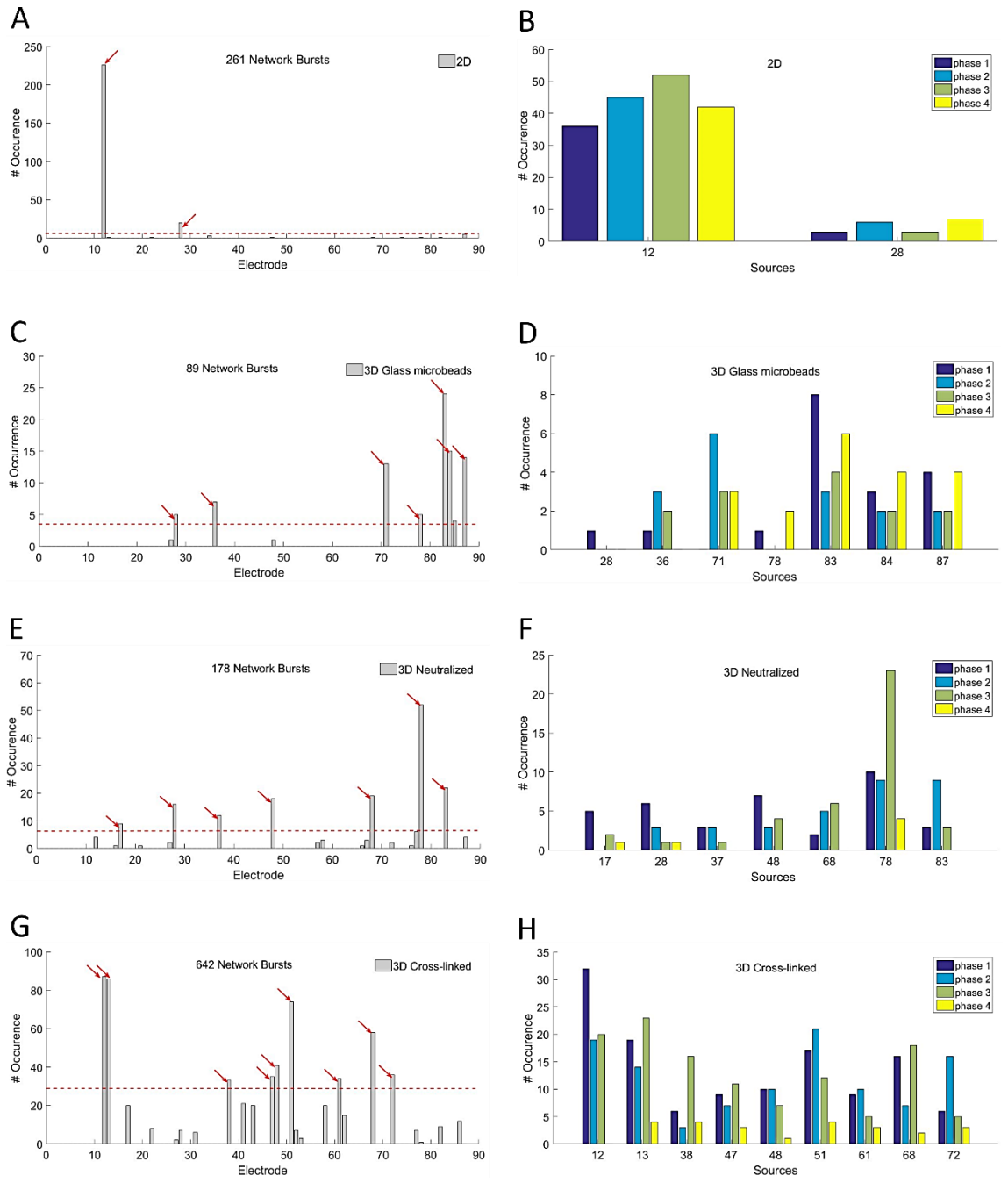

Figure 2.12. Signal sources evaluated in a recording phase of 30 min for 2D (A), 3D grown onto glass microbeads (C), 3D neutralized chitosan (E) and 3D cross-linked CS/TPP (G) hippocampal neuronal cultures. The number of occurrence of the sites where burst initiated is reported. The sources are the electrodes from which the signal starts in at least 5% of all network burst. The threshold is indicated by a dashed red line and the sources are indicated with arrows. (B), (D), (F) and (H) represent signal sources evaluated in four recording phases of 5 min each for 2D, 3D on glass microbeads, 3D neutralized chitosan and 3D cross-linked CS/TPP hippocampal neuronal cultures, respectively. The number of occurrence for each source is reported.

By looking at Figure 2.12 (D), it is clear that sources change in different recording phases. In particular, the electrodes 83, 84 and 87 are the unique reliable sources. The others change in different experimental phases. Thus, this system presents a complex organization in which the sources are not reliable. This is an indirect proof of the fact that there is the presence of real sources in the upper layers.

In Figure 2.12 (E) is shown the signal sources evaluation in a recording phase of 30 min for a 3D hippocampal neuronal network assembled onto neutralized chitosan microbeads. In this type of configuration, there are few network bursts but a lot of sources (seven) with low occurrence.

To verify if the system presents a reliable behavior, I evaluate the signal sources in four different experimental phases (5 min for each phase). By looking at Figure 2.12 (F), it is possible to observe that the electrodes 28 and 78 are the unique reliable sources. The others change in different experimental phases. These features suggest that 3D neutralized chitosan hippocampal network exhibits a complex and not reliable dynamics like in 3D hippocampal networks on glass microbeads. The behavior observed puts such 3D neutralized chitosan network closer to 3D networks on glass microbeads systems than 2D ones.

Finally, in Figures 2.12 (G) and (H), is reported the signal sources evaluation in the case of 3D hippocampal neuronal network grown onto cross-linked CS/TPP microbeads. In this configuration, it possible to observe that there are a lot of sources (nine) with high occurrence but at the same time a lot of number of network bursts.

Moreover, by looking at Figure 2.12 (H), we can see that the unique not reliable source is the electrode 12. The other sources remain the same in all the experimental phases taking into account. These features suggest that this type of system shows a complex dynamics but at the same time reliability of the sources. The behavior observed puts such 3D cross-linked CS/TPP neuronal network system between standard 3D networks on glass microbeads and 2D networks.

The previous results evaluated taking into account a single representative experiment, were further globally quantified by evaluating the number of network bursts and the relative sources detected in different experiments.

In Figure 2.13 are represented the network bursts number and the sources detected in four experiments during 30 minutes of recordings. By looking at the grey bars (i.e. number of network bursts detected in 30 minutes of recording) it is possible to observe that the number of network bursts exhibited by the 2D and 3D cross-linked CS/TPP neuronal network are higher than those detected by the other ones ($NB_{2D} = 432 \pm 210$, $NB_{3D\ Cross-linked} = 619 \pm 79$).

In the 3D neuronal network on glass microbeads and on neutralized chitosan microbeads, instead, there were fewer network burst than those detected from other networks in 30 minutes of recording ($NB_{3D\ microbeads} = 182 \pm 70$, $NB_{3D\ Neutralized} = 289 \pm 105$). By looking at the black bars (i.e. number of sources evaluated in 30 minutes of recording), the three types of 3D neuronal networks exhibits more sources than the 2D one.

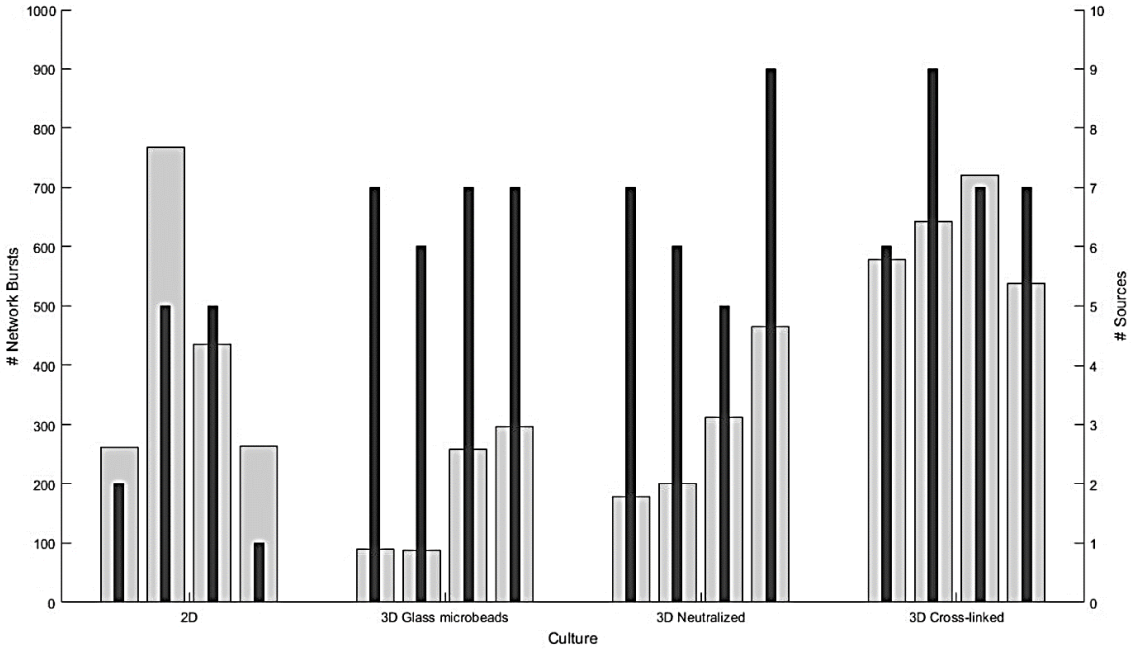

Figure 2.13. Number of network burst (grey bars) and number of sources (black bars) evaluated in 30 minutes of recording. Each bar represents a single experiment (four experiments for the 2D neuronal network and four experiments for the 3D ones).

Summarizing, 2D neuronal network exhibits a lot of network burst and few sources; in the 3D neuronal network on glass microbeads, on the contrary, few network burst and more sources are detected. 3D neuronal network on neutralized chitosan microbeads shows a lot of sources and few network bursts like in the case of 3D network on glass microbeads; in the 3D neuronal network on cross-linked CS/TPP microbeads, a lot of sources and at the same time a lot of network bursts are observed.
In order to compare the observed behavior, I evaluated the percentage of sources related to the number of network bursts (i.e. SNB).

$$SNB = \frac{\sharp\, Sources}{\sharp\, Network\ Bursts} * 100 \tag{2.1}$$

The SNB values evaluated for all the performed experiments are reported in Figure 2.14. 2D neuronal network exhibit a very low value of SNB (0.7 ± 0.3): it indicates the presence of a lot of network burst with respect to the number of sources.
The value of SNB evaluated for the 3D neuronal network on glass microbeads, instead is higher than the one shown by the other networks (4.9 ± 1.8). It means that there are a lot of sources with respect to the number of network burst detected. The SNB plot highlights that 3D neuronal network grown on neutralized chitosan and cross-linked CS/TPP microbeads lie between standard 2D and 3D network on glass microbeads.
In particular, the obtained results suggest that the 3D neutralized chitosan network exhibits a dynamics closer to the one shown by 3D network on glass microbeads; instead, the 3D cross-linked CS/TPP network shows features close to the one exhibited by both standard 2D neuronal network and 3D network on glass microbeads.

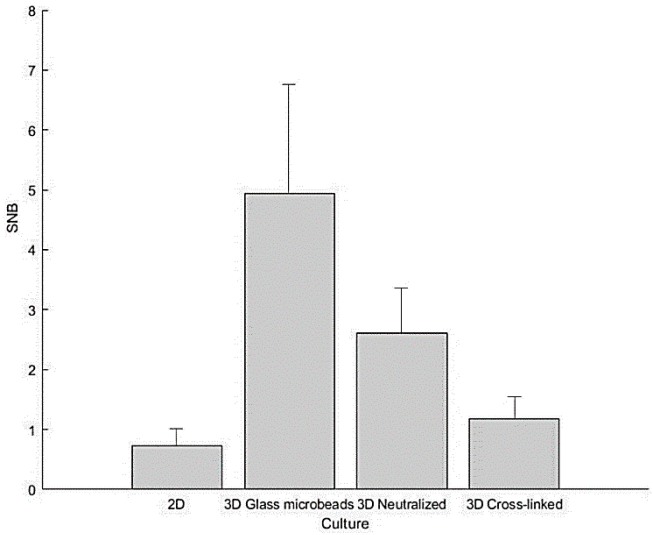

Figure 2.14. SNB values (percentage of sources within respect to the number of network burst) evaluated in 30 minutes of recording for all the experiment performed.

Summarizing, in 2D neuronal network the propagation of the signal is continuous. This system is simple, stereotyped, organized and there is reliability of the sources. These features indicate a closed system in which no external inputs arrives to modulate the activity. Thus, the 2D neuronal network continues to repeat the same pattern of activity. The 3D neuronal networks, instead, exhibit a more complex system in which the propagation of the signal is discontinuous.

Especially, 3D network on neutralized chitosan microbeads shows a dynamics closer to that one expressed by 3D network on glass microbeads. Thus, the activity of this system is modulated by external input: there are real sources in the upper layers, from which the signal starts and reaches the sub-networks coupled to the MEA device modulating their activity. Instead, in the 3D network on cross-linked CS/TPP microbeads, the expressed dynamics is similar to that one exhibited by both standard 2D and 3D neuronal network on glass microbeads.

As shown before, the source is the site from which the signal (i.e. network bursts) starts. In Figure 2.15, the MEA electrode layout is depicted: one source is represented with a red electrode. The distance that the signal travels is evaluated as the physical distance from the source electrode to the other electrode involved in the network burst. The time that the signal needs to reach another electrode involved into the network burst starting from the source (i.e. d1) is the latency of the signal (Streit et al. 2001, Tscherter et al. 2001).

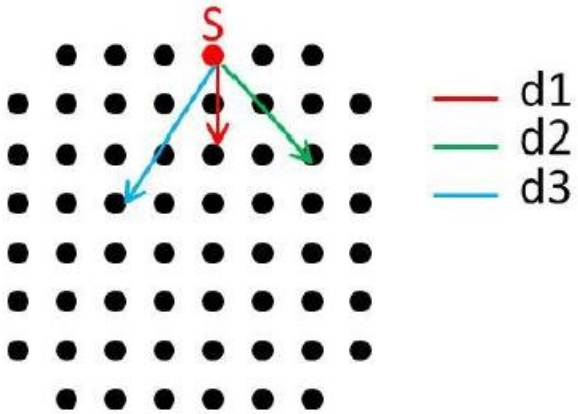

Figure 2.15. Sketch that represents the 8x8 MEA electrode layout. A source is depicted with a red electrode. The arrows indicated three different distance that the signal travels with relative latencies.

By computing the latency values and relating it to the distance that the signal travels, it is possible to quantify the speed propagation of the signal. The average of the latencies over all bursts from the same source was calculated for each electrode (Streit et al. 2001, Tscherter et al. 2001).

Figure 2.16 reports the latency map for all the four configurations of neuronal network taking into account. Latency map indicates the timing that the signal needs for propagating from one representative source to the other parts of the network. The colors of the lines presented in the latency map indicate how long it takes the wave-front of the burst to reach the different electrodes.

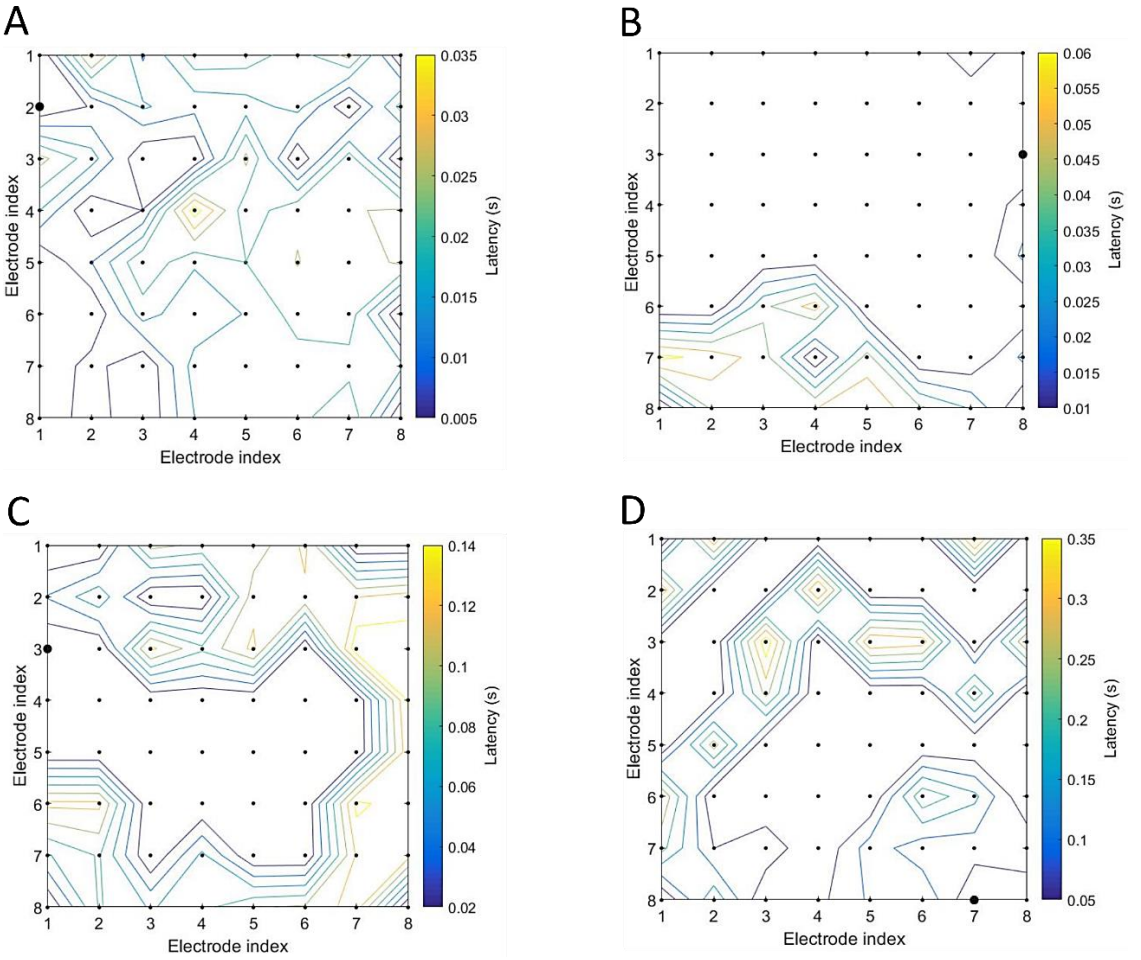

Figure 2.16. Timing that the signal needs for propagating from one representative source to the other parts of the 2D (A), 3D on glass microbeads (B), 3D cross-linked CS/TPP (C) and 3D neutralized chitosan (D) hippocampal neuronal network. The representative source is indicated with a bold point.

In the case of 2D neuronal network, the propagation of the signal is continuous and fast. The signal starts from the source and reaches immediately the electrodes that are closer. Then, in a continuous way, the wave-front of the signal arrives at the distant sites.

By looking at Figure 2.16 (A), it is possible to observe that in this type of configuration the latency values span from 5 ms to 35 ms. These latency values are lower than those detected in the three types of 3D neuronal network. This behavior is mainly due to the fact that in the 3D neuronal network configuration the propagation of the signal is discontinuous and slow. The signal starts from the source and reaches in a random way the other parts of the network (Figures 2.16 (B), (C) and (D)).

The observed features of the 3D neuronal network models are further highlighted in Figure 2.17, where the distance/latency correlation for each type of neuronal culture taking into account is shown.

By looking at Figure 2.17 (A), it is possible to observe that in case of a 2D neuronal network, there is a clear (i.e. linear) relationship between latency and distance. The wave-front of the signal arrives immediately at the sites that are close to the initiation site, then it reaches the more distant sites. Due to the linear distance/latency correlation, it was possible to evaluate the speed of the propagation of the signal which corresponds to the slope of the curve. The obtained value is of about 35 mm/s that is comparable with previous results (Bonifazi et al. 2005, Pasquale et al. 2008, Frega et al. 2014). Instead, in the case of 3D neuronal network configuration, the propagation of the signal is long. Figure 2.17 (B), (C) and (D) show how in the 3D neuronal network there is a random relationship between latency and distance: the signal that starts from one site could perform the same distance both in a very fast way and with high latency. Because of the not clear latency-distance correlation ratio, it is not possible to evaluate the speed of the signal propagation.

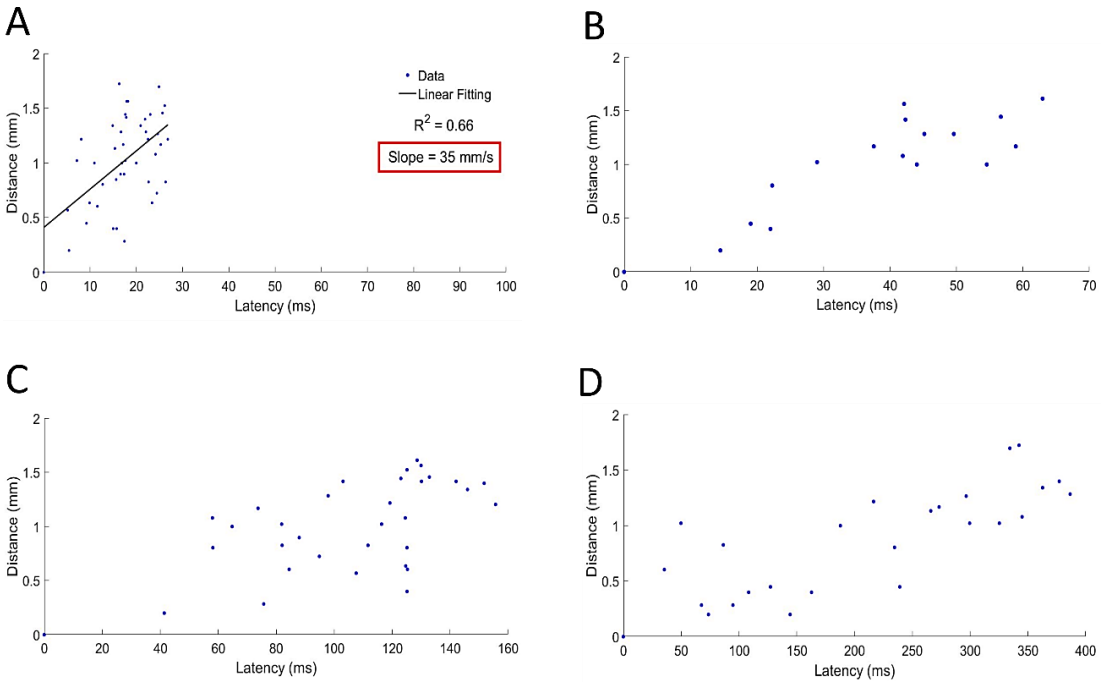

Figure 2.17. Distance-latency correlation in case of 2D (A), 3D on glass microbeads (B), 3D cross-linked CS/TPP (C) and 3D neutralized chitosan (D) hippocampal neuronal network.

Summarizing, in the 3D neuronal network configuration, the latency values are higher than the ones detected in the 2D neuronal network model. Thus, the propagation of the signal in the 3D neuronal network systems is slower than the 2D one.
Moreover, there is a not linear relationship between latency and distance which does not allow to estimate the signal propagation speed. The higher latency values observed in the 3D neuronal network configuration is mainly due to the variability in the connectivity pathway that is present in the 3D structure: the signal can pass through possible paths going up and down to the 3D layers.
In addition, the 3D cross-linked CS/TPP neuronal network shows latency values higher than those detected in 2D and 3D neuronal network on glass microbeads. Instead, in the case of 3D neutralized chitosan neuronal network, the propagation of the signal is much more slower than the one observed in the other cultures.
This feature suggests that the 3D neuronal network assembled onto neutralized chitosan microbeads-based scaffold represents the 'true' 3D neuronal model with respect to the other 3D neuronal models taking into account.

Finally, I also performed an amplitude analysis of the spikes detected by using planar MEA in all the four types of neuronal network under investigation.
In Figure 2.18 (A), (B), (C) and (D) is reported the spikes amplitude distribution for the 2D, 3D on glass microbeads, 3D cross-linked CS/TPP and 3D neutralized chitosan hippocampal neuronal network, respectively.
Moreover, I estimated the probability density function of the spikes amplitudes for each type of culture taking into account (Figure 2.18 (E)). By looking at Figure 2.18 (E), it possible to observe that the 3D cross-linked CS/TPP neuronal network exhibits spikes with an amplitude much more higher than those obtained in the other cultures, reaching about 200 μV of amplitude. Instead, the 3D neutralized chitosan neuronal network shows spikes with amplitude lower than other cultures (< 80 μV).

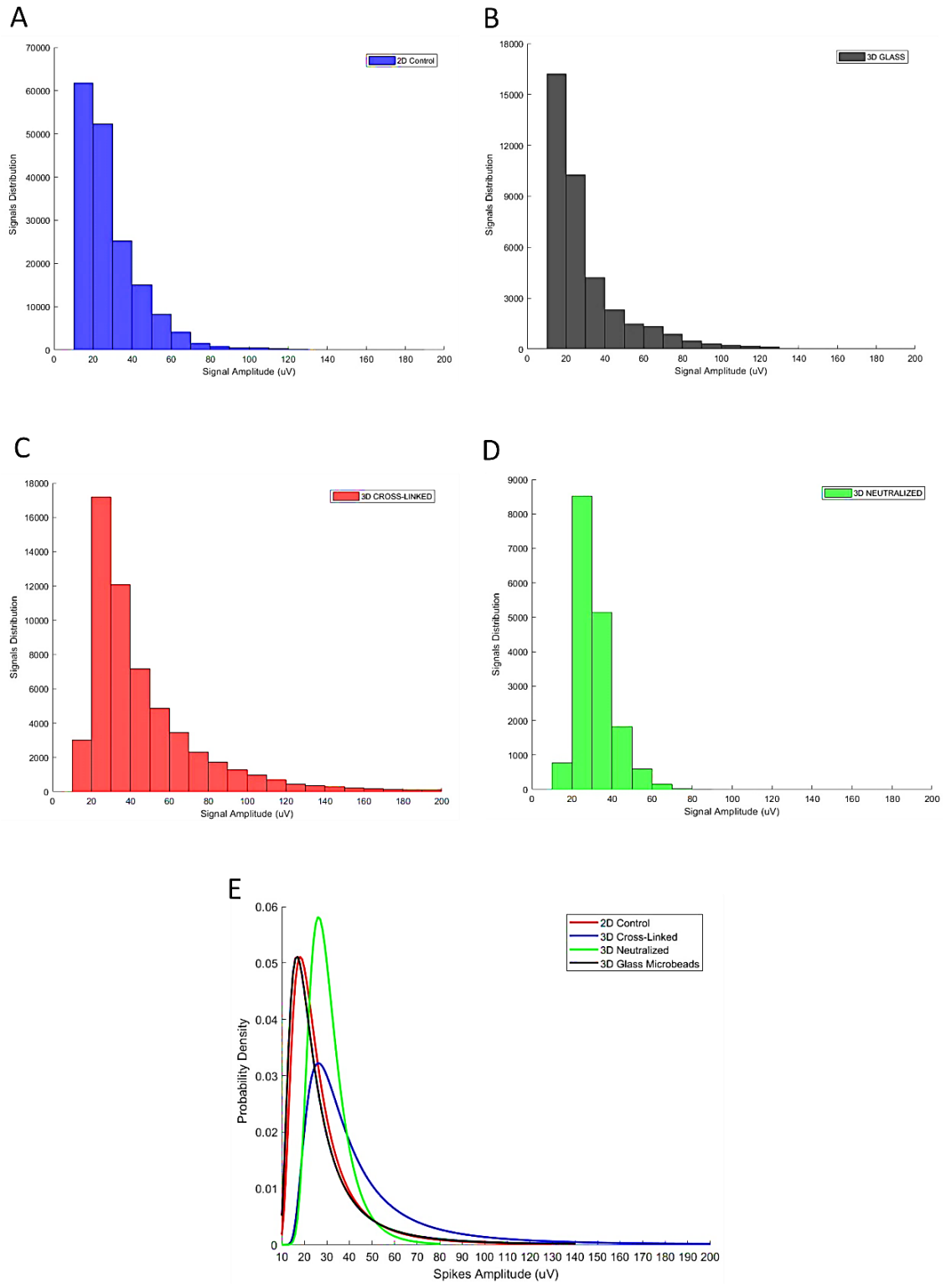

Figure 2.18. Signals amplitude distribution in 2D (A), 3D on glass microbeads (B), 3D cross-linked CS/TPP (C) and 3D neutralized chitosan (D) hippocampal neuronal network. (E). Probability density function of the spikes amplitude in 2D (red), 3D on glass microbeads (dark), 3D cross-linked CS/TPP (blue) and 3D neutralized chitosan (green) hippocampal neuronal network.

2.1.2.2 Soft Chitosan Microbeads Scaffold for 3D Functional Neuronal Networks

The availability of 3D biomimetic *in vitro* neuronal networks of mammalian neurons represents a pivotal step for the development of brain-on-a-chip experimental models to study neuronal (dys)functions and particularly neuronal connectivity for applications ranging from basic neuroscience to drug screening (Pautot et al. 2008, Bosi et al. 2015). As previously reported, the use of hydrogel-based scaffolds for the development of 3D cell cultures has been extensively studied in the last years (Mahoney et al. 2006, Tibbitt et al. 2009, Magin et al. 2016). However, limited work on biomimetic 3D neuronal cultures has been carried out to date.

In this respect, in another work, Dr. Laura Pastorino and her group have further explored and exploited the use of chitosan (CHI) microbeads to actively support 3D functional neuronal cultures coupled to MEAs (Tedesco et al. 2018).

In this study, they reported a detailed characterization of such widely popular polysaccharide, mimicking the physico-chemical characteristics of the extracellular matrix (ECM), for the growth of *in-vitro* 3D neuronal networks.

My contribution to this work was the electrophysiological characterization of 3D hippocampal neuronal networks grown onto the fabricated CHI microbeads. I specifically analyzed the expressed dynamics of such 3D chitosan engineered hippocampal neuronal networks comparing the obtained results with the one reported in a previous work, where glass microbeads were used as a 3D scaffold for neuronal growth (Frega et al. 2014).

In the last few years, polysaccharides have been proposed and widely used as biomimetic materials for scaffold fabrication for a huge variety of cell types (Frampton et al. 2011, Broguiere et al. 2016). However, the use of polysaccharides for 3D neuron cultures has been quite limited as compared to other cell types. Very few studies have addressed the use of chitosan, and the electrophysiological behavior of chitosan-based 3D neuronal cultures is still unknown (Lozano et al. 2015, Huang et al. 2016). This polysaccharide is well known for its biocompatibility, biodegradability, muco-adhesiveness, antibacterial and antifungal activity (Anitha et al 2014).

Interestingly, as previously stated, chitosan enhances neuron attachment, proliferation and neurite extension, and exerts a potent neuroprotective action.

In this work, Dr. Laura Pastorino and coworkers first prepared 2D physically cross-linked chitosan films in order to evaluate their interaction with neurons and obtain information on the bioactivity of chitosan in terms of cell adhesion and network development.

Then, physically cross-linked chitosan microbeads were fabricated by an aerodynamically assisted jetting technique. Specifically, two CHI concentrations were tested for microbeads fabrication, namely 1% and 2% w/v.

Subsequently, they characterized the fabricated CHI microbeads by optical and atomic force microscopies (AFM) in view of their use as scaffolds for neuronal growth. The obtained results indicated a spherical shape and a size ranging from 40 to 90 μm for both 1% and 2% CHI microbeads. The stiffness of 1% CHI microbeads was found to be comparable to that of brain tissue. Moreover, a difference in the stiffness, among 1% and 2% CHI microbeads, was observed and could be attributed to the increase in the concentration of CHI, corresponding to an increase in the density of the polymeric chains. Regarding AFM, darker areas on the microbeads surface were revealed. These characteristics combined with the bioaffinity of CHI, due to the presence of primary amines, contributed to the formation of a dense neuronal network onto CHI microbeads.

3D neuronal constructs were then developed and implemented following the same procedure reported in a previous work in which the scaffold made of glass microbeads was used to actively support the growth of neurons (Frega et al. 2014).

The so obtained 3D chitosan engineered neuronal networks were characterized morphologically by transmission electron microscopy (TEM), by immunofluorescence techniques and 3D imaging with a confocal microscope. Specifically, the scaffold topography, characterized by confocal microscopy, showed that while the micro-scale dendritic extensions were distributed on the external surface of the CHI microbeads, the nano-scale ones tended to penetrate the hydrogel, contributing to the formation of a compact structure.

This speculation was confirmed by TEM analysis, which put in evidence that CHI microbeads are enveloped in a dense network of neuronal dendrites and axons. At the same time, there was clear evidence that smaller dendrites are allowed to enter and spread inside the CHI microbeads, providing its porosity to neuronal dendrites.

Figure 2.19 shows the neuronal network development around the CHI microbeads (A, C) and around glass microbeads (B). It can be observed (Figure 2.19 (A), left and middle) neuronal soma from which rich neuritic arborizations depart. This is particularly evident around the CHI microbead surfaces while it becomes partially fragmented due to the penetration of neurites into the microporous volume of the microbeads (white arrows). In the case of the glass microbeads, the neuronal network development was only confined onto the surface of microbeads, without any fragmentation (Figure 2.19 (B), left). The shape of the soma was found to be spherical in both cases (Figure 2.19 (A) and (B), middle), as the one observed *in vivo*.

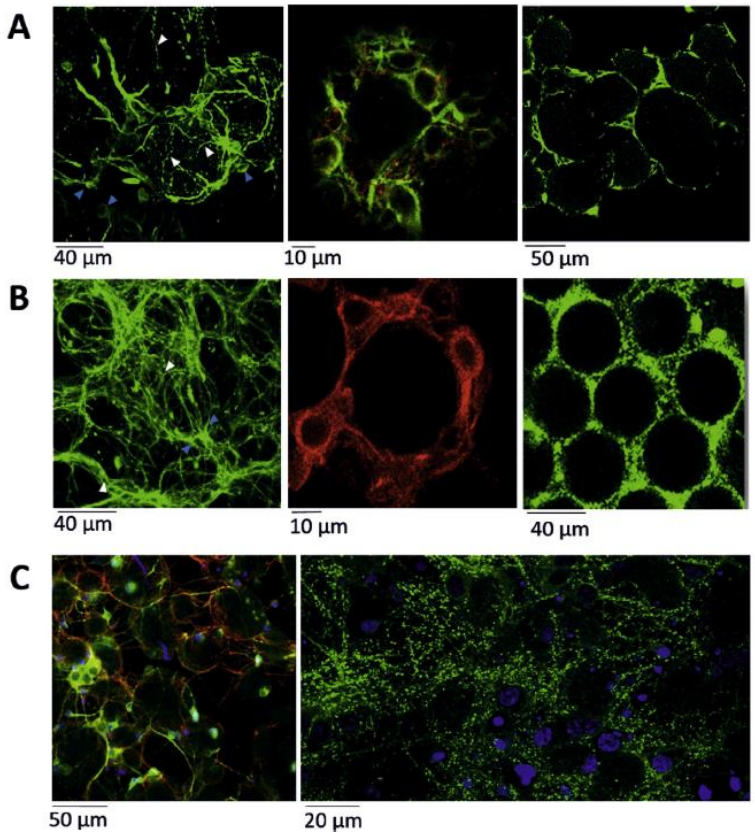

Figure 2.19. Confocal microscope images of 3D neural network at DIV 25: (A) 3D neural network on 2% CHI microbeads (left), single 2% CHI microbead surrounded by almost six neurons (middle) and a section of 3D neural network on 2% CHI microbeads (right), MAP-2 (green) and Synapsin (red). (B) 3D neuronal network on glass microbeads (left), single glass microbead surrounded by five neurons (middle) and a section of 3D neural network on glass microbeads (right), MAP-2 (green and red). The blue arrows point the cell soma while the white one points neuritic fragmentation. (C) 3D neural network on 2% CHI microbeads (left) labeled for MAP-2 (green), Tubulin bIII (red) and DAPI (blu), 3D neural network on 2% CHI microbeads (right) labeled for Synapsin (green) and DAPI (blue).

Once the 3D neuronal networks on CHI microbeads were characterized, the neurons-microbeads assembly was coupled to a planar MEA to record the electrophysiological activity of the 3D networks.

Then, I performed functional characterization of such 3D neuronal networks on CHI microbeads. Specifically, in order to perform the electrophysiological analysis of the 3D networks grown onto CHI microbeads and to compare the obtained results with the ones reported in a previous work (Frega et al. 2014), CHI microbeads were pre-treated with adhesion proteins (a. p.), then mixed with neurons and finally plated onto MEA.

As reported by Frega and coworkers (Frega et al. 2014), before this final step, a 2D neuronal network was directly coupled to the active area of MEA in order to establish a good communication between the 3D culture and the underlying microelectrodes. Figure 2.20 (A) shows the spontaneous activity (raw signal) of 10 s of a 3D CHI network as recorded from one microelectrode and characterized by two bursts and random spikes. The global electrophysiological behavior of representative 3D networks is qualitatively showed in the raster plots of Figure 2.20 (B) and (C), where 300 s of spontaneous activity are displayed. In both experimental conditions (CHI, Figure 2.20 (B) and glass microbeads, Figure 2.20 (C)), quasi-synchronous network bursts (NB) are mixed with random spiking activity. However, 3D networks with CHI microbeads scaffold exhibit a global activity characterized by longer bursts than glass microbeads ones. After 21 DIV, I recorded 30 min of spontaneous activity of n = 3 CHI 1% networks, and n = 3 CHI 2% networks, and I compared the obtained results to n = 3 cultures where the 3D scaffold was realized by means of glass microbeads.

Figures 2.20 (D)-(I) shows the parameters extracted from the analyzed spike data. CHI 1% networks presented values of MFR (2.3 ± 0.14 spikes/s), statistically different from the CHI 2% ones (0.86 ± 0.05 spikes/s; $p < 0.001$) but similar to the MFR of the 3D glass microbeads networks (2.97 ± 0.55 spikes/s). All the 3D experimental configurations display high values of random spiking activity (Figure 2.20 (E)): specifically, CHI 1% and 2% networks show higher (statistically significant) values with respect to glass microbeads ones.

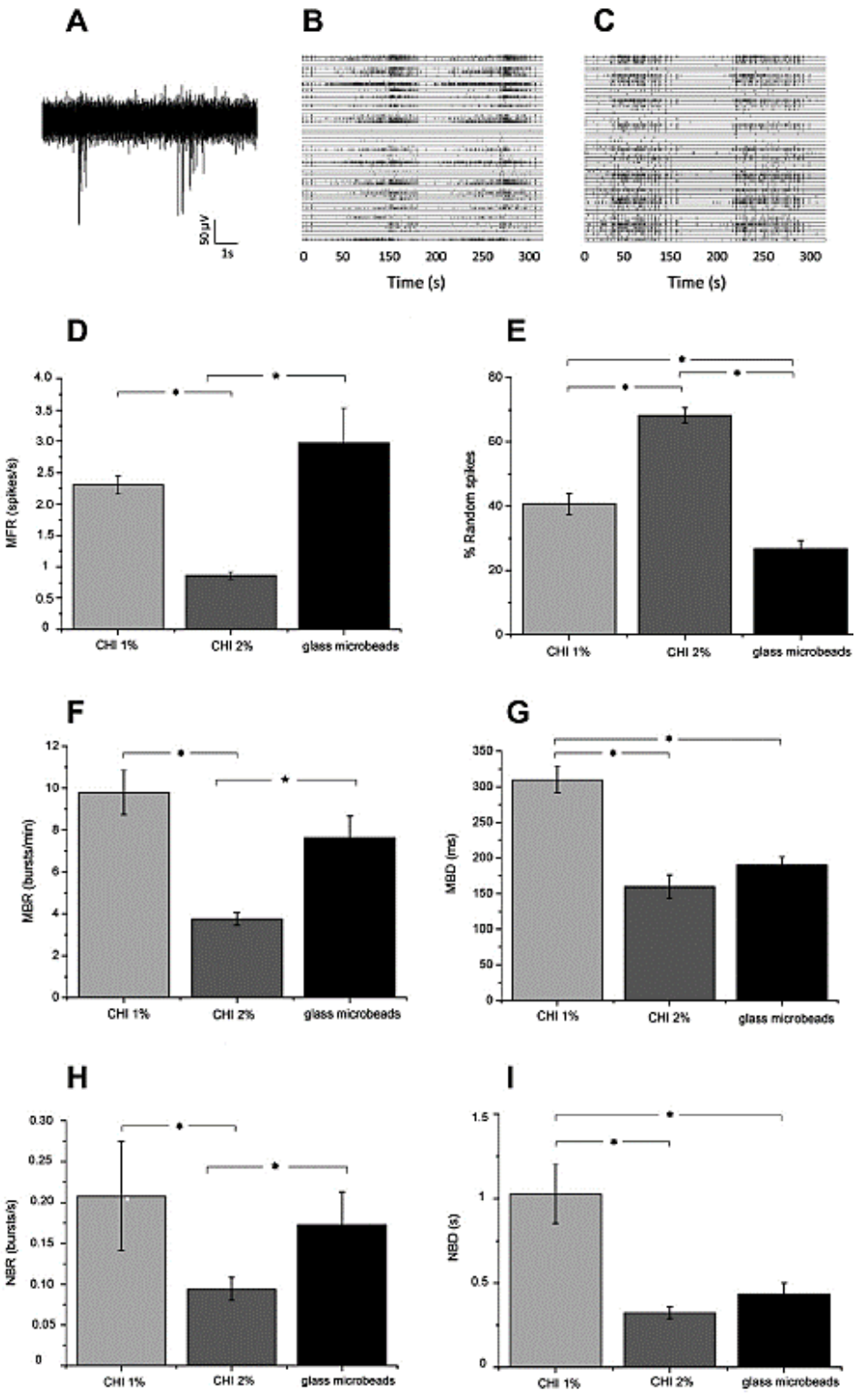

Figure 2.20. Spontaneous activity characterization: (A) 10 s of raw data recorded from a single microelectrode. Raster plot showing 300 s of spontaneous activity of 3D network on (B) CHI 1% microbeads and (C) on glass bead; (D) mean firing rate, (E) percentage of random spiking activity, (F) mean bursting rate, (G) mean burst duration, (H) network bursting rate, (I) network bursts duration. (Kruskal-Wallis, $*p \leq 10^{-3}$).

Regarding the bursting behavior, the MBR of CHI 2% networks showed the lowest value (3.74 ± 0.31 (bursts/min)) which is significantly different ($p < 0.001$) from the CHI 1% and glass microbeads networks. On the other way, round (Figure 2.20 (G)), CHI 1% networks exhibited a MBD (310.5 ± 18.19 (ms)) significantly higher ($p < 0.001$) than the other two configurations that share similar MBD values (175.10 ± 16.41 ms and 190.70 ± 10.53 ms for CHI 2% and glass microbeads).

Finally, the NB activity was investigated by computing the network mean bursting rate (NBR; Figure 2.20 (H)) and duration (NBD; Figure 2.20 (I)). NBR was similar for CHI 1% and glass microbeads networks and statistically different with respect to CHI 2% networks. Again, for the NBD, CHI 1% was different from CHI 2% and glass microbeads that are in turn characterized by shorter bursts (0.32 ± 0.036 s and 0.43 ± 0.067 s, respectively).

Summarizing, I found that the 3D neuronal networks developed onto CHI microbeads presented electrophysiological patterns similar to the ones observed for the glass microbeads in terms of the percentage of random spiking and bursting behavior. As already observed by Frega and coworkers (Frega et al. 2014), in the case of glass microbeads, the percentage of random spiking of the 3D CHI networks presents higher values than those observed in 2D cultures. Here I found a further increase of random spiking with respect to the 3D glass microbeads networks.

Moreover, I observed that 3D CHI 1% networks show more synchronous bursts (MBR, NBR), with respect to 3D CHI 2% with associated longer duration for both bursts and network bursts. This activity indicates the formation of a very dense network with a high degree of connectivity as also suggested by the immunostaining for Synapsin (Figure 2.19 (C) right).

Therefore, the 3D CHI model presents possible advantages that would merit further investigations: (i) stiffness similar to the living brain tissue; (ii) no need for pre-treatment with a. p.; (iii) high-level of connectivity; (iv) *in vivo* like electrophysiological behavior. In conclusion, CHI seems to be a promising scaffolding-support for developing 3D neuronal networks towards the design and implementation of brain-on-a chip microsystems.

Arrays of 3D microelectrodes ad-hoc designed would provide easier physical integration with the culture and more resolved access to the electrophysiological network activity.

2.1.2.3 Structurally and functionally interconnected 3D *in vitro* neuronal assemblies coupled to Micro-Electrode Arrays

Over the last years, there has been a growing interest in interconnected neuronal assemblies (mostly 2D (Pan et al. 2015, Kanagasabapathi et al. 2011)) to investigate, in a controllable setting, functional interaction among cell assemblies or interplay between neurons from different brain regions (e.g., cortex and thalamus (Kanagasabapathi et al. 2012)).

As a step forward in the direction of 'organ-on-chip' (Williamson et al. 2013), here I present a simple method, developed by Dr. Mariateresa Tedesco and coworkers at the University of Genoa (Genoa, Italy), for building interconnected 3D neuronal networks coupled to Micro-Electrode Array (MEA) substrates. Particularly, they designed a confinement structure made of PDMS (poly-dimethyl-siloxane) for realizing two structurally and functionally interconnected 3D neuronal networks *in vitro*. The interconnectivity between the 3D sub-populations was obtained by means of two groups of ten micro-channels with specific spacing and heights, in which neurites and cell bodies adhering to the MEA substrate, guarantee, in principle, a bi-directional way of communication.

My contribution to this work was the network dynamics characterization and functional connectivity estimation of such 3D interconnected *in-vitro* neuronal assemblies. Specifically, I evaluated the network dynamics in terms of spiking and bursting activity. Then, by applying a recently developed cross-correlation based algorithm (Pastore et al. 2016), I estimated the functional connectivity to prove inter- and intra-assemblies connections and thus actual functional interaction between the two neuronal assemblies.

In Figure 2.21 (A) and (B) are shown the two compartment's layout and the realized PDMS structure coupled to the MEA device. In Figure 2.21 (C), a zoom of a small portion of the 3D culture with neurons embedding the microbeads is presented to highlight the ability of the culture to form a dense network of neurites embedding the self-assembled microbeads. Figure 2.21 (D) shows actual 3D interconnected culture by means of one of the two groups of micro-channels. Finally, Figure 2.21 (E) displays the bottom part of the

cortical culture (i.e., the one adhering to the MEA substrate) in one compartment with neurites bundles (and a few soma) entering the micro-channels (Microtubuline Associated Protein MAP-2, green for cytoskeleton and synaptophysin, red for presynaptic vesicles).

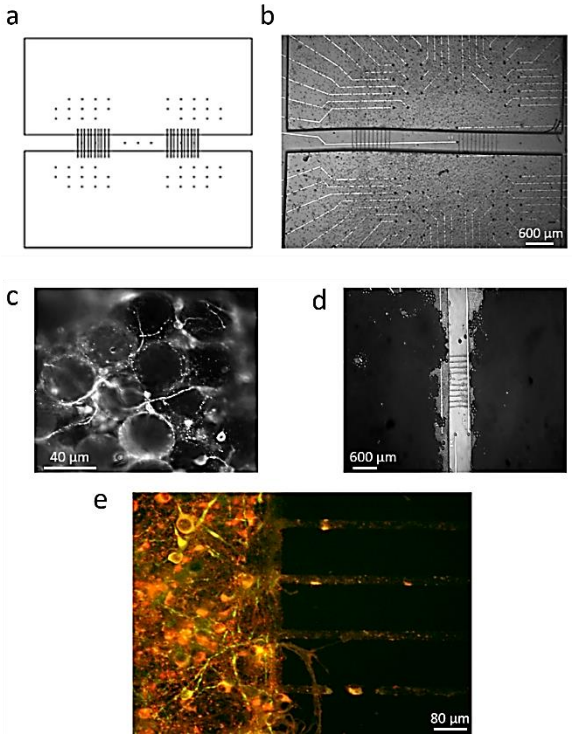

Figure 2.21. (A) Design of the (silicon) master for realizing the PDMS confinement structures. Spacing between the two blocks of channels is 1000 µm. (B) PDMS structure coupled to MEA. (C) Cortical neurons grown on 3D self-assembled glass microbeads showing immunoreactivity to the beta-3 Tubulin cytoskeletal marker. (D) 3D cultures interconnected by means of one of the two groups of micro-channels. (E) Dense staining (red) for presynaptic protein synaptophysin. Synapses are defined as puncta distributed within MAP-2 positive (green) dendrites. Neurite bundles are clearly visible within the micro-channels.

Spontaneous electrophysiological activity of the two interconnected 3D cortical neuronal networks was recorded by means of 60-4QMEA devices (Figure 2.22 (A): the red and blue square profiles represent the two compartments of the mask hosting the 3D sub-populations) during the third week *in vitro* corresponding to a stable state of maturation of the network. The results presented in this work come from two MEAs of interconnected 3D cortical cultures and two control 2D cortical cultures. Each experiment lasted 30 minutes. Data were acquired by using the MEA 2100 System (MCS) at 10 kHz sampling frequency. Raw signals were peak detected by means of the threshold-based precise timing spike detection (PTSD) algorithm (Maccione et al. 2009).

Network dynamics of the two 3D cell populations was then analyzed off-line by using a custom software package named SpyCode (Bologna et al. 2010) developed in MATLAB (The Mathworks, Natick, MA, USA).

Figure 2.22 (A) shows the layout of the MEA device highlighting the two compartments (red and blue) while figure 2.22 (B) presents 5 min of spontaneous activity of a representative experiment of a 3D cortical culture at DIV 21.

For the sake of clarity, the activity of the two interconnected populations is represented in blue and red for the two compartments. It can be noticed that the recorded electrophysiological activity of each sub-population shows the typical signatures of a true 3D network (i.e. reduced global synchrony and more pronounced spiking activity at single channel level) as previously demonstrated (Frega et al. 2014).

Figure 2.22 (C) and (D) show raw data of a representative channel of the two compartments, respectively. Besides differences in the amplitude, both channels show a sustained spontaneous activity.

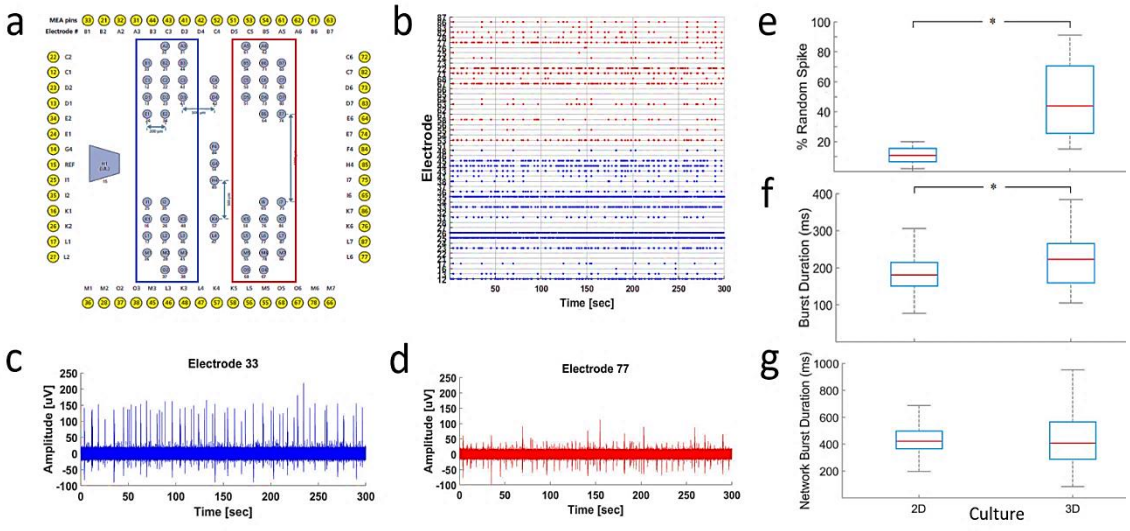

Figure 2.22. Spontaneous activity of interconnected 3D neuronal networks. (A) 60-4QMEA layout (adapted from the MCS website (http://www.multichannelsystems.com). Blue and red boxes represent the left and right compartment, respectively. (B) Raster plot showing 300 s of spontaneous activity of the left (blue dots) and right (red dots) compartment of a representative 3D cortical culture. (C), (D) raw data of a representative channel of the left (electrode 33) and right (electrode 77) side. (E), (F) and (G) boxplot showing percentage of random spikes (Mann-Whitney U-test, $|U|=2\cdot10^{-10}$), burst duration (Mann-Whitney U-test, $|U|=3\cdot10^{-3}$) and network burst duration of the two interconnected 3D cell populations compared with the ones of 2D interconnected control system, respectively. Parameters were evaluated for the active channels of the entire dataset. Asterisks above the plots indicate statistically significant differences.

Figure 2.22 (E), (F) and (G) shows boxplots of the percentage of random spikes (i.e., spikes not belonging to a burst), burst duration and network burst duration of each single compartment of the two interconnected 3D cortical cultures.

To quantify the level of integration inside each neuronal population as well as the level of segregation between them, I characterized functional connectivity by applying a cross-correlation algorithm (Pastore et al. 2016) to the spike trains. From the adjacency (i.e., connectivity) matrix, I discarded (thresholding procedure) the noisier and weaker connections and I quantified the inter- and intra-connectivity links. Figures 2.23 (A) and (B) show the percentage of links intra- and inter-compartments of two different culture experiments. I noticed that the estimated interconnectivity (about 57% for both the presented experiments) between the two 3D cell populations is higher than the intra-connectivity of each of the two compartments for both experiments. Finally, in Figure 2.23 (C), I present the estimated connectivity map of one experiment to illustrate intra- and inter-compartment links.

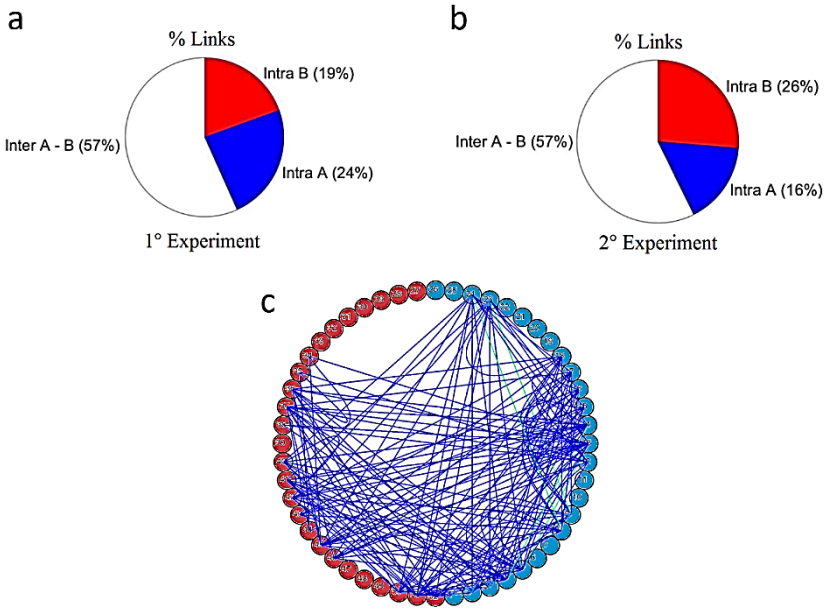

Figure 2.23. Functional connectivity of 3D interconnected assemblies. (A), (B) Percentage of links intra- and inter-compartments of 3D interconnected cortical cultures evaluated during the first and second experiment, respectively. Red and blue slices represent the two different compartments. (C) Connectivity map showing links intra- and inter-compartments of one experiment. Electrodes of the two compartments are depicted in blue and red, respectively.

The new proposed experimental paradigm presents a real 3D architecture mimicking the *in vivo* condition and exhibiting spontaneous activity with structural and functional connections between the two compartments. The obtained results suggest new avenues for the use of such an *in vitro* 3D model for studying brain (dys)function and for co-culturing neuronal cells towards the development of 'organ-on-chip' microsystems.

2.2 Three-Dimensional Micro-Electrode Arrays (3D-MEAs)

Over the past two decades, several studies have been devoted to the introduction of integrated microfabrication approaches for the development of *in-vitro* three-dimensional Micro-Electrode arrays (3D-MEAs).

Thiebaud and coworkers (Thiebaud et al. 1997 and 1999) reported one of the first approaches in this area. They showed fabrication, characterization and initial electrophysiological evaluation of a 3D MEA device consisting of 34 silicon nitride passivated protruding microelectrodes of total height 47 μm of which only the top 15 μm are exposed Pt-tips. They have further demonstrated the use of the MEA as a biosensor by recording the response of a toxin (picrotoxin) from hippocampal slices of rats.

In 2001 and 2002, Metz and co-authors (Metz et al. 2001) and Heuschkel and collaborators (Heuschkel et al. 2002) reported fabrication of 30-70 μm tall tip-shaped protruding microelectrodes in polyimide and glass respectively as shown in Figure 2.24. In the case of the polyimide devices, the electrodes are made of platinum and are constructed using anisotropic etching of silicon to create V-shaped sharp grooves and finally released by sacrificially etching the silicon away. Heuschkel and coworkers performed a comparison between the planar and 3D protruding electrode configuration by stimulation and recording from acute rat hippocampus slices. They simulated 2D and 3D microelectrodes and found that the signals from a 3D microelectrode are 2–3 times superior in magnitude than those from a 2D counterpart.

In another study (Nam et al. 2006), Heuschkel and co-authors extended the usefulness of such 3D tip MEAs to interface with dissociated neuronal cultures. Neural recording and stimulation were readily possible and the quality of the recorded signals was comparable to those from conventional 2D flat type electrodes with the advantage of reduced noise

level. They observed that many neurons grew directly on protruding electrode surface, appearing to make excellent contact. Moreover, a larger than usual portion of extracellular spikes had large positive peaks, while most of the spikes from conventional two-dimensional electrode arrays had large negative spikes.

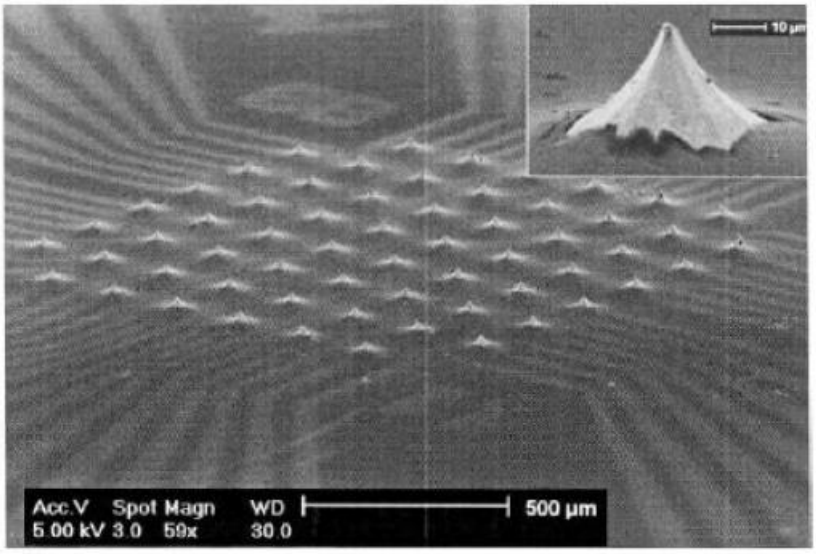

Figure 2.24. 3D tip-shaped electrodes fabricated by etching glass. Height of the electrodes is around 60 µm. (From Heuschkel et al. 2002).

Other integrated microfabrication approaches for *in-vitro* 3-D MEAs have been reported by Chu et al. (Chu et al. 2005) and Takei et al. (Takei et al. 2007). The features common to these fabrication approaches area: 1. The MEAs are all silicon-based devices. So the biocompatibility and cost-effectiveness are debatable; 2. These involve a combination of ICP, KOH or XeF_2 etching processes to create 3D electrodes in silicon. In the case of Takei et al., an exotic yet unproven technique to grow silicon tubes on a wafer by vapor-liquid-solid (VLS) technique is reported; 3. All these technologies provide electrodes that are less than 100 µm tall.

A different 3D-MEA microfabrication approach reported in literature has been proposed by Rajaraman and collaborators (Rajaraman et al. 2007). They employed a laser-scribing technique coupled with electroplating to fabricate 3D protruding towers array coupled with microfluidic ports for *in-vitro* neuronal cells and tissue slice interfacing (Rajaraman et al. 2007). A schematic illustration of the proposed 3D-MEA with metal traces to define the electrodes and a central fluidic port with neuronal culture all around the MEA is showed in Figure 2.25. Nutrients were flowing through the fluidic ports to keep cells alive

for longer periods of time. An excimer laser was used to define patterns in a polymer mold layer that is vapor-deposited on a 3D microfluidic SU-8 substrate. Metal is then electroplated through this mold to fabricate electrodes at multiple heights resulting in a multi-level electrode structure.

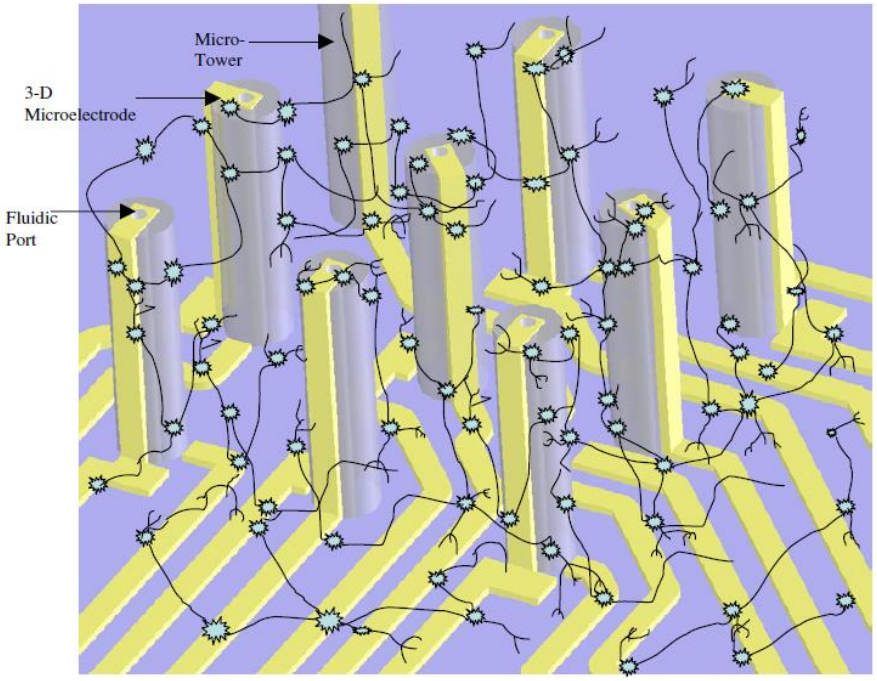

Figure 2.25. Conceptual view of the 3D coupled microelectrode, microfluidic array with neuronal culturing. (From Rajaraman et al. 2007).

An alternative approach with a similar goal was described by Musick and coworkers (Musick et al. 2009). They proposed electrically and fluidically active 3D-MEAs realized by stacking individually patterned thin films, each of which constitutes either an electrode to record and stimulate neurons or a fluidic layer used to load cells, nutrient delivery or waste removal. The electrode layers had a physical matrix to support neuronal growth and enable recording and stimulation of neurons.

In 2010, Charvet and coworkers (Charvet et al. 2010) showed a different approach for the fabrication of a new generation of compact and versatile 3D-MEA devices for both *in-vitro* and *in-vivo* recording and stimulation of large neural networks. They have developed a full modular 256-channel MEA system based on integrated electronics. They reported a specific technique based on the alternation of isotropic and non-isotropic etching steps to achieve high electrode aspect ratios and different shapes of tip electrodes. Figure 2.26 shows the high-density array of 3D tip-shaped microelectrodes.

The different shapes of the developed tip electrodes using alternations of isotropic and anisotropic etching processes are also reported in Figure 2.26.

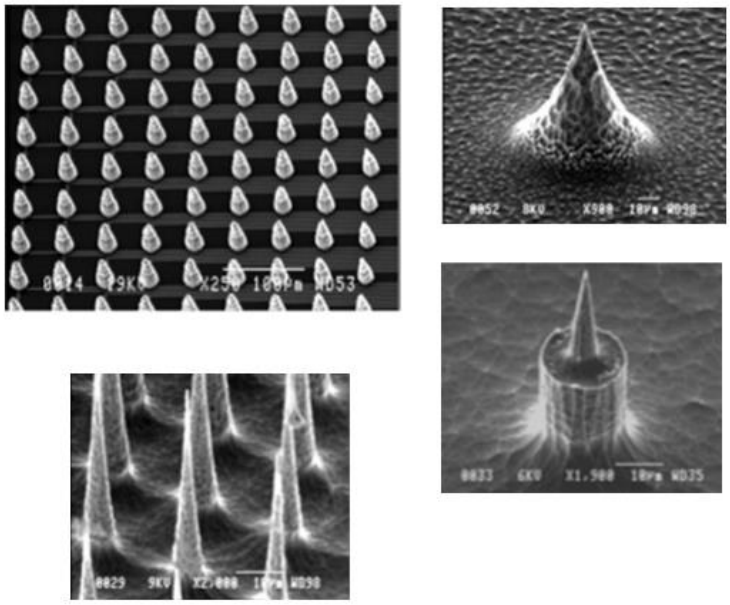

Figure 2.26. High-density arrays of 3D tip-shaped electrodes. 3D-tip electrodes were fabricated using alternations of isotropic and anisotropic etching approaches. Different shapes were achieved using different etching and mask parameters. (From Charvet et al. 2010).

In another study, Rajaraman and coworkers (Rajaraman et al. 2011) proposed a novel method based on Metal transfer micromolding (MTM) technology to achieve 3D-MEAs for use with *in-vitro* acute brain slices. Metal transfer micromolding was introduced as a manufacturing technology for producing nonplanar metallized patterned microelectromechanical-systems devices such as MEAs on polymeric substrates. Such technology provides a self-aligned metallization scheme that eliminates the need for complex 3D lithography and allows to fabricate MEAs on polymeric substrates.

The developed 3D-MEA devices were further packaged on glass substrates and insulated using parylene deposition. Recording sites were defined using laser micromachining and RIE etching. Figure 2.27 shows a schematic of such a device, with the closer inset depicting the electrode area.

The design chosen for the 3D MEA was a 5 × 5 array of metallized towers in the center of the chip and electrodes at the bottom of each tower (2-D counterparts).

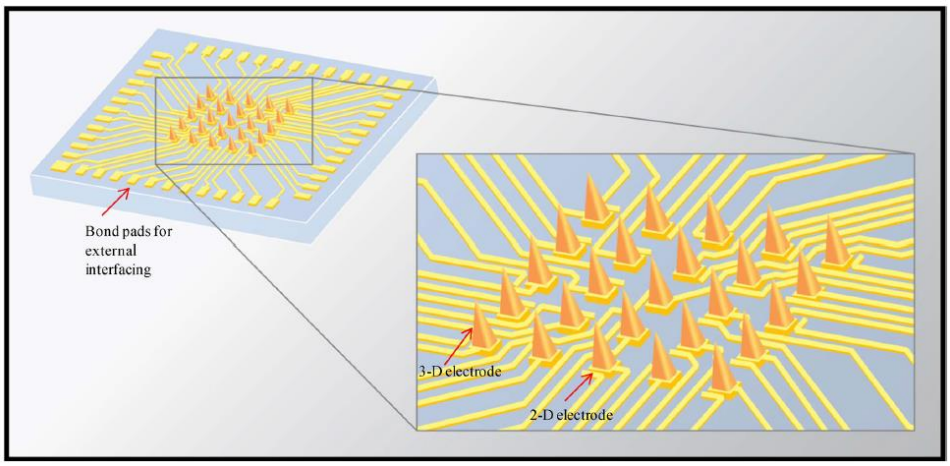

Figure 2.27. Schematic of the metal-transfer-micromolded 3D MEA. The inset on the right shows the electrode area with 25 metallized towers (3D electrodes) and 25 electrode traces (2D electrodes). (From Rajaraman et al. 2011).

In a more recent study, Lei Zuo and collaborators (Lei Zuo et al. 2017) reported a high-density multiple three-dimensional microelectrode arrays for stimulation and recording of extracellular neural signals of brain slices. They proposed a different way to better approach the neurons in the tissue slices for efficient neurons recording. The developed 3D-MEAs allowed to precisely position the individual electrodes by piezoelectric-based actuators to penetrate the inactive tissue layer and get closer to the active neurons so as to optimize the recording and stimulation of electrical field potentials.

2.2.1 3D Engineered Neuronal Networks coupled to 3D-MEAs: a new experimental model for *in-vitro* electrophysiology

In this section, I report the study and characterization of a new *in-vitro* experimental paradigm constituted by 3D engineered neuronal networks coupled to innovative 3D-MEAs devices. The advantage of such a model is clearly its improved representation of the actual *in-vivo* environment while maintaining some of the advantages (controllability, observability) of *in-vitro* systems.

In this work, I performed electrophysiological spontaneous activity characterization of 3D engineered hippocampal neuronal networks coupled to innovative 3D-MEAs (i.e. devices constituted by 3D gold ball-shaped microelectrodes positioned at different heights). I characterized first the electrical properties of such devices (i.e., impedance) and then I used the 3D-MEA to record the spontaneous activity of 3D neuronal networks at different days of development.

Moreover, I estimated the functional connectivity within and between different layers of the 3D neuronal structure to prove and point out actual functional inter- and intra-level connections in the 3D neuronal network.

The three-dimensional Micro-Electrode Arrays (3D-MEAs) used in this work is composed of 60 gold ball-shaped microstructures positioned at different heights (diameter of a single ball = 50 µm). Each gold ball-shaped microelectrode corresponds to a different level of the 3D chip (i.e. planar, 50-µm-, 100-µm- and 150-µm-high level).

A PMMA (Poly(methyl methacrylate)) thin-film was used as passivation layer to isolate and passivate the microstructures sidewalls and conductive tracks of the 3D chips from the direct contact of the active cells. Thus, the only conductive part of the device exposed to the direct contact of living neurons is the top side of such ball-shaped microelectrodes. Therefore, recordings from *in-vitro* neuronal cell cultures were performed only from the tip of the ball-shaped microstructures.

Figure 2.28 (A) shows an overview of the complete, assembled and packaged 3D-MEA device. The overall dimension of the PCB was designed to be 49 mm × 49 mm to comply with the standard holder of the Multichannel System acquisition setup (MEA 2100, MCS, Reutlingen, Germany).

In Figure 2.28 (B), an overview of the 3D-MEA layout is shown. It is possible to observe four counter electrodes (exposed area = 0.68 mm^2) positioned at the four corners of the recording area of the electrodes. The bold black circle positioned at the center of the 3D-MEA layout represents the reference electrode (exposed area radius = 340 µm). An enlargement of the electrodes recording area with the correspondences electrode-level of the 3D neuronal structure is reported in Figure 2.29 (A).

Moreover, by looking at Figure 2.29 (B), it is possible to observe a rendering 3D of the max projection of a single electrode of about 150-µm-high.

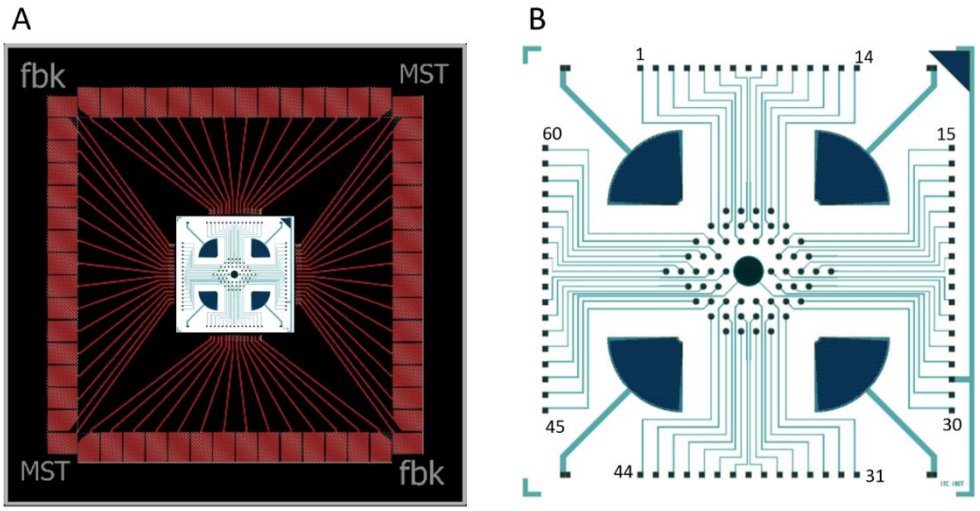

Figure 2.28. (A). Overview of the complete and packaged 3D-MEA device. We can clearly see the MEA at the center, the conductive tracks, and the PCB macropads for external electronics interfacing. (B). Overview of the 3D-MEA layout.

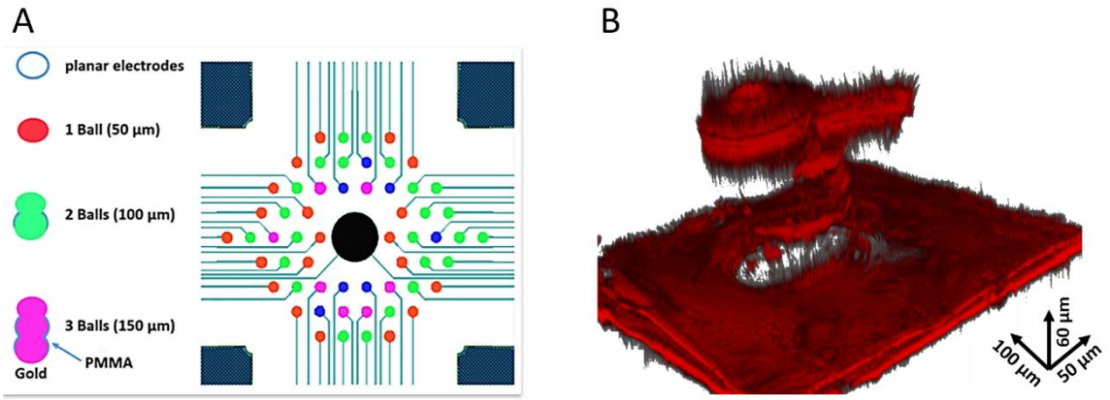

Figure 2.29. (A). Enlargement of the 3D-MEA layout where each electrode corresponds to a different level (n=4) of the 3D ball-shaped MEAs. Blue (n=7), red (n=20), green (n=24) and purple (n=7) electrodes correspond to the planar, first (50 µm), second (100 µm) and third (150 µm) layer of the 3D neuronal structure, respectively. (B). Confocal image that shows rendering 3D of the max projection of a single electrode (h=150 µm).

As first step, I performed an electrical characterization of such 3D-MEAs in order to estimate the electrical properties of the fabricated 3D chips. Electrochemical impedance spectroscopy (EIS) based-experimental set-up was used to carry out impedance measurements of the electrodes. A schematic of the impedance measurement experimental set-up employed in this work is shown in Figure 2.30. Such experimental set-up was based on a dual phase lock-in amplifier (SIGNAL RECOVERY Model 5110) connected to an external function generator (HP 33120A) and an Ag/AgCl reference electrode used to complete the circuit and collect the current which flows through the electrochemical cell.

To measure the impedance, the waveform generator was used to apply a small amplitude (5-15 mV) sinusoidal perturbation of a given frequency to the working/excitation microelectrode under investigation and the dual phase lock-in amplifier was used to measure the resulting AC current which flows through the device. Especially, the lock-in amplifier translates the collected current to a voltage by the integrated transimpedance amplifier and then demodulates the voltage into the in-phase ($V_{OUT,I}$) and quadrature ($V_{OUT,Q}$) components. Magnitude of the impedance was then calculated from the so obtained real and imaginary part.

Measures were performed between the excitation microelectrode under test, the Ag/AgCl reference electrode and the conducting media (Phosphate-buffered saline solution (PBS)). The process was repeated for seven selected microelectrodes of each level of a 3D chip and by sweeping the frequency from 10 Hz to 10 kHz to compute impedance at each frequency value.

Figure 2.31 shows the measured impedance magnitude values as function of the frequency for a 3D ball-shaped gold MEA evaluated over each level of such 3D device. It is possible to observe that the impedance magnitude decreases as the frequency of the AC input signal increases. The impedance values of each level ranges from a few mega ohms at low frequency (10 Hz) to a few kilo ohms at higher frequency (10 kHz).

Each data point of the curves represents mean and standard error of the mean evaluated over seven selected microelectrodes of each level of the 3D-MEA under test.

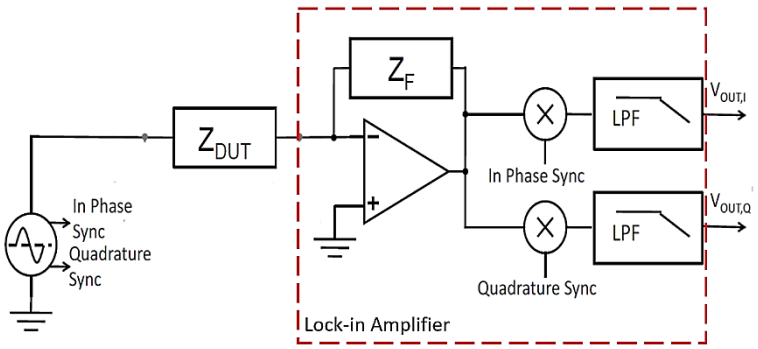

Figure 2.30. Impedance measurement scheme using lock-in amplifier with integrated transimpedance amplifier. Z_{DUT} represents the unknown impedance of the electrode under test. Z_F is the feedback impedance of the current to voltage converter.

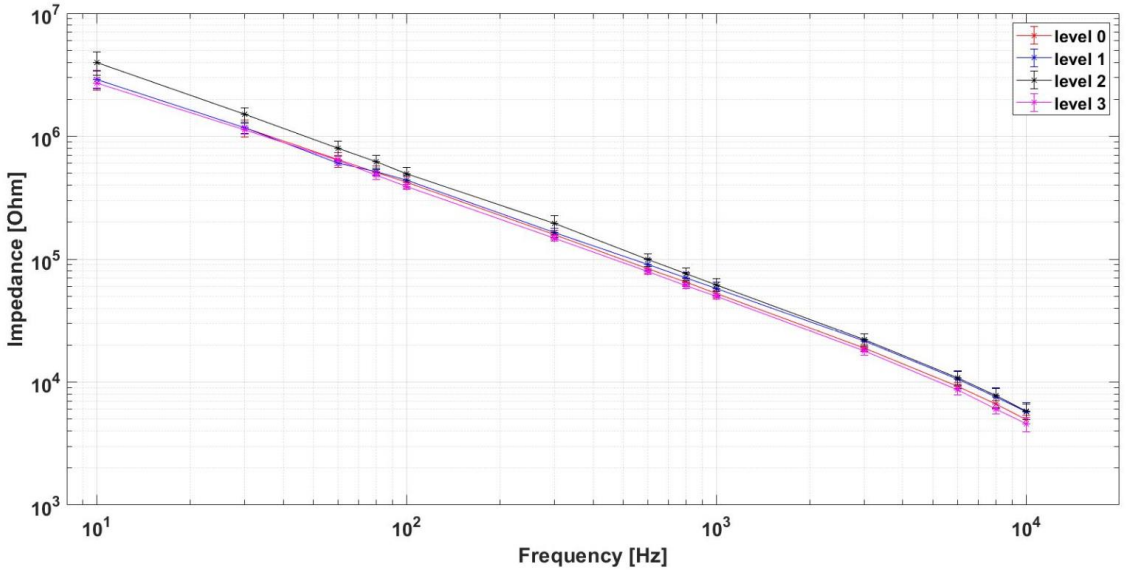

Figure 2.31. Measured impedance values versus frequency for a 3D-MEA chip evaluated over each level (n=4) of the 3D device in a PBS (Phosphate buffered Saline) solution. A 10 mV, [10-10000] Hz AC voltage signal was applied to the electrodes during the measurements. Each data point of the curves represents mean and standard error of the mean evaluated over seven selected microelectrodes of each level of the 3D chip under test.

Once the electrical properties of the ball-shaped 3D-MEAs have been evaluated, I performed spontaneous electrophysiological activity recordings of 3D hippocampal neuronal networks assembled onto glass microbeads-based scaffold at 15 and 19 days *in vitro* (DIVs) by means of such 3D-MEAs, previously described, and fabricated at the Bruno Kessler Foundation (FBK, Trento, Italy).

The electrophysiological activity was acquired with the 2100 System (MEA 2100-System, MCS), and signals were sampled at 10 kHz. Recordings were performed for 30 min outside the incubator at a temperature of 37°C. To prevent evaporation and changes of the pH medium, a slow flow of humidified gas (5% CO_2) was constantly delivered during sessions into a small plastic box covering the experimental MEA setup.

The 3D neuronal construct, made up of 3D hippocampal neuronal network grown onto glass microbeads-based scaffold, was developed and implemented by following the same approach described by Frega and coworkers (Frega et al. 2014).

In Figure 2.32 (A), a zoom of a small portion of the 3D culture with neurons embedding the microbeads is presented to highlight the ability of the culture to form a dense network of neurites embedding the self-assembled microbeads. Such ability of the 3D culture is further stressed in Figure 2.32 (B), where the neuronal network is able to growth and spread on and around the top side of a 3D ball-shaped microelectrode (white arrow) allowing good measurement conditions.

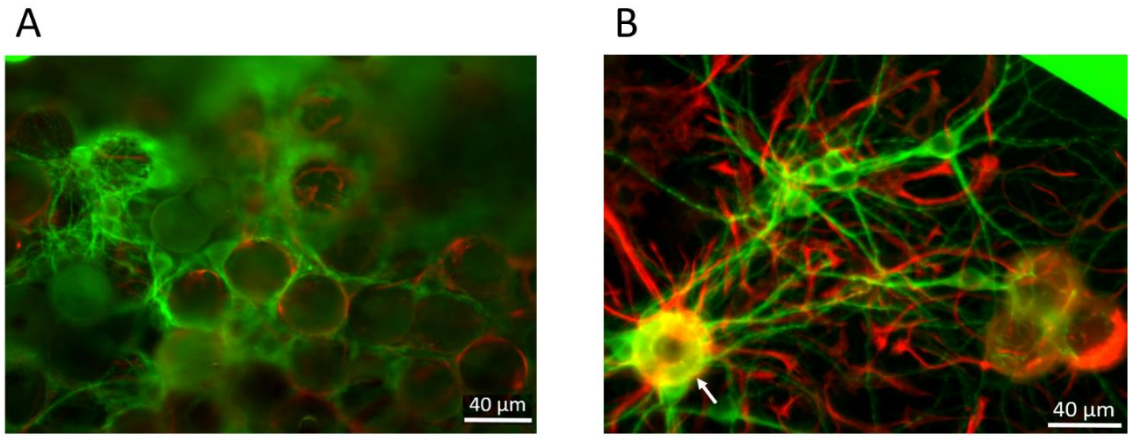

Figure 2.32. Immunofluorescence of 3D hippocampal neuronal culture grown on (A) 3D self-assembled glass microbeads and (B) top side of a 3D ball-shaped microelectrode (white arrow) at DIV19 where green color represents the MAP-2 dendritic protein and the red color represents GFAP intermediate filament of glia cells. Scale bar: 40 µm.

Regarding the data analysis, I used a custom software package named SpyCode (Bologna et al. 2010) developed in MATLAB (The Mathworks, Natick, MA, USA). The acquired raw signals were peak detected by means of the threshold-based precise timing spike detection (PTSD) algorithm (Maccione et al. 2009). Burst detection was performed according to the method described in (Pasquale et al. 2010). A burst is a sequence of spikes having an ISI (inter-spike interval, i.e., time intervals between consecutive spikes) smaller than a reference value (set at 100 ms in the experiments), and containing at least a minimum number of consecutive spikes (set at 5 spikes).

To quantify the network dynamics properties, from the obtained spike trains, the following metrics have been computed: mean firing and bursting rate (MFR, MBR). Data were expressed as mean ± standard error of the mean.

Statistical analysis was then performed to determine significant differences between each sample pairs by using MATLAB. Since data do not follow a normal distribution (evaluated by the Kolmogorov-Smirnov normality test), I performed a non-parametric Mann-Whitney U-test.

Finally, by applying a cross-correlation algorithm recently developed and implemented in the software package SpiCodyn (Pastore et al. 2018), I estimated the functional connectivity to prove inter- and intra-level connections and thus actual functional interactions within and between each layer of the 3D neuronal network structure. Figure 2.33 (A) shows 2 min of spontaneous electrophysiological activity of a representative experiment of a 3D hippocampal neuronal network at DIV 15.

For the sake of clarity, the activity recorded from the planar, 50 µm-, 100 µm- and 150 µm-high 3D ball-shaped microelectrodes is reported in blue, red, green and violet, respectively. In this way, it is possible to observe and understand how the network dynamics changes in different layers of the 3D structure. Especially, at this day of the development, I found a network dynamics composed mainly of a mean percentage of random spikes (i.e. the fraction of spikes outside bursts) of about 20 % in correspondence of each level of the 3D neuronal structure.

Similarly, Figure 2.33 (B) shows a raster plot of the spontaneous activity of a representative experiment of the same 3D culture at DIV 19. In this case, it can be noticed that the signature of the network dynamics presents a wide repertoire of activities characterized of both synchronous bursts and random spikes at the single channel-neuron level.

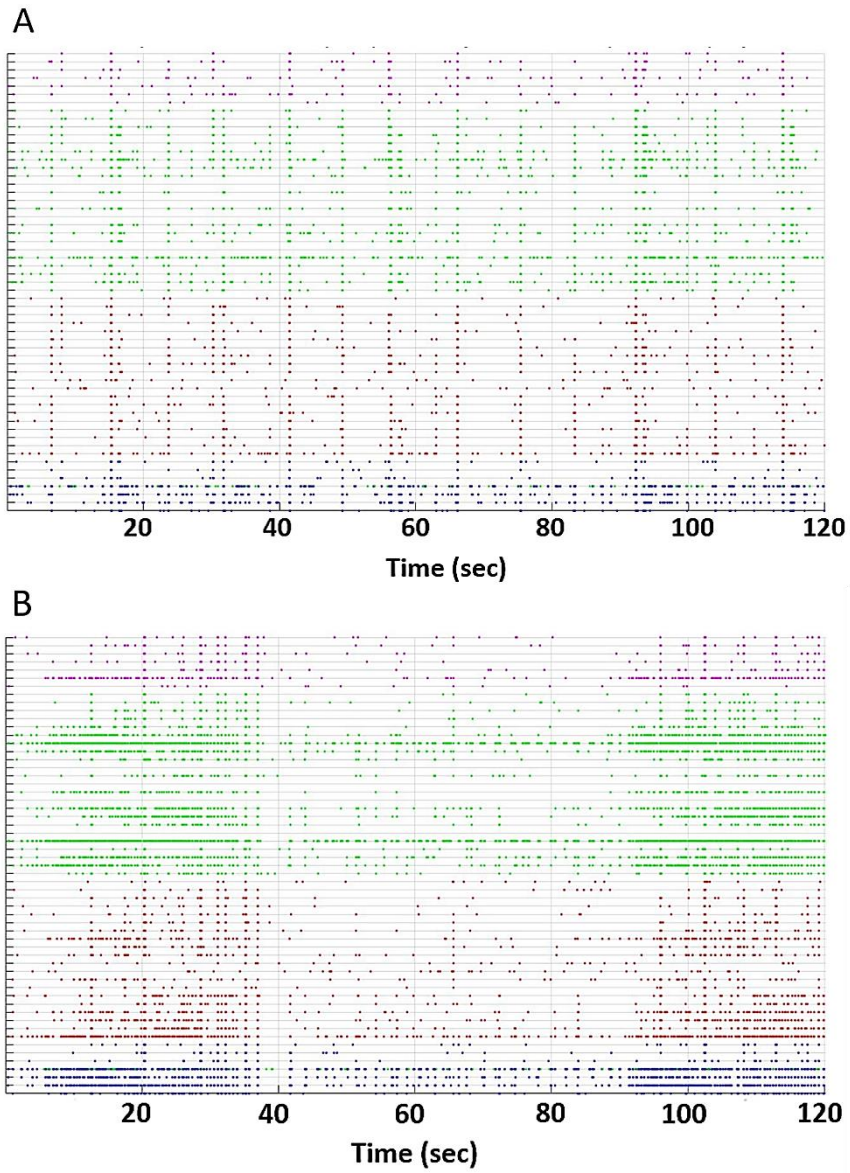

Figure 2.33. (A) and (B) raster plot showing 120 s of spontaneous activity of 3D hippocampal neuronal network on glass microbeads at DIV 15 and DIV 19, respectively; blue, red, green and violet color refers to the activity recorded from the planar, first, second and third layer of the 3D structure, respectively.

I also evaluated the mean firing and bursting rate, the mean burst duration and percentage of random spikes in all (n=3) the performed experiments at DIV 19 of development. Regarding the frequency of firing, I observed a higher level of MFR in correspondence of the planar and second layer of the 3D neuronal structure than the first and third ones (Figure 2.34 (A)). Specifically, in correspondence of the second layer, there are MFR values statistically different ($p < 0.001$) from those recorded in the other ones. Regarding the bursting behavior, the MBR values detected in the second layer are significantly higher ($p < 0.001$) with respect to the other ones (Figure 2.34 (B)). Instead, the duration of bursts is similar for all the four levels of the 3D neuronal structure (250 ± 40 ms). Regarding the percentage of random spikes, it is possible to notice no significant differences between each layer.

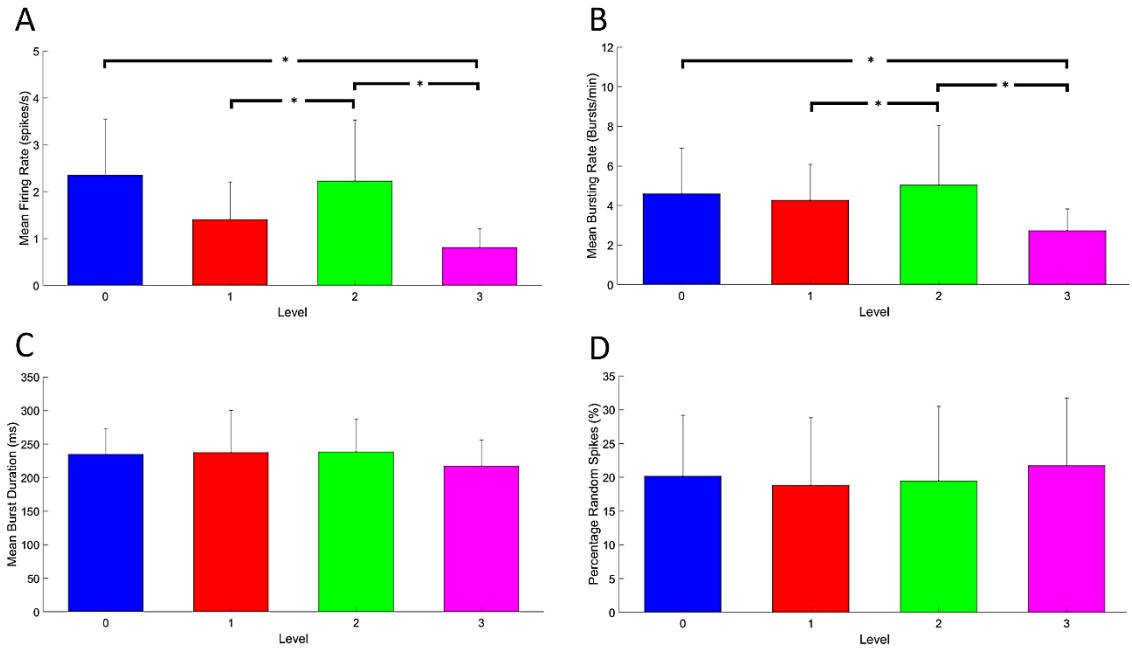

Figure 2.34. (A) Mean Firing Rate, (B) Mean Bursting Rate, (C) Mean Burst Duration and (D) Percentage of Random Spikes evaluated over each layer of a representative 3D hippocampal neuronal network. (Mann-Whitney U-test, * $P_{VALUE} \leq 10^{-3}$).

Finally, I estimated the functional connectivity within and between the four levels of the 3D neuronal network structure by means of a cross-correlation algorithm recently developed and implemented in the software package SpiCoDyn (Pastore et al. 2018). From the adjacency matrix (i.e., connectivity), I discarded (thresholding procedure) the noisier and weaker connections and I quantified the inter- and intra-level connectivity links.

Figure 2.35 (A) shows the percentage of links intra- and inter-levels of one representative experiment. As previously stated (cf., caption of Figure 2.29), the first and second layer contain a larger number of electrodes than the other ones. Thus, I expected a much higher level of interconnectivity (about 29 %) between the first and second layer than other inter- and intra-connectivity.

Moreover, I also quantified the delay values of the signal propagation within and between the four layers of a representative 3D hippocampal neuronal network grown onto glass microbeads-based scaffold.

Especially, I studied and analyzed the mean timing (i.e. delay) that the signal needs to propagate from one electrode of a level (e.g. level 0) to another one belonging to the same level (level 0) or to a different level (e.g. level 1).

In Figure 2.35 (B) and (C), I reported the intra- and inter-level delay values of the propagation of the signal, respectively. As it is expected, there are no differences between the mean intra-level delay values; instead, regarding the signal propagation delay between each layer of the 3D neuronal structure, it is possible to notice that the mean delay between the planar and third level is higher than the one between the planar and first and between the planar and second. Furthermore, at the same time, the timing the signal needs to propagate from the first level to the last level of the 3D structure is higher than the one between the first and second and between the second and third.

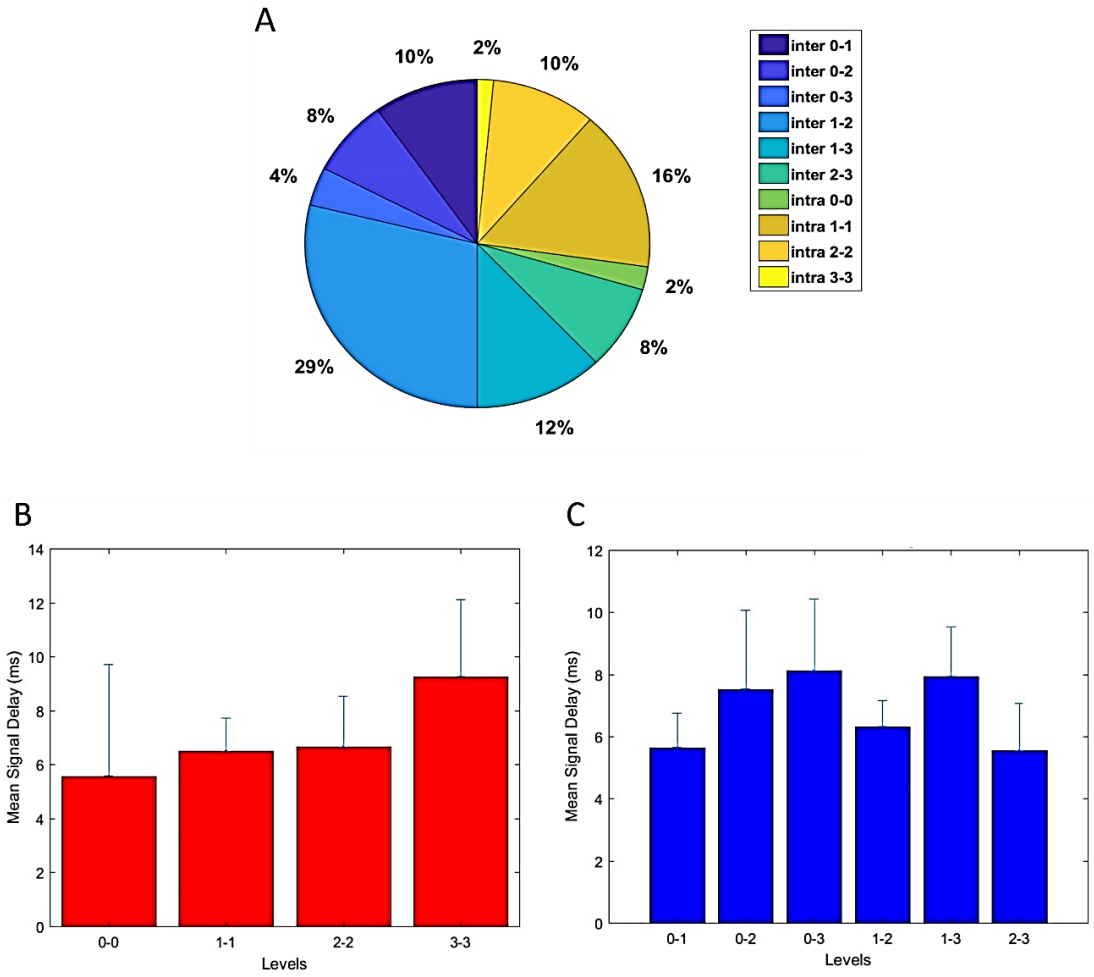

Figure 2.35. (A) Percentage of links intra- and inter-level of a 3D hippocampal neuronal network evaluated during one representative experiment. (B) and (C) mean intra- and inter-level delay values of the signal propagation in a representative 3D hippocampal neuronal network, respectively.

In summary, the new developed experimental platform constituted by 3D engineered neuronal networks coupled to 3D-MEAs represents a complete 3D-3D *in-vitro* neuronal system. This model allows to record the electrophysiological activity of the 3D neuronal network from different locations in the 3D space and to study how the network dynamics changes in different layers of the 3D structure. Such a system can be considered a more physiological model of a real brain structure and it could be further engineered to constitute bio-hybrid microsystems towards the development of brain-on-a-chip for neurophysiological investigations. Moreover, it could be used as an operational platform to study brain pathology or pharmacological treatments.

References

Anitha A., et al. (2014). Chitin and chitosan in selected biomedical applications. *Prog. Polym. Sci*, vol. 39, no. 9, pp. 1644-1667.

Borkholder D.A. (1998). Cell Based Biosensors using Microelectrodes. *Department of Electrical Engineering, Stanford University, Palo Alto, CA.*

Bonifazi P., Ruaro M. E., et al. (2005). Statistical properties of information processing in neuronal networks. *Eur J Neurosci*, vol. 22, no. 11, pp. 2953-2964.

Brewer G. J., Boehler M. D., et al. (2009). Neuron network activity scales exponentially with synapse density. *J Neural Eng,* 6(1): 014001.

Berdondini, L., Imfeld K., et al. (2009). Active pixel sensor array for high spatio-temporal resolution electrophysiological recordings from single cell to large scale neuronal networks. *Lab on a chip*, vol. 9, no. 18, pp. 2644-51.

Berdondini L., Massobrio P., et al. (2009). Extracellular recordings from locally dense microelectrode arrays coupled to dissociated cortical cultures. *Journal of Neuroscience Methods*, vol. 177 no. 2, pp. 386-96.

Bologna L. L., Pasquale V., Garofalo M., Gandolfo M., Baljon P. L., Maccione A., Martinoia S., and Chiappalone M. (2010). Investigating neuronal activity by SPYCODE multi-channel data analyzer, *Neural Netw,* vol. 23, pp. 685-97.

Bosi S., Rauti R., Laishram J., Turco A., Lonardoni D., Nieus T., Prato M., Scaini D., and Ballerini L. (2015). From 2D to 3D: novel nanostructured scaffolds to investigate signalling in reconstructed neuronal networks. *Sci Rep*, 24;5:9562.

Broguiere N., Isenmann L., Zenobi-Wong M. (2016). Novel enzymatically cross-linked hyaluronan hydrogels support the formation of 3D neuronal networks. *Biomaterials*, vol. 99, pp. 47-55.

Chu H.-Y., Kuo T.-Y., Chang B., Lu S.-W., Chiao C.-C., and Fang W. (2005). Development of the Three Demensional Multi-Electrode Array for Neural Interfacing. *Solid-State Sensors, Actuators and Microsystems, 2005. Digest of Technical Papers. TRANSDUCERS '05. The 13th International Conference on, IEEE,* pp. 1804-1807.

Chiappalone M., Bove M., et al. (2006). Dissociated cortical networks show spontaneously correlated activity patterns during in vitro development. *Brain Research*, vol. 1093, no.1, pp. 41-53.

Charvet G., Rousseau L., Billoint O., Gharbi S., Rostaing J.-P., Joucla S., Trevisiol M., Bourgerette A., Chauvet P., Moulin C., Goy FB., Mercier B., Colin M., Spirkovitch S., Fanet H., Meyrand P., Guillemaud R., Yvert B. (2010). BioMEA^{TM}: A versatile high-density 3D microelectrode array system using integrated electronics. *Biosensors and Bioelectronics*, vol. 25: 1889–1896.

Cullen D. K., Wolf J. A., et al. (2011). Neural tissue engineering and biohybridized microsystems for neurobiological investigation in vitro (Part 1). *Critical reviews in biomedical engineering*, vol. 39, no. 3, pp. 201-40.

DeBusschere B.D., and Kovacs G.T.A. (2001). Portable cell-based biosensor system using integrated CMOS cell-cartridges. *Biosensors and Bioelectronics,* vol. 16, pp. 543-556.

Eytan D., and Marom S. (2006). Dynamics and effective topology underlying synchronization in networks of cortical neurons. *J Neurosci*, vol. 26, no. 33, pp. 8465-8476.

Franks W., Heer F., McKay I., Taschini S., Sunier R., Hagleitner C., Hierlemann A., and Baltes H. (2003). CMOS monolithic microelectrode array for stimulation and recording of natural neural networks. *TRANSDUCERS, Solid-State Sensors, Actuators and Microsystems, 12th International Conference on,* pp. 963-966.

Frey U., Sanchez-Bustamante C. D., et al. (2007). Cell recordings with a CMOS high-density microelectrode array. *Conf Proc IEEE Eng Med Biol Soc*, pp. 167-70.

Frampton J.P., et al. (2011). Fabrication and optimization of alginate hydrogel constructs for use in 3D neural cell culture. *Biomed. Mater* 6 (1), 015002.

Frega M., Tedesco M., Massobrio P., Pesce M., and Martinoia S. (2014). Network dynamics of 3D engineered neuronal cultures: a new experimental model for in-vitro electrophysiology. *Scientific Reports 4*, Article number: 5489.

Gross G.W., Rieske E., Kreutzberg G.W., and Meyer A. (1977). A new fixed-array multi-microelectrode system designed for long-term monitoring of extracellular single unit neuronal activity in vitro. *Neuroscience Letters,* vol. 6, no. 2-3, pp. 101-105.

Gross G.W. (1979). Simultaneous single unit recording in vitro with a photoetched laser deinsulated gold multimicroelectrode array. *IEEE Trans. Biomed. Eng.,* vol. BME-26, no. 5, pp. 273-279.

Gandolfo M., Maccione A., et al. (2010). Tracking burst patterns in hippocampal cultures with high-density CMOS-MEAs. *Journal of Neural Engineering,* 7(5): 056001.

Heuschkel M.O., Fejtl M., Raggenbass M., Bertrand D., and Renaud P. (2002). A three-dimensional multi-electrode array for multi-site stimulation and recording in acute brain slices. *Journal of Neuroscience Methods,* vol. 114, no. 2, pp. 135-148.

Heer F., Hafizovic S., Franks W., Blau A., Ziegler C., and Hierlemann A. (2006). *CMOS microelectrode array for bidirectional interaction with neuronal networks. IEEE Journal of Solid-State Circuits,* vol. 41, no. 7, pp. 1620-1629.

Huang C., et al. (2016). The migration and differentiation of hUC-MSCs(CXCR4/GFP) encapsulated in BDNF/chitosan scaffolds for brain tissue engineering. *Biomed. Mater,* 11 (3) 035004.

Irons H. R., Cullen D. K., et al. (2008). Three-dimensional neural constructs: a novel platform for neurophysiological investigation. *J Neural Eng,* vol. 5, no 3, pp. 333-41.

Kanagasabapathi T. T., Ciliberti D., Martinoia S., Wadman W. J., and Decre M. M. J. (2011). Dual compartment neurofluidic system for electrophysiological measurements in physically segregated and functionally connected neuronal cell culture. *Frontiers in Neuroengineering,* vol. 4.

Kanagasabapathi T. T., Massobrio P., Barone R. A., Tedesco M., Martinoia S., Wadman W. J., *et al.* (2012). Functional connectivity and dynamics of cortical-thalamic networks co-cultured in a dual compartment device. *Journal of Neural Engineering,* vol. 9.

Lozano R., et al. (2015). 3D printing of layered brain-like structures using peptide modified gellan gum substrates. *Biomaterials,* vol. 67, pp. 264-273.

Janders M., Egert U., Stelzle M., and Nisch W. (1996). Novel thin film titanium nitride micro-electrodes with excellent charge transfer capability for cell stimulation and sensing applications. *Engineering in Medicine and Biology Society. Bridging Disciplines for Biomedicine. Proceedings of the 18th Annual International Conference of the IEEE,* pp. 245-247.

Kim D., Kim S.-M., Lee S., and Yoon M.-H. (2017). Investigation of neuronal pathfinding and construction of artificial neuronal networks on 3D-arranged porous fibrillary scaffolds with controlled geometry. *Scientific Reports,* volume 7, Article number: 7716.

May G.A., Shamma S.A., and White R.L. (1979). A tantalum-on-sapphire microelectrode array. *Electron Devices, IEEE Transactions on,* vol. 26, no. 12, pp. 1932-1939.

Maher M.P., Pine J., Wright J., and Tai Y.C. (1999). The neurochip: a new multielectrode device for stimulating and recording from cultured neurons. *Journal of Neuroscience Methods,* vol. 87, no. 1, pp. 45-56.

Metz S., Heuschkel M.O., Valencia Avila B., Holzer R., Bertrand D., and Renaud P. (2001). Microelectrodes with Three-Dimensional Structures for Improved Neural Interfacing. *Proc. of 23rd Annual EMBS Intr. Conf., IEEE,* pp. 765-768.

Marom S. and Shahaf G. (2002). Development, learning and memory in large random networks of cortical neurons: lessons beyond anatomy. *Quarterly Reviews of Biophysics,* vol. 35, no. 1, pp. 63-87.

Mahoney M.J., Anseth K.S. (2006). Three-dimensional growth and function of neural tissue in degradable polyethylene glycol hydrogels. *Biomaterials,* vol. 27, no. 10, pp. 2265-2274.

Macis E., Tedesco M., et al. (2007). An automated microdrop delivery system for neuronal network patterning on microelectrode arrays. *J Neurosci Methods,* vol. 161, no. 1, pp. 88-95.

Musick K., Khatami D., and Wheeler B. C. (2009). Three-dimensional micro-electrode array for recording dissociated neuronal cultures. *Lab Chip,* 9(14): 2036.

Maccione A., Gandolfo M., Massobrio P., Novellino A., Martinoia S., and Chiappalone M. (2009). A novel algorithm for precise identification of spikes in extracellularly recorded neuronal signals. *Journal of Neuroscience Methods,* vol. 177, pp. 241-249.

Marconi E., Nieus T., et al. (2012). Emergent functional properties of neuronal networks with controlled topology. *PLoS One,* 7(4): e34648.

Müller J., Ballini M., Livi P., Chen Y., Radivojevic M., Shadmani A., Viswam V., Jones I. L., Fiscella M., Diggelmann R., Stettler A., Frey U., Bakkum D. J., and Hierlemann A. (2015). High-resolution CMOS MEA platform to study neurons at subcellular, cellular, and network levels. *Lab Chip,* vol. 15, no. 13, pp. 2767-2780.

Magin C.M., Alge D.L., Anseth K.S. (2016). Bio-inspired 3D microenvironments: a new dimension in tissue engineering. *Biomed. Mater,* 11 (2), 022001.

Novak J.L., and Wheeler B.C. (1986). Recording from the Aplysia Abdominal-Ganglion with a Planar Microelectrode Array. *IEEE Transactions on Biomedical Engineering,* vol. 33, no. 2, pp. 196-202.

Nisch W., Bock J., Egert U., Haemmerle H., and Mohr A. (1994). A thin film microelectrode array for monitoring extracellular neuronal activity in vitro. *Biosensors and Bioelectronics,* vol. 9, pp. 737-741.

Nam Y., Wheeler B. C., Heuschkel M. O. (2006). Neural recording and stimulation of dissociated hippocampal cultures using microfabricated three-dimensional tip electrode array. *Journal of Neuroscience Methods,* vol. 155, pp. 296–299.

Pine J. (1980). Recording Action Potentials from Cultured Neurons with Extracellular Microcircuit Electrodes. *Journal of Neuroscience Methods,* vol. 2, pp. 19-31.

Pautot S., Wyart C., et al. (2008). Colloid-guided assembly of oriented 3D neuronal networks. *Nature Methods,* 5(8): 735-740.

Pasquale V., Massobrio P., et al. (2008). Self-organization and neuronal avalanches in networks of dissociated cortical neurons. *Neuroscience,* vol. 153, no. 4, pp. 1354-1369.

Pasquale V., Martinoia S., Chiappalone M. (2010). A self-adapting approach for the detection of bursts and network bursts in neuronal cultures. *J. Comput. Neurosci,* vol. 29, no. 1, pp. 213-229.

Pan L., Alagapan S., Franca E., Leondopulos S., DeMarse T.B., and Wheeler B. C. (2015). An *in vitro* method to manipulate the direction and functional strength between neural populations. *Frontiers in Neural Circuits,* vol. 9.

Pastore V. P., Poli D., Godjoski A., Martinoia S., and Massobrio P. (2016). ToolConnect: a functional connectivity toolbox for *in vitro* networks. *Frontiers in Neuroinformatics,* vol. 10.

Pastore V.P., Godjoski A., Martinoia S., Massobrio P. (2018). SPICODYN: A Toolbox for the Analysis of Neuronal Network Dynamics and Connectivity from Multi-Site Spike Signal Recordings. *Neuroinformatics,* vol. 16, no. 1, pp. 15-30.

Rolston J. D., Wagenaar D. A., et al. (2007). Precisely timed spatiotemporal patterns of neural activity in dissociated cortical cultures. *Neuroscience,* vol. 148, no. 1, pp. 294-303.

Rajaraman S., Choi S.-O., Shafer R., Ross J. D., Vukasinovic J., Choi Y., DeWeerth S. P., Glezer A., and Allen M. G.. (2007). Microfabrication technologies for a coupled three-dimensional microelectrode, microfluidic array. *J. Micromech. Microeng,* vol. 17, pp. 163–171.

Rajaraman S., Choi S.O., McClain M. A., Ross J. D., LaPlaca M. C., and Allen M. G. (2011). Metal-Transfer-Micromolded Three-Dimensional Microelectrode Arrays for *in-vitro* Brain-Slice Recordings. Journal of Microelectromechanical systems, vol. 20, no. 2.

Streit J., Tscherter A., et al. (2001). The generation of rhythmic activity in dissociated cultures of rat spinal cord. *Eur J Neurosci,* vol. 14, no. 2, pp. 191-202.

Stett A., Egert U., Guenther E., Hofmann F., Meyer T., Nisch W., and Haemmerle H. (2003). Biological application of microelectrode arrays in drug discovery and basic research. *Analytical and Bioanalytical Chemistry,* vol. 377, no. 3, pp. 486-495.

Thomas C. A., Springer P. A., et al. (1972). A miniature microelectrode array to monitor the bioelectric activity of cultured cells. *Exp Cell Res*, vol. 74, no. 1, pp. 61-6.

Tatic-Lucic S., Tai Y.-C., Wright J.A., and Pine J. (1994). Silicon-Micromachined Cultured Neuron Probes for In Vivo Studies of Neural Networks. *Proc. of ASME winter Annual Meeting, ASME*.

Thiebaud P., DeRooij N.F., KoudelkaHep M., and Stoppini L. (1997). Microelectrode arrays for electrophysiological monitoring of hippocampal organotypic slice cultures. *IEEE Transactions on Biomedical Engineering*, vol. 44, no. 11, pp. 1159-1163.

Thiebaud P., Beuret C., Koudelka-Hep M., Bove M., Martinoia S., Grattarola M., Jahnsen H., Rebaudo R., Balestrino M., Zimmer J., and Dupont Y. (1999). An array of Pt-tip microelectrodes for extracellular monitoring of activity of brain slices. *Biosensors & Bioelectronics*, vol. 14, no. 1, pp. 61-65.

Tscherter A., Heuschkel M. O., et al. (2001). Spatiotemporal characterization of rhythmic activity in rat spinal cord slice cultures. *Eur J Neurosci*, vol. 14, no. 2, pp. 179-90.

Takei K., Kawashima T., Takao H., Sawada K., and Ishida M. (2007). Si Micro Probe and SiO_2 Micro Tube Array with NMOSFETs. *Transducers 2007: The 14th International Conference on Solid-State Sensors, Actuators and Microsystems IEEE*, pp. 1381-1384.

Tibbitt M.W., Anseth K.S. (2009). Hydrogels as extracellular matrix mimics for 3D cell culture. *Biotechnol. Bioeng*, vol. 103, no. 4, pp. 655-663.

Tedesco M.T., Di Lisa D., Massobrio P., Colistra N., Pesce M., Catelani T., Dellacasa E., Raiteri R., Martinoia S., Pastorino L. (2018). Soft chitosan microbeads scaffold for 3D functional neuronal networks. Biomaterials, vol. 156, pp. 159-171.

Wagenaar D. A., Madhavan R., et al. (2005). Controlling bursting in cortical cultures with closed-loop multi-electrode stimulation. *The Journal of Neuroscience*, vol. 25, no. 3, pp. 680-688.

Wagenaar D. A., Nadasdy Z., et al. (2006). Persistent dynamic attractors in activity patterns of cultured neuronal networks. *Phys Rev E Stat Nonlin Soft Matter Phys*, 73(5 Pt 1): 051907.

Williamson A., Singh S., Fernekorn U., and Schober A. (2013). The future of the patient-specific Body-on-a-chip. *Lab on a Chip*, vol. 13.

Zuo L., Yu S., Briggs C.A., Kantor S., Pan J.Y. (2017). Design and Fabrication of a Three-Dimensional Multi-Electrode Array for Neuron Electrophysiology. *Journal of Biomechanical Engineering*, 139(12):121011.

Chapter 3

A NEW PILLAR-SHAPED GOLD 3D-MEA FOR *IN-VITRO* ELECTROPHYSIOLOGICAL RECORDINGS

In this chapter, I report the design, microfabrication, characterization and experimental validation of an innovative and truly 3D pillar-shaped gold Micro-Electrode Array (3D-MEA) designed and developed in IBM Almaden Research Center (San Jose, CA, USA) for *in-vitro* electrophysiological applications. The capability of the fabricated 3D-MEAs to record spontaneous activity from 3D engineered neuronal cultures and both 4-AP-induced epileptiform-like and electrically-evoked activity from mouse cortico-hippocampal brain slices is successfully demonstrated.

3.1 Introduction

Microelectrode arrays (MEAs) represent a powerful and popular tool to study single neurons and functional organization of neuronal networks and brain slices. As previously stated at the beginning of section 2.1, several multi-electrode array devices integrating planar (2D) metal electrodes were designed and fabricated in the past 35 years for extracellular stimulation and recording from cultured neuronal cells and organotypic brain slices.

In the last years, several studies have been devoted to the introduction of new *in-vitro* experimental models constituted of 3D engineered neuronal networks coupled to 2D-MEAs (Frega et al. 2014, Tedesco et al. 2018).

3D engineered neuronal networks coupled to planar MEAs, represent a powerful-complementary-alternative and interesting tool capable of better emulating *in-vivo* neurophysiology than standard 2D *in-vitro* neuronal systems. The use of MEA devices allows to better study and understand the functional properties of biomimetic 3D neuronal networks.

However, the existing proposed 3D *in-vitro* neuronal models lack of appropriate microtransducers arrays that can be coupled to such models to record the electrophysiological activity of the 3D networks. 2D-MEAs allow to record the electrophysiological activity of the 3D network only from the bottom layer (i.e. the one directly coupled to the planar MEAs).

Thus, to further develop and optimize such 3D neuronal network systems and to study and understand how the 3D neuronal network dynamic changes in different layers of the 3D structure, new 3D recording/stimulating devices should be constructed. Overall, planar MEAs are limited in their applicability to 3D *in-vitro* neuronal constructs (like tissue slices or 3D dissociated cultures) mainly due to attenuation of the electrical signal from the active cells (leading to poor signal-to-noise ratios (SNRs)) as the neuron-microelectrode distance increases. Thus, a technology that combines 3D functionality (hopefully higher than 100 µm), scalability, and mass manufacturability is required to address the current and future needs of the *in vitro* electrophysiological, neurophysiological, and pharmacological communities (Rajaraman et al 2011).

Therefore, in order to study complex network morphologies and 3D neuronal networks or tissue slices which contain substantial 3D neuronal structures, three-dimensional micro-electrode arrays (3D-MEAs) are required.

3D-MEAs such as 3D protruding fingers ('towers') with embedded microelectrodes positioned at different heights, tip-shaped or needle-shaped 3D protruding microstructures, or sandwich-structure (i.e. standard MEA from the bottom side and a planar multi-channel recording structure on the upper side) can be developed to interface with 3D neuronal constructs (brain slices or 3D neuronal cultures) and record the activity of such 3D neuronal systems from both the bottom, middle and upper layers.

Thus, there is a tremendous need to fabricate new 3D recording devices able to record spontaneous or/and stimulus-evoked electrophysiological activity of 3D neuronal structures from different locations in the 3D space. The design and development of innovative and truly 3D-MEAs would open new perspectives for *in-vitro* neurophysiological studies and would allow to study and characterize a complete 3D-3D *in-vitro* neuronal models.

3.2 Concept and Design of 3D pillar-shaped gold MEAs

Technology that uses 3D functionality higher than 100 µm is required to address the current and future needs of the *in-vitro* electrophysiological, neurophysiological and pharmacological communities. Toward such a goal, in this work, I successfully demonstrate an innovative microfabrication approach to implement a novel 3D-MEA with heights of 105 ± 5 µm for *in-vitro* 3D neuronal cell cultures and tissue slices interfacing.

Figure 3.1 shows an optical photograph of the developed 3D device, with the closer inset depicting the electrodes recording area. The design chosen for the 3D-MEA includes a square recording area of 5 mm x 5 mm. In this area, 60 pillar-shaped gold microelectrodes are aligned in an 8 x 8 grid (except the four electrodes at the corners) with inter-electrode distances of 200 µm. The pillar-shaped gold microstructures in the center of the chip have a height of 105 ± 5 µm and a diameter of about 60 µm and 45 µm at the top and bottom side, respectively. All the 60 electrodes can be individually addressed electrically at the periphery of the chip. The external bond pads at the periphery serve this purpose.

The conductive tracks are used to electrically connect the pillar-shaped gold microelectrodes to the external macropads. Both tracks and sidewalls of such 3D pillar-shaped gold microstructures are completely passivated by using an oxide bi-layer composed of Silicon (Si) and Titanium (Ti) oxide. Thus, only the top side of these gold pillars is used as recording/stimulation area of the chip and is exposed to the direct contact of the active cells. The overall chip dimensions are designed to be 49 mm x 49 mm to be compatible with standard holder of the Multichannel System acquisition set-up (MEA 2100-System, Multichannel System, Reutlingen, Germany).

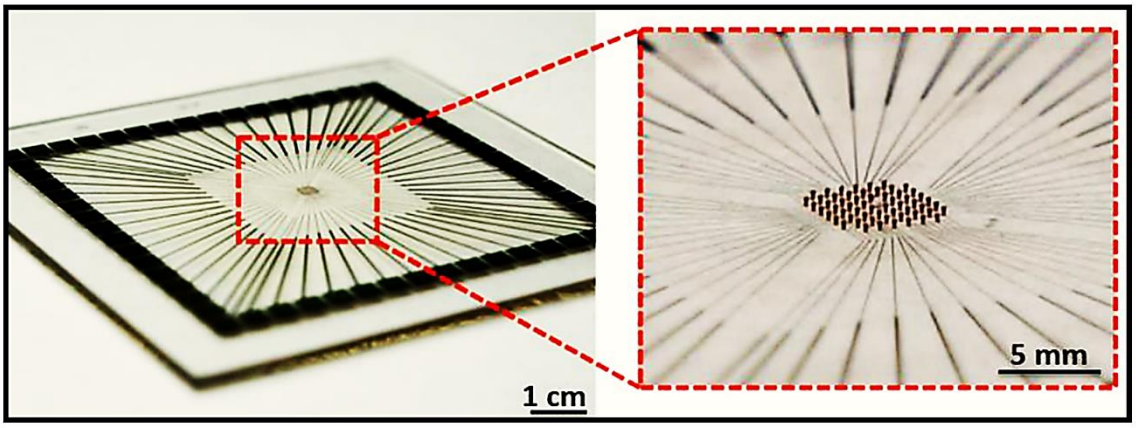

Figure 3.1. Optical photograph of the proposed pillar-shaped gold 3D-MEA. The inset on the right shows the electrodes recording area with 60 3D pillar-shaped gold microstructures (height 105 ± 5 µm).

These 3D pillar-shaped gold microelectrodes have been carefully designed to be interfaced with 3D *in-vitro* neuronal structures like 3D cell cultures and acute brain slices. In this work, I successfully demonstrate the capability of the developed 3D-MEAs to record the spontaneous electrophysiological activity of 3D engineered *in-vitro* neuronal networks from different locations in the 3D space. Moreover, recordings of both epileptiform-like and electrical-evoked electrophysiological activity from mouse acute brain slices have been successfully demonstrated with these 3D-MEAs.

In this research, two 3D-MEA technologies have been designed and developed to perform preliminary characterization of such 3D devices. The first one, called 3D-MEA all pillars, has been described above. Just to remind, this technology includes 60 pillar-shaped gold microelectrodes of height 105 ± 5 µm with a diameter of about 60 µm and 45 µm at the top and bottom side, respectively. The only area of the chip exposed to the direct contact of the active cells is the top side (recording/stimulation area) of such gold pillars. As

previously stated, the other parts of the chip are completely passivated. The second one, called 3D-MEA half/half, has the same geometrical properties of the aforementioned 3D-MEA all pillars but presents a simple gradient structure composed of both 100-µm-high pillar-shaped gold microelectrodes and planar gold microelectrodes. Only the top side (~60 µm in diameter) of the 3D pillars and the surface area of the planar round-shaped electrodes (~45 µm in diameter) are exposed to the direct contact of the active neurons. Other areas of the chip (i.e. conductive tracks and sidewalls of the pillars) are completely passivated.

3.3 Materials and Methods

In this section, I report a detailed description of the microfabrication process employed to fabricate the 3D pillar-shaped gold MEAs. Then, I describe the experimental setup used to carry out impedance measurement of the electrodes of the developed 3D chips. Subsequently, the method used for the preparation of mouse cortico-hippocampal brain slices and 3D engineered cortical neuronal networks coupled to the fabricated 3D-MEAs to experimentally validate such 3D devices is showed. In addition, the experimental setup used for performing electrophysiological recordings from both mouse acute brain slices and 3D cortical neuronal cultures with the developed 3D chips is reported.

3.3.1 Microfabrication of 3D Pillar-Shaped Gold MEAs

A specific microfabrication method based on standard photolithography and electroplating processes has been carefully designed and developed to build arrays of 3D microelectrodes onto borosilicate glass substrates. The process begins with the realization of gold standard 60-channel planar MEA (60 µm electrode diameter, 200 µm spaced) directly onto glass substrate. The fabrication process of such 2D-MEA is detailed in subsection 3.3.1.1 and showed in figure 3.2. Then, 3D pillar-shaped gold microstructures are realized through gold electroplating directly on the top side of such standard planar MEA. As previously stated, two types of 3D-MEA technologies have been developed and fabricated. The first one, called 3D-MEA all pillars, is constituted of 60 gold microelectrodes of height 105 ± 5 µm. The second one, called 3D-MEA half/half, is constituted of both 100-µm-high gold microelectrodes and planar gold microelectrodes.

The fabrication process of 3D-MEA all pillars and 3D-MEA half/half is reported in subsection 3.3.1.2 and 3.3.1.3, respectively. The ideal process flow of such 3D-MEAs is shown in details in figure 3.3.

3.3.1.1 2D-MEA on glass substrate

The process starts with spin-coating of 800-Å-thick anti-reflective material (DUV 42P) onto glass substrate and soft-baking for 1 min at 110 and 205 °C (Figure 3.2 (A)). DUV 42P anti-reflective coatings are able to control reflection and light absorption during photolithography steps. Highly reflective materials (i.e. the underlying glass substrate) would cause light from the exposure to bounce back into the photoresist, resulting in phenomena such as standing waves and reflective notching. These defects could ruin the fidelity of the pattern in the photoresist. Anti-reflective coatings can mitigate and control these reflections.

Then, 600-nm-thick lift-off resist (LOR 5A) and positive-tone photoresist (~1.3 µm MEGAPOSIT™ SPR™ 670) are spin-coated onto the DUV 42P layer and soft-baked for 1.30 min at 180 °C and 95 °C, respectively (Figure 3.2 (B)). LOR resists are based on polydimethylglutarimide (PMGI) material. Its unique properties enable LOR products to perform exceptionally well when used, either as a sacrificial layer or as an undercut layer in bi-layer lift-off processing. Used beneath photoresists in a bi-layer resist stack, such materials allow to obtain very high-resolution metallization (<0.25 µm), easy process tuning, high yields, and superior deposition line width control.

A first photolithography step is then performed to realize an MEA pattern made up of 60 planar gold microelectrodes (60 µm electrode diameter, 200 µm spaced) arranged over an 8 x 8 square grid (except the four electrodes at the corners), directly on the glass substrate.

Thus, SPR 670 positive photoresist is exposed to UV light (Figure 3.2 (C)), post-exposure baked (1.30 min at 95 °C) and developed in Tetramethylammonium Hydroxide (TMAH) solution, 25 wt. % in water, for 1.30 min. The underlying LOR 5A layer being TMAH-soluble is developed at the same time (Figure 3.2 (D)). A layer of Cr/Au (5 nm/100 nm) is then deposited onto the substrate surface by means of thermal evaporation (Figure 3.2 (E)).

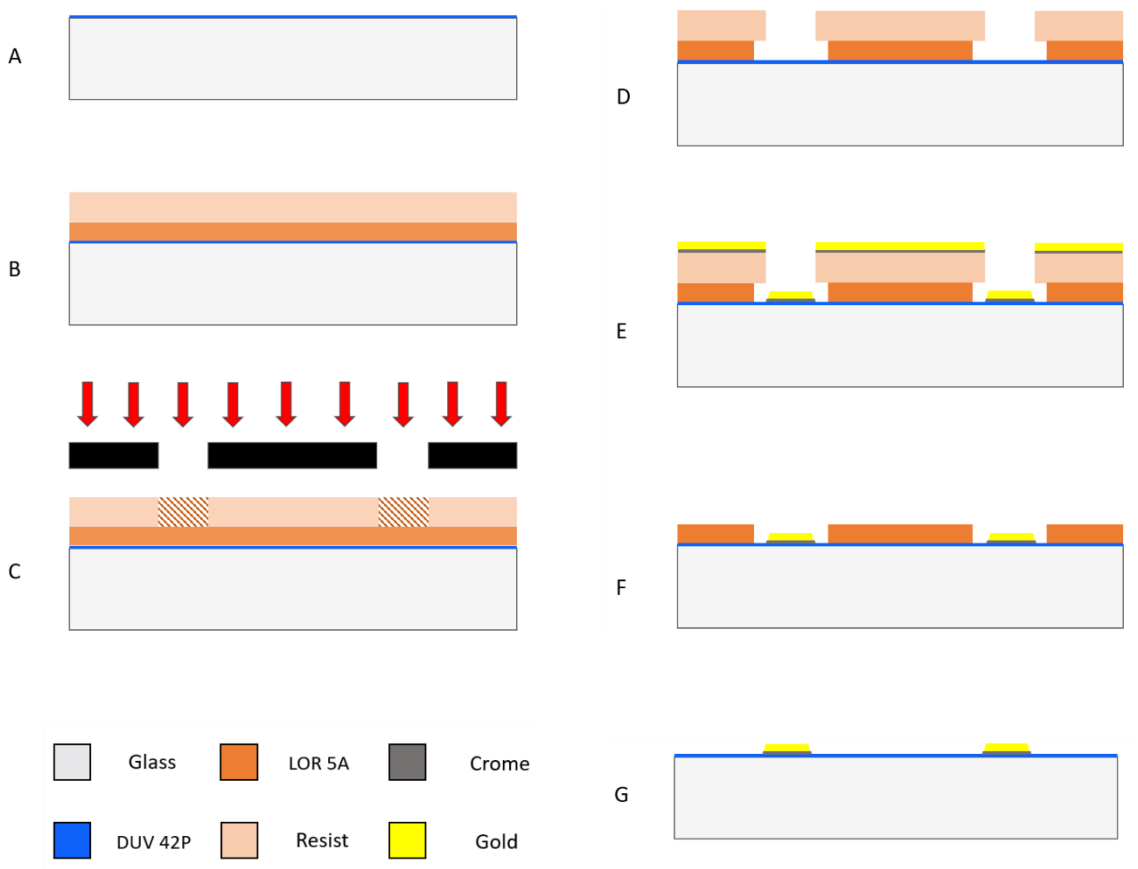

Figure 3.2. Fabrication process flow for gold 2D-MEA on glass substrate. (A) Coat and soft-bake DUV 42P. (B) Coat and soft-bake LOR 5A and SPR 670 resist. (C) Expose SPR 670 resist. (D) Develop SPR 670 resist and LOR 5A. LOR 5A develops isotropically, creating a bi-layer reentrant sidewall profile. (E) Cr/Au thin-film deposition. The reentrant profile ensures discontinuous film deposition. (F) Lift-off UV-light unexposed resist. (G) Remove LOR 5A residual layer, leaving only the desired film.

In addition, a Lift-off process is performed to remove UV-light unexposed photoresist and the overlying metal film by dipping the substrate in N-Methyl-2-pyrrolidone (NMP) solvent with ultrasonic waves (Figure 3.2 (F)). Finally, the sample is washed in TMAH for 2 min to remove LOR 5A residual layer, leaving only the desired film onto the glass substrate (Figure 3.2 (G)).

Figure 3.4 (A) shows optical micrograph of the gold standard 60-channel planar MEA fabricated directly onto glass substrate and obtained by using the fabrication process described above.

3.3.1.2 3D-MEA all pillars on glass substrate

Since the electrodes surface had to be the only conductive area of the 3D chips in contact with the neuronal cells, it has been necessary to passivate the surface of the signal lines (i.e. electrical interconnection between the electrodes and external bond pads) by using negative-tone photoresist (SU-8 2005) as insulation layer. SU-8 resist consists of a polymeric epoxy resin by dissolving in an organic solvent and adding a photoacid generator. Thanks to its high sensitivity, excellent chemical resistance, good compatibility with electroplating, highly uniform coating, vertical sidewalls, low edge bead, SU-8 appears to be an ideal photoresist for MEMS fabrication.

Therefore, 5.3-µm-thick SU-8 layer is spin-coated onto the substrate surface and soft-baked for 2 min at 65 °C and then for 5 min at 95 °C to passivate the 3D-MEA chip (Figure 3.3 (A)). Before SU-8 deposition, the sample is washed in acetone, isopropanol and water, dehydrated at 130 °C for 5 min and cleaned with O2 plasma (5 s) to improve the SU-8 adhesion.

A second photolithography step is then performed to realize a through-holes pattern in the SU-8 layer in correspondence to the position of each electrode. Thus, SU-8 negative photoresist is exposed to UV-light (Figure 3.3 (B)), post-exposure baked (2 min at 65 °C and 5 min at 90 °C) and developed in Ethyl-lactate with ultrasonic waves for 3 min (Figure 3.3 (C)). The substrate is then rinsed with isopropanol and dried with clean air.

Figure 3.4 (B) shows optical micrograph of the through-holes pattern (5.3 µm thick) realized in the SU-8 negative photoresist in correspondence to the position of each electrode.

At the end of the photolithography process described earlier, a lot of strengths remain inside the SU-8 photoresist, which can create cracks on the surface or even delamination of the layer. Therefore, the SU-8 layer is exposed to UV-light (3 min) and then hard-baked for 5 min at 150 °C to successfully carry out a cross-linking process of such negative photoresist. The Hard bake heats the SU-8 to suppress these strengths. Thanks to it, some cracks disappear and the SU-8 photoresist becomes harder.

A shadow mask (i.e. mask constituted of full and empty parts) is then realized and applied to the sample surface to allow Al (130 nm) thin-film deposition only on the external bond pads of the 3D-MEA chip by means of thermal evaporation. In this way, a common conductive line between the external macropads is realized and employed to successfully

carry out gold electrodeposition directly on the electrodes surface during the next electroplating steps. Indeed, such conductive line will be connected to the negative pole of an external power supply which will cause a constant current to flow through an electrolytic cell during the electroplating process allowing the growth of the gold only on the surface area of the electrodes.

Figure 3.5 (A) shows a schematic of the shadow mask applied to the sample surface to allow Al thin-film deposition on the external bond pads of the 3D chip. As previously stated, such a step is necessary to allow the gold electroplating process only on the surface area of the gold microelectrodes.

In Figure 3.5 (B) is showed the experimental setup used for performing the gold electrodeposition. By taking a look at Figure 3.5 (B), it possible to observe that the experimental setup for gold electroplating is typically constituted of an external power supply which causes a constant current to flow through an electrolytic cell. Such a cell is typically composed of a negative electrode (cathode), a positive electrode (anode) and the plating solution (bath). Cathode represents the substrate to be plated and through which the direct current flows. The anode is made of a conducting material which serves merely to complete the circuit. Bath is composed of an aqueous solution of gold cyanide (electrolyte). Thus, a first gold electrodeposition step, called 'pre-plating', is then performed to create pillar-shaped gold microstructures (~5.3 µm thick) in correspondence to the position of each electrode (Figure 3.3 (D)). Such a step is necessary to make easier the second and truly gold electroplating process for realizing 100-µm-high pillar-shaped gold microstructures.

The 'pre-plating' process is performed using a plating current density of 20 $\mu A/cm^2$ for 8 min in a plating bath composed of an aqueous solution of gold cyanide ($Au(CN)_2$). Moreover, a constant bath temperature (~60 °C) and a stirrer speed of 1200 rpm are used to reduce stress in the electroplated gold. Gold ions in the solution migrate only to the conductive and exposed area of the 3D device (electrodes surface area) where gold reduction reactions and gold thin-film deposition occurs. Before the 'pre-plating' step, the sample is cleaned with O_2 plasma (30 s) to remove SU-8 residual from the surface area of the gold planar microelectrodes.

In Figure 3.4 (C) is showed optical micrograph of the 5.3-µm-high pillar-shaped gold microstructures in correspondence to the position of each electrode developed during the 'pre-plating' step.

Then, a thick positive-tone photoresist (AZ IPS528) is spin-coated onto the substrate surface and soft-baked for 11 min at 65 °C, 11 min at 95 °C and 8 min at 130 °C to obtain 50-µm thick layer. A second AZ IPS528 layer is then spin-coated and soft-baked with the same parameters to finally obtain 100-µm thick positive photoresist (Figure 3.3 (E)). Prior the thick photoresist deposition, the sample is washed in acetone, isopropanol and water, dehydrated at 130 °C for 5 min and cleaned with O_2 plasma (4 s) to improve the thick photoresist adhesion on the substrate surface.

A third and last photolithography process is performed to realize a through-holes pattern in the 100-µm thick AZ IPS528 layer in correspondence to the position of each electrode. Thus, the thick photoresist is exposed to UV-light for 60 s (Figure 3.3 (F.1)), post-exposure baked (2 min at 90 °C and 4 min at 100 °C) and developed in TMAH for ~30 min (Figure 3.3 (G.1)).

The action of TMAH has to be much aggressive to guarantee a complete opening of the holes in the UV-light exposed thick photoresist. A Reactive-ion Etching (RIE) process (etching time: 3 min) is then performed to clean the holes and remove waste materials (i.e. resist residual) deposited on the bottom side of the holes during the thick resist development. Such an RIE step is strongly necessary to successfully allow good and uniform growth of the gold through the 100-µm-deep holes in the AZ IPS528 photoresist. Therefore, a second and truly gold electroplating process is performed to realize 100-µm thick pillar-shaped gold microstructures in correspondence to the position of each electrode (Figure 3.3 (H.1)). Such electroplating process is performed using a plating current density of 5 $\mu A/cm^2$ for 1 h and then 10 $\mu A/cm^2$ for 3 h.

After the electroplating step, the thick positive photoresist and the common conductive Al line between the external bond pads are removed by washing the sample in acetone and in sulfuric acid (H_2SO_4), respectively. In this way, only the desired pillar-shaped gold 3D-MEA remains onto the borosilicate glass substrate (Figure 3.3 (I.1)).

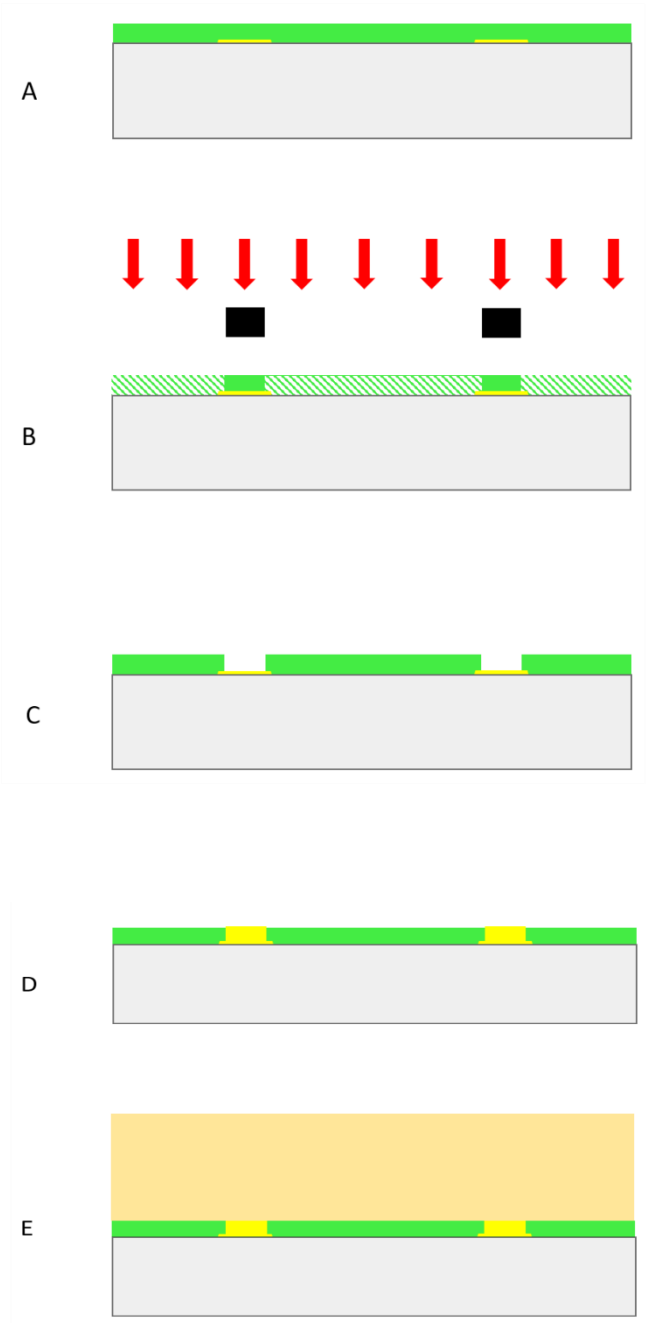

Figure 3.3. Fabrication process flow for gold 3D-MEA all pillars and gold 3D-MEA half/half on glass substrate. Continued.

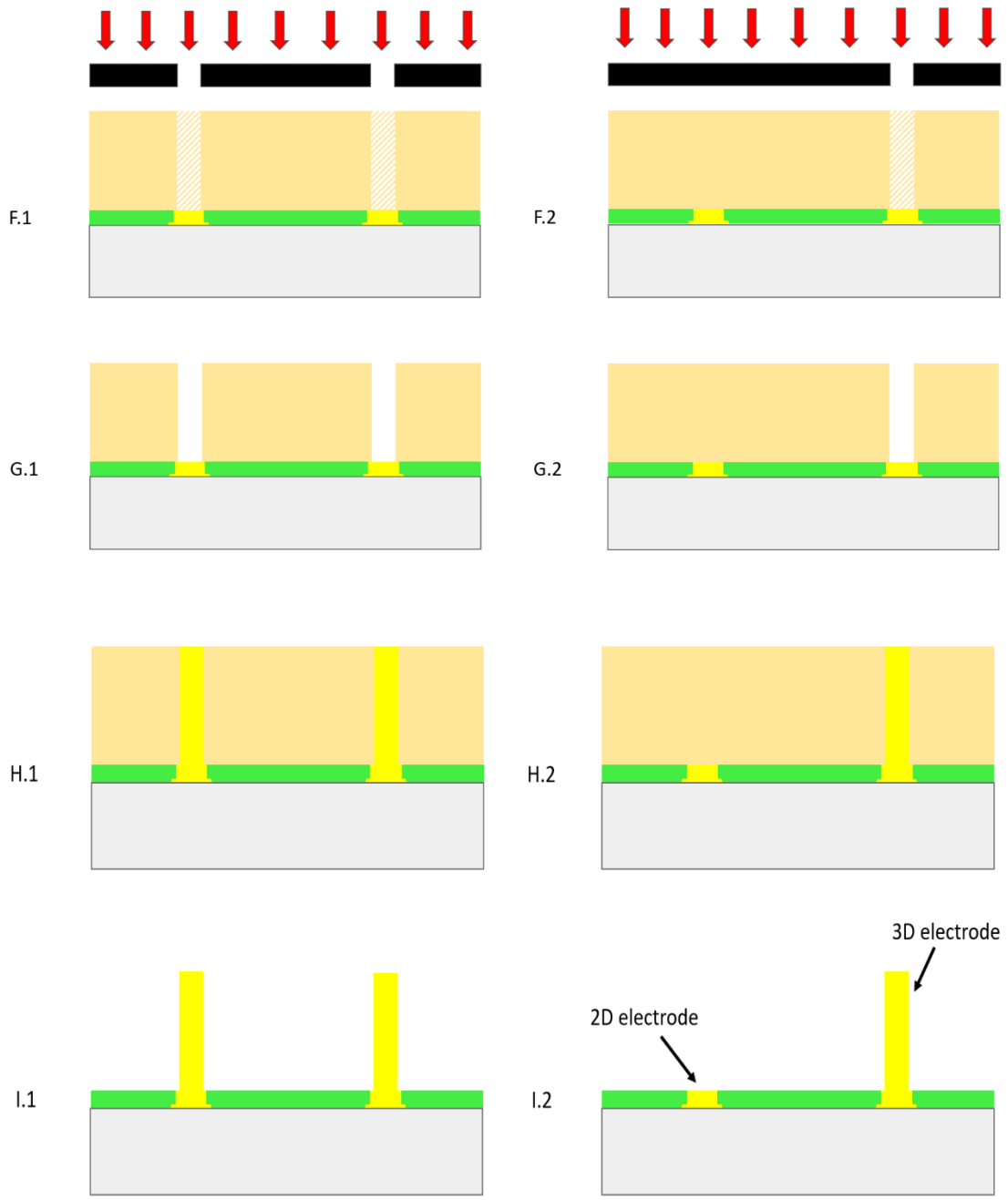

Figure 3.3. Fabrication process flow for gold 3D-MEA all pillars and gold 3D-MEA half/half on glass substrate. Continued.

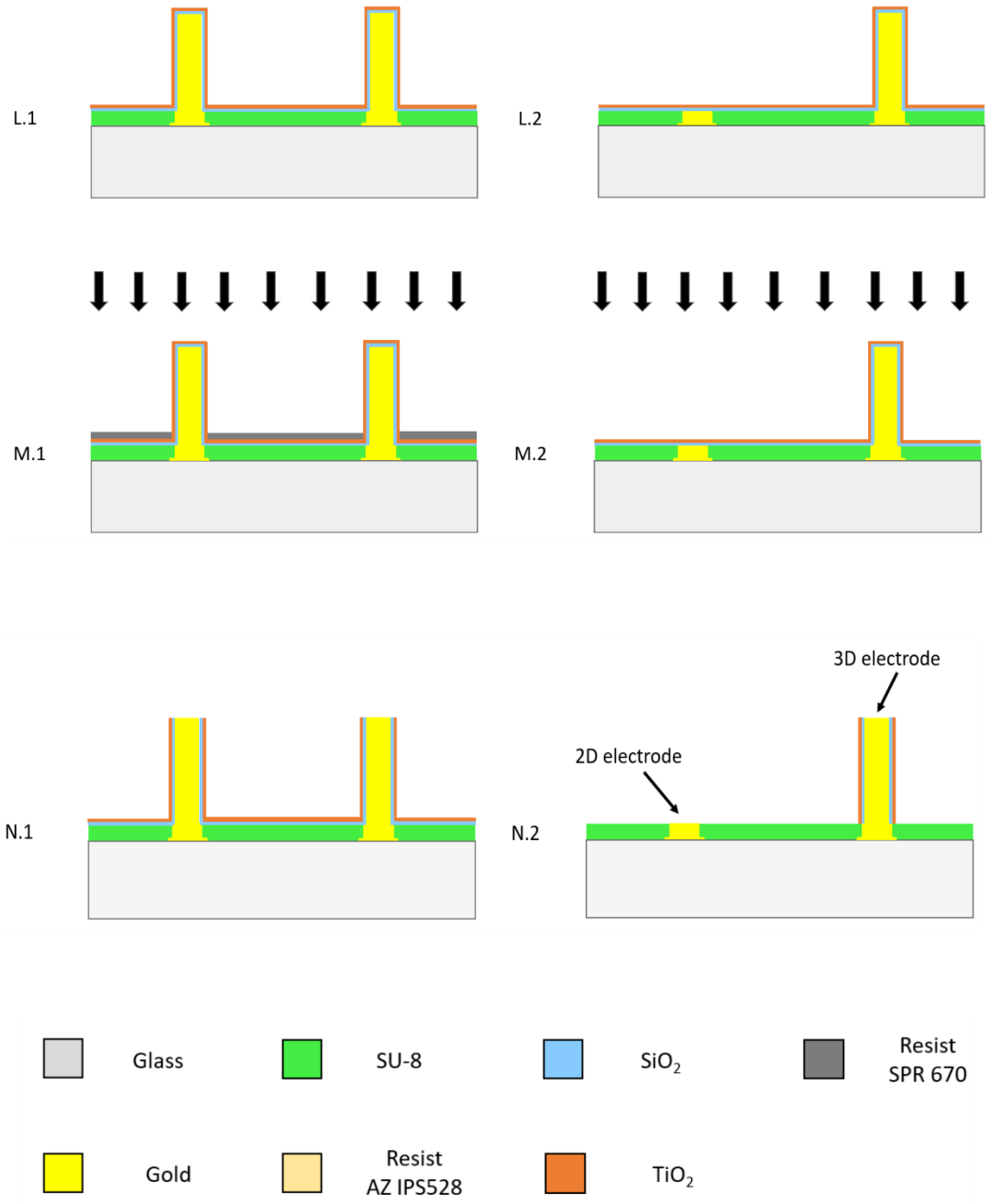

Figure 3.3. Fabrication process flow for gold 3D-MEA all pillars and gold 3D-MEA half/half on glass substrate. (●.1) and (●.2) refers to 3D-MEA all pillars and 3D-MEA half/half fabrication process, respectively. (A) Coat and soft-bake SU-8 negative resist (5.3 µm thick) to obtain a first passivation of 3D-MEA chips. (B) Expose SU-8 resist. (C) Develop SU-8 resist. (D) First gold electrodeposition (pre-plating process). (E) Coat and soft-bake AZ IPS528 resist (100 µm thick). (F.1) , (F.2) Expose AZ IPS528 resist. (G.1) , (G.2) Develop AZ IPS528 resist. (H.1) , (H.2) Second gold electrodeposition. (I.1), (I.2) AZ IPS528 resist removing, leaving only the desired 3D-MEA onto glass substrate. (L.1) , (L.2) Second passivation of 3D-MEA chips by means of SiO2 and TiO2 thin-film deposition. (M.1) , (M.2) Oxide bi-layer anisotropic etching (RIE) process to define recording sites on 3D-MEA devices. (N.1) , (N.2) Final 3D-MEAs.

To further improve the passivation of the fabricated 3D-MEA chips, a first SiO_2 (~230 nm) thin-film is coated onto the sample surface in a uniform way by means of sputter deposition. In addition, atomic layer deposition (ALD) technique is used to coat a second TiO_2 (~100 nm) thin-film onto the sample surface (Figure 3.3 (L.1)). Such thin-film deposition method (i.e. ALD) allows to further passivate and insulate the surface of the conductive tracks and the sidewalls of the pillars from the direct contact of the active cells.

Since the top side of the fabricated 3D pillar-shaped gold microstructures had to be the only exposed area of the 3D chip, it has been necessary to remove the oxide bi-layer only from such area of the 3D device.

To remove the oxide double-layer from the top side of the pillars, an anisotropic etching via RIE is employed (SiO_2 etching time: 6.5 min, TiO_2 etching time: 7 min) (Figure 3.3 (M.1)). Prior to such anisotropic etching, the oxide bi-layer deposited onto the surface of the tracks, has been protected by deposition of a few micron thick SPR 670 layer to avoid oxide etching during the RIE process. Thus, the surface of the signal lines and the sidewalls of the pillars remain completely passivated by the oxide bi-layer. Instead, the only conductive part of the 3D-MEA chip exposed to the direct contact of the cells remains the top surface area of the gold pillars (recording/stimulation sites).

After etching, 3D-MEA device is washed in acetone, isopropanol and water to remove the SPR 670 resist residual previously used to protect the oxide bi-layer, deposited on the surface of the tracks, from the etching via RIE (Figure 3.3 (N.1)).

In summary, electrophysiological recordings and stimulation from *in-vitro* 3D neuronal cultures or acute brain slices can be performed only from the top surface area of such 3D 100-µm-high pillar-shaped gold microelectrodes. The other parts of the 3D chip remain, as previously stated, completely passivated.

3.3.1.3 3D-MEA half/half on glass substrate

The fabrication process employed to develop 3D-MEAs half/half diverges from the process flow described in section 3.3.1.2 on few steps.

First, it is realized an only half through-holes pattern in the 100-µm thick positive photoresist during the third photolithography process (Figure 3.3 (F.2) and 3.3 (G.2)). Thus, only 30 100-µm-deep holes are opened in the AZ IPS528 photoresist and gold is

only electroplated through these holes (Figure 3.3 (H.2)). Therefore, at the end of the second electroplating process, the device will be constituted of half 100-µm-high pillar-shaped gold microelectrodes and half planar gold microelectrodes (Figure 3.3 (I.2)). Passivation of such 3D-MEA half/half chip is obtained by means of SiO_2 and then TiO_2 deposition as reported in the previous section (Figure 3.3 (L.2)). Then, an oxide double-layer anisotropic etching process via RIE is performed to define the recording sites (i.e. top side of the gold pillars and surface area of the planar gold microelectrodes) (Figure 3.3 (M.2)).

In this way, the surface of the signal lines remains only passivated and insulated by the SU-8 layer. Instead, the sidewalls of the pillars remain passivated by the oxide bi-layer. Thus, the only conductive parts of the 3D-MEA chip exposed to the direct contact of the active cells is the surface area of the gold planar microelectrodes and the top side of the gold pillars (Figure 3.3 (N.2)).

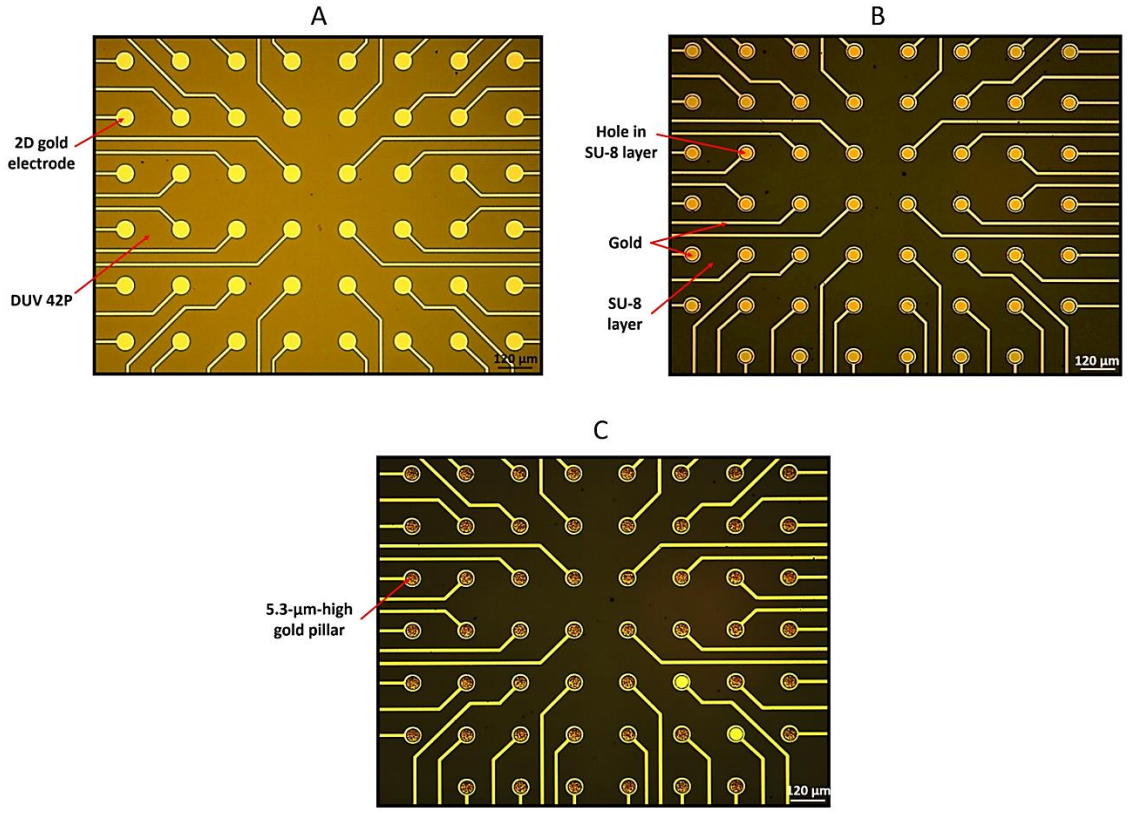

Figure 3.4. Optical micrographs of (A) gold 60-channel standard planar MEA, (B) SU-8 negative photoresist-through-holes pattern (5.3-µm thick) in correspondence to the position of each electrode, and (C) preliminary gold electrodeposition ('pre-plating') for realizing 5.3-µm-high-pillar-shaped microstructures.

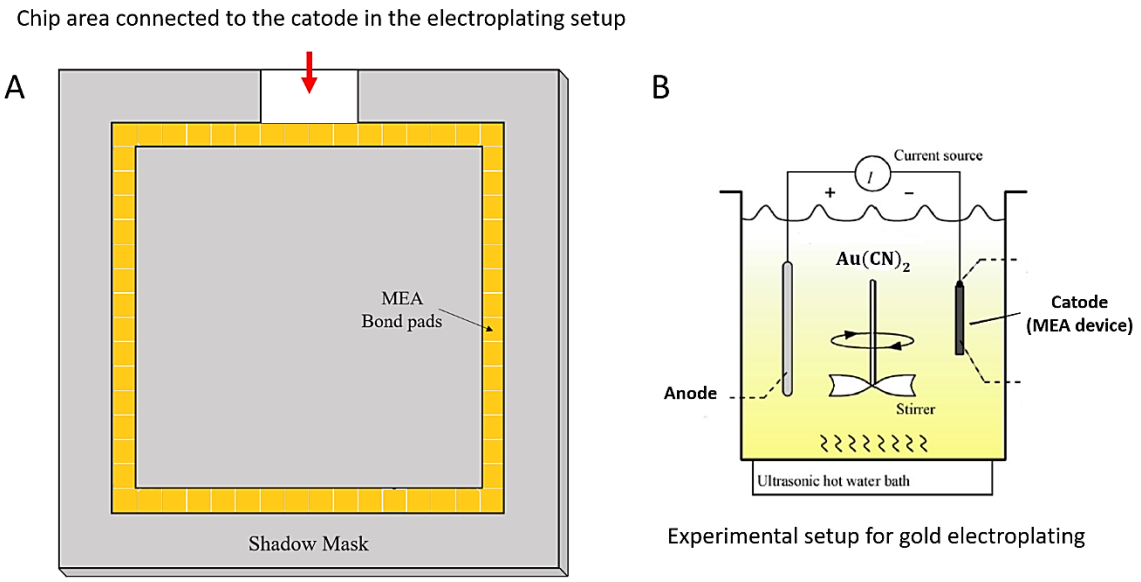

Figure 3.5. (A) schematic of the shadow mask applied to the MEA surface for Aluminium (Al) thin-film deposition on the external bond pads and on the chip area marked by the red arrow, which is connected to the cathode during the gold electroplating. This step is mandatory for performing the electroplating process. (B) Experimental setup used for gold electrodeposition on the surface area of the electrodes.

In Summary, the proposed microfabrication process is simple, flexible and easy to be implemented. It allows to realize layout of 3D pillar-shaped electrodes with different heights through electroplating on the top side of a standard planar MEA. By changing the thickness of the photoresist, it is possible to achieve arrays of 3D pillar-shaped electrodes with a height of 100 µm, 150 µm, and more than 200 µm.

3.3.2 Impedance Measurement System

Over the past decade, many studies have been devoted to the introduction of measurement platforms or systems to make impedance measurements (Merrill et al. 2005, Xu et al. 2009, Rottignini et al. 2011, Puia et al. 2013, Park et al. 2015, Gu et al. 2015, Rocka et al. 2016, Viswa et al. 2016, Dragas et al. 2017).

In this study, electrochemical impedance spectroscopy (EIS)-based experimental setup was implemented to characterize, in a systematic way, the electrical properties of the fabricated 3D-MEAs in order to determine the exact value of the individual impedance of the electrodes across the frequency spectrum of interest. The developed experimental setup was based on a dual phase lock-in amplifier (SIGNAL RECOVERY Model 5110) connected to an external function generator (HP 33120A) and an Ag/AgCl reference electrode used to complete the circuit and collect the current which flows through the electrochemical cell.

To measure the impedance, the waveform generator was used to apply a small amplitude (5-15 mV) sinusoidal perturbation of a given frequency to the working/excitation microelectrode under investigation and the dual phase lock-in amplifier was used to measure the resulting AC current, which flows through the device.

Specifically, the lock-in amplifier translates the collected current (I) to a voltage (V) by the integrated trans-impedance amplifier (TIA) and then demodulates the voltage (V) into the in-phase (X) and quadrature (Y) components. Magnitude ($|Z|$) and phase (φ_z) of the impedance were then calculated from these X&Y data as follows:

$$|Z| = \frac{|V_{stim}|}{|I|} \tag{3.1}$$

$$\varphi_z = \tan^{-1}\left(\frac{Y}{X}\right) \tag{3.2}$$

Where $|I| = |V|/G$, $|V| = \sqrt{X^2 + Y^2}$, G is the TIA conversion gain and V_{stim} is the applied input sinusoidal perturbation.

Impedance measurements were performed in a PBS (Phosphate-buffered saline) solution between the working electrode under test and the Ag/AgCl reference electrode. The process was repeated for all the microelectrodes of a 3D chip by sweeping the frequency from 10 Hz to 10 kHz to compute impedance at each frequency value.

In Figure 3.6 is showed a schematic of the impedance spectroscopy experimental setup used in this work to measure the impedance of the electrodes of the fabricated 3D-MEAs.

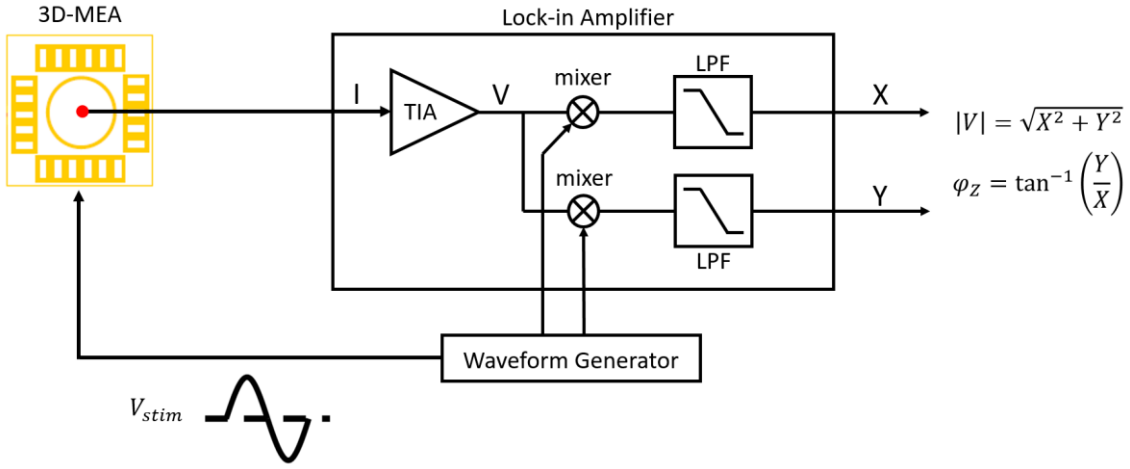

Figure 3.6. Schematic illustrating the electrochemical impedance spectroscopy experimental setup used to carry out impedance measurements of the fabricated 3D-MEA devices. The red bold circle represents the Ag/AgCl reference electrode dipped in the PBS solution and used to collect the current, which flows through the electrochemical cell.

3.3.3 Preparation of Acute Brain Slices

Horizontal cortico-hippocampal slices were prepared as shown by Farisello et al. (2012). Mice were anesthetized with halothane (Sigma-Aldrich, Milan, Italy) and decapitated; the brain was quickly removed and immersed in an ice-cold "cutting" solution composed of (in millimolars) 125 NaCl, 25 $NaHCO_3$, 25 glucose, 2.5 KCl, 1.25 NaH_2PO_4, 1 $CaCl_2$, 2 $MgCl_2$, 0.4 ascorbic acid, 2 NaPyruvate, 3 myo-inositol, and saturated with 95% O_2 and 5% CO_2. Horizontal mouse cortico-hippocampal slices (250 μm thick) (as shown by Bischofberger et al., 2006) were cut using an HM 650 vibratome (Microm International GmbH, Walldorf, Germany) in ice-cold oxygenated cutting solution. Slices were first incubated in cutting solution at 35 °C for 30 min and then transferred to a "submerged" recording chamber in a "standard recording" solution composed of (in millimolars) 125

NaCl, 25 $NaHCO_3$, 25 glucose, 2.5 KCl, 1.25 NaH_2PO_4, 2 $CaCl_2$, and 1 $MgCl_2$. This solution was constantly oxygenated and superfused at a rate of 1.5 mL/min. All experiments were carried out in accordance with the guidelines established by the European Communities Council (Directive of 24 November 1986) and approved by the National Council on Health and Animal Care.

3.3.4 Preparation of 3D Cell Cultures

Cortical neurons were dissociated from E18 Sprague Dawley rats (Charles River Laboratories, Milan). The procedure was approved by the European Animal Care Legislation and by the guidelines of the University of Genova. The day before the plating, 3D-MEAs were sterilized at 120 °C in the oven, and the glass microbeads (40 µm in diameter) were sterilized with ethanol at 70% for 1–2 hours. The sterilized material was therefore exposed to the coating treatment with adhesion protein Laminin (L-2020 Sigma) and Poly-Lysine (P-6407 Sigma) at 0.05 mg/ml overnight in incubator at 37 °C. The adhesion factors were removed and the treated glass surfaces washed with sterile water. 3D-MEAs were left to dry inside the laminar hood. Lastly, a PDMS mask (Corning Sigma) was put on the electrodes area to constraint it. From each embryo, cortical neurons were removed and placed into ice-cold Hank's balanced salt solution. The tissue was then dissociated in 0.125% of Trypsin/Hank's solution containing 0.05% of DNAse (D-5025 Sigma-Aldrich) for 15–18 min at 37 °C. The supernatant solution was removed and the enzymatic digestion was stopped by adding 10% fetal bovine serum (FBS) in Neurobasal medium for 5 min. Medium with FBS was removed and replaced with Neurobasal medium supplemented with B27, 1% Glutamax, gentamicin 10 mg/ml (Gibco Invitrogen). Glass microbeads were then placed onto a porous membrane (Transwell®, Millipore) where they self-assembled forming a compact monolayer. Dissociated cortical neurons were cultured on such coated microbeads in order to obtain a cell density of about 1500 cells/mm^2. At the same time, some cortical cells were plated directly onto the ground of the 3D-MEA surface, defined by the PDMS mask. The assembly of neurons with microbeads was then moved from the Transwell® membrane and deposited onto the 2D neuronal network previously coupled to the 3D-MEA device to obtain a packed three dimensional assembly.

The obtained 3D cortical neuronal cultures were maintained in a humidified CO_2 atmosphere at 37 °C for 18 days. Half of the media was replaced once a week. No antimitotic drug was added to prevent glia proliferation since glial cells are essential elements for healthy development of neuronal networks. As previously stated, glass microbeads (distributed by Distrilab-Duke Scientific) were used as a scaffold to create the 3D neuronal networks. The cell density and the thickness of the reconstructed tissue can be tuned depending on the diameters of the sphere and the number of transferred layers. Glass microbeads with a diameter of 40 µm (certified mean diameter of 42.3 ± 1.1 µm) were used and 5 to 8 layers were stacked.

3.3.5 3D-MEA Recordings Experimental Setup

In this section, I report the experimental setup used to perform electrophysiological recordings from both mouse acute brain slices and 3D *in-vitro* cortical neuronal networks with the fabricated 3D-MEAs.

3.3.5.1 Acute Brain Slices Recordings

Slices were transferred over a 3D-MEA and kept in place by the use of a small U-shaped platinum anchor with a grid of nylon threads to enhance the coupling between the tissue slices and 3D-MEA chip. MEAs were also coated with poly-ornithine (500 µg/ml, Sigma-Aldrich, Milan, Italy) to provide a good surface coating and improve the adhesion of tissue slices on the top surface area of the developed 3D pillar-shaped microelectrodes. MEA recording chamber was continuously superfused at rate of 1.5 ml/min with a standard recording solution (artificial cerebrospinal fluid, ACSF) composed of (mM): 125 NaCl, 25 $NaHCO_3$, 25 $C_6H_{12}O_6$, 2.5 KCl, 1.25 NaH_2PO_4, 2 $CaCl_2$, 1 $MgCl_2$. The bath temperature was monitored and maintained at 33 °C throughout the all (n=3) performed experiments. Then, 4-aminopyridine (4-AP) (500 µM, Sigma-Aldrich, Milan, Italy) was continuously bath perfused in order to induce spontaneous epileptiform-like discharges in the acute brain slices. 4-AP-induced epileptiform-like activity, in the form of interictal (I-IC) and ictal (IC) events, was recorded by means of such pillar-shaped gold 3D-MEAs and acquired with the 2100 System (MEA 2100-System, MCS). Signals were sampled at 10 kHz and recordings were performed in 30 min sessions under 4-AP bath application.

Moreover, acute brain slices were also electrically stimulated. Especially, electrical stimuli were delivered by using the 2100-System-integrated stimulus generator, which supplies current or voltage pulses to be applied through selected electrodes of the MEA. Voltage pulses were applied through one MEA electrode to locally stimulate the slice. Stimuli were sent from the selected electrode at a frequency of 0.3 Hz for 5 min with an amplitude of 3 V peak-to-peak. The stimulus pulse was biphasic (positive first) and lasted for 100 µs with 50% duty cycle.

3.3.5.2 3D Cell Cultures Recordings

The spontaneous electrophysiological activity of 3D cortical neuronal networks was recorded at 18 days *in vitro* (DIV) by means of the fabricated pillar-shaped gold three-dimensional Micro-Electrode arrays (3D-MEAs). The electrophysiological activity was acquired with the 2100 System (MEA 2100-System, MCS), and signals were sampled at 10 kHz throughout the all (n=2) performed experiments. Recordings were performed for 30 min outside the incubator at a temperature of 37 °C. To prevent evaporation and changes of the pH medium, a slow flow of humidified gas (5% CO_2, 5% O_2, 5% N_2) was constantly delivered during the measurement sessions into a small plastic box covering the experimental MEA setup.

3.4 Testing and Experimental Results

The fabricated 3D-MEAs have been characterized through both electrical and electrophysiological tests. For the electrical characterization, an electrochemical impedance spectroscopy-based experimental setup has been used to measure the impedance of the electrodes and the impedance spectrum of the device has been measured and evaluated in the frequency range of interest.

For the biological characterization, the 3D-MEAs have been experimentally validated by performing *in-vitro* tests with 3D engineered neuronal networks and mouse acute brain slices. These tests along with the obtained results are described in details in the next sub-sections.

Moreover, the advantages of such 3D-MEA devices with respect to standard planar MEA and previously reported 3D-MEA technologies have been highlighted and discussed.

3.4.1 Advantages of 3D Pillar-Shaped gold MEAs

The fabricated chips have a dimension of 49 x 49 x 2 mm to comply with standard holder of the Multichannel System acquisition setup (MEA 2100, MCS, Reutlingen, Germany). The 3D-MEAs are composed of pillar-shaped gold microstructures of height 105 ± 5 µm and diameter of about 60 µm and 45 µm at the top and bottom side, respectively. The SEM images in Figures 3.7 (A), (B) and (C) show such a bit irregular pillar-shaped gold microstructures at different view planes. The distance between each electrode is 200 µm. Figure 3.7 (D) shows a close-up view of one 3D electrode. The insert on the left represents an enlargement of the sidewall of such pillar-shaped microelectrode. The sidewall insulation oxide bi-layer composed of SiO_2 (∼230 nm) and TiO_2 (∼100 nm) is clearly observed.

It is important to underline that such a bit irregular shape of the pillars is mainly due to the effects resulting from the 100-µm-thick positive photoresist (AZ IPS528) exposure to the UV-light.

The developed 3D-MEAs present several advantages with respect to 2D and previous 3D electrode arrays reported in literature for use with acute brain slices. As it was postulated (Heuschkel et al. 2002), 3D sharp tip-shaped protruding electrodes with a height of about 50 µm should improve recording in acute slices by reducing the distance between active cells and recording electrodes and should allow better measurement and stimulation conditions by overcoming the dead-cell layer problem as compared to planar electrode arrays.

In this work, I successfully demonstrate that 3D pillar-shaped microelectrodes with height up to 110 µm and planar round-shaped top surface area (about 60 µm in diameter) can enhance the tissue slice adhesion on the top side of such microstructures and allow better contact between the tissue and the 3D-MEA chip. In this way, better cells and/or tissue slice coupling to the 3D pillar-shaped electrodes and reduced leakage currents can be achieved without slice penetration and damage and/or laceration of the tissue as it might be expected when using sharp tip- or needle-shaped protruding electrodes to overcome the dead-cell layer problem.

Such a good coupling between the tissue and the developed 3D electrodes allows to record stronger signals with larger amplitude and to improve recording and stimulation performances in a non-invasive way with respect to previously reported 3D electrode

arrays.

In this study, other approaches have been employed to enhance the tissue slice adhesion on the top side of the fabricated 3D pillar-shaped microstructures and thus, achieve a better coupling between the tissue and the 3D electrodes. Firstly, 3D-MEAs were coated with poly-ornithine to provide a good surface for the adhesion of brain slices. Secondly, to achieve good contact between the tissue and the 3D-MEA chip, slices were transferred over the 3D-MEA and kept in place by using a small U-shaped platinum anchor with a grid of nylon threads that was positioned on the top of the tissue slice. Therefore, such 3D pillar-shaped MEA devices can represent a good and alternative non-invasive technology, which allow better recording and stimulation conditions in acute brain slices without slice penetration with respect to previously developed 3D tip-shaped protruding electrode arrays.

In Figure 3.8, is showed a sketch illustrating the tissue slice/3D electrodes configuration. As previously stated, the shape of the pillar-shaped microstructures is a bit irregular. Such a property promotes a good contact between the slice and the top side of the 3D electrodes. Moreover, in the case of 3D MEA half/half configuration, the realized 3D pillar-shaped electrodes present an increased recording area (about 60 µm in diameter) as compared to 2D counterparts (about 45 µm in diameter). This increase in surface area reduces electrode impedance, which increases recorded signal amplitudes.

Furthermore, 3D electrodes also present a geometrical advantage when used for electrical stimulation. Due to a larger electrode surface area than 2D one, the electrode can store a larger electrical charge and thus can deliver a higher safe injected charge. In addition, a more reasonable comparison between signals recorded with 3D and planar electrodes can be performed because both 3D and 2D electrodes present a flat round-shaped recording area.

Summarizing, with respect to previously developed 3D sharp tip- or needle-shaped protruding electrode arrays, which needed to penetrate the tissue slice in order to reduce as much as possible the distance with the active living neurons, the fabricated 3D pillar-shaped electrodes with height up to 110 µm and planar round-shaped recording area (about 60 µm in diameter) allow to obtain a good coupling to the slice without penetration, damage and/or laceration of the tissue.

In this way, better recording and stimulation performances can be achieved and thus, stronger signals with larger amplitudes can be obtained with such 3D pillar-shaped microelectrodes.

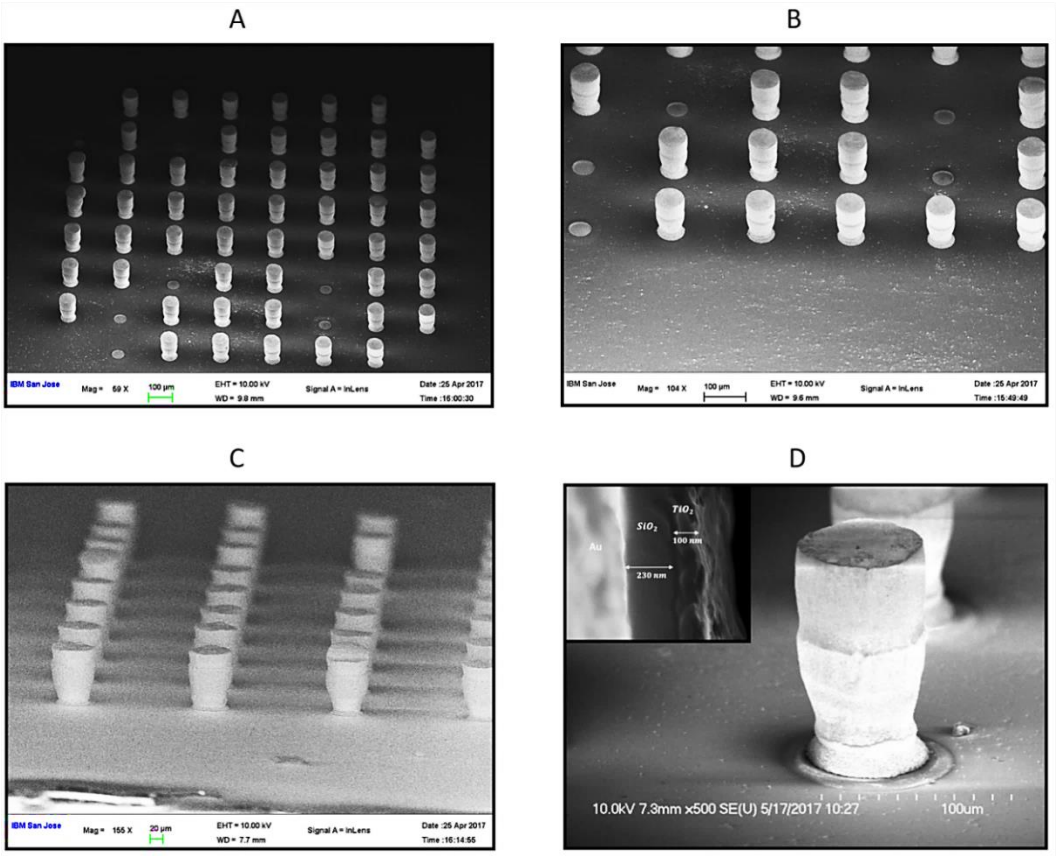

Figure 3.7. SEM images (A), (B) and (C) of the developed 3D-MEA constituted of 3D pillar-shaped gold microstructures. The lacking of some 3D pillars is mainly due to interruption of their corresponding signal lines. (D) SEM image showing a close-up view of one a bit irregular 3D pillar-shaped microelectrode. The insert on the left shows the oxide bi-layer used for the pillar sidewalls insulation.

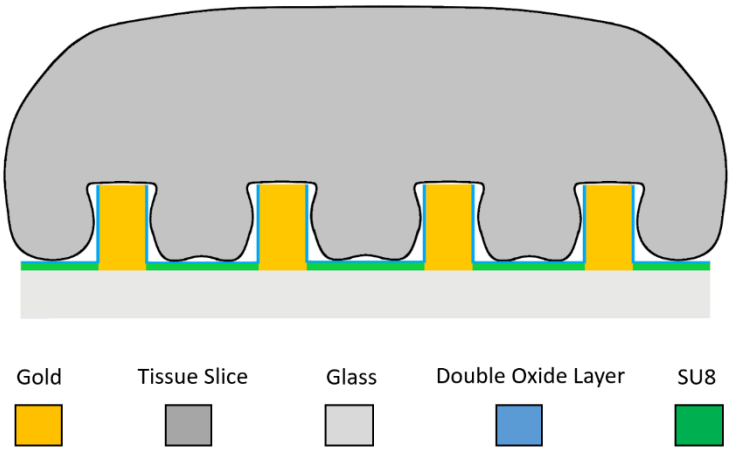

Figure 3.8. Schematic cross-section of the tissue slice/3D-MEA configuration.

3.4.2 Electrical Characterization

In this section, I discuss the electrical properties of the fabricated 3D-MEAs showing the impedance spectrum of such 3D devices in the frequency range of interest.

3.4.2.1 Impedance Results

I characterized the electrical properties of the fabricated 3D-MEAs to evaluate the individual impedance of the electrodes across the frequency spectrum of interest (10Hz - 10kHz).

Impedance spectroscopy based-experimental setup has been employed to carry out impedance measurements of electrodes as described in the previous section 3.3.2. Measures were performed between the microelectrode under test and an Ag/AgCl reference electrode in a PBS solution. Figure 3.9 shows the measured impedance magnitude values as function of the frequency for both 3D pillar-shaped and standard planar MEAs.

Specifically, the red curve is related to a 60-channel standard MEA constituted of planar microelectrodes of 30 µm in diameter and inter-electrode distances of 200 µm. The blue one is related to the 3D electrodes of a 3D-MEA half/half chip and the black one to a 3D-MEA all pillars device. As it is expected, the impedance magnitude decreases as the frequency of the AC input signal increases.

The impedance values of the 3D-MEAs chips range from a few mega ohms at low frequency (10 Hz) to tens of kilo-ohms at a higher frequency (10 kHz). Moreover, due to an increased electrode surface area, the 3D electrodes show an impedance value lower than 2D one across the whole frequency spectrum. Each data point of the curves represents the mean and standard error of the mean evaluated over thirty selected microelectrodes of each chip.

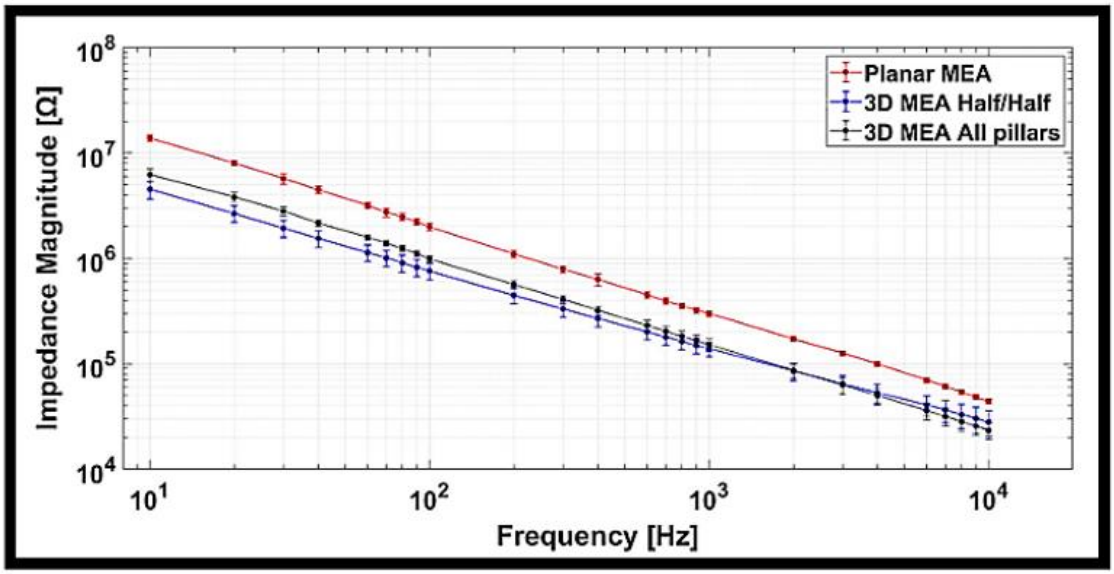

Figure 3.9. Impedance characterization. Measured impedance Z versus frequency for planar and 3D-MEAs in a PBS (Phosphate buffered Saline) solution. A 10 mV, [10-10000] Hz AC voltage signal was applied to the electrodes during the measurements. Each data point of the curves represents the mean and standard error of the mean evaluated over thirty selected microelectrodes of each chip.

3.4.3 Biological Characterization

In this section, I report the electrophysiological characterization of the fabricated 3D-MEA devices. I successfully demonstrate the capability of the developed 3D-MEAs to record electrophysiological activity from 3D *in-vitro* neuronal structures. *In-vitro* tests with 3D engineered neuronal cultures and mouse cortico-hippocampal brain slices have been performed to experimentally validate such fabricated 3D chips.

3.4.3.1 Electrophysiological Results from 3D Engineered Neuronal Networks

Preliminary electrophysiological results of the developed 3D-MEAs have been obtained from 3D *in-vitro* cortical neuronal networks grown onto glass microbeads-based scaffold. The 3D neuronal networks have been prepared and assembled onto the glass microbeads by following the procedure described in the previous section 3.3.4.

Electrophysiological recordings from 3D (n=2) cortical neuronal cultures have been performed after 18 days *in vitro* (DIV) by means of such 3D-MEAs.

To quantify the network dynamics properties, from the obtained peak trains, the following metrics have been computed. The mean firing rate, i.e. the number of spikes per second of each channel and the percentage of random spikes, i.e. the fraction of spikes outside bursts were evaluated. Moreover, the frequency (mean bursting rate) and duration (mean burst duration) of bursts were estimated. The network dynamics of the 3D cortical neuronal networks has been analyzed as described in the APPENDIX A.2.

Figure 3.10 (A) shows the layout of the 3D-MEA device involved in this analysis, where the blue and red boxes include the planar and the 3D 100-µm-high electrodes, respectively.

Raster plot in figure 3.10 (B) shows the global electrophysiological behavior of a representative 3D cortical neuronal network, where 300 s of spontaneous activity is displayed. For the sake of clarity, the activity recorded by means of planar and 3D 100-µm-high electrodes is represented in blue and red, respectively.

It can be noticed that the recorded electrophysiological activity of the 3D cortical neuronal culture shows the typical signatures of a true 3D network characterized by both network bursts and random spikes regions.

Figures 3.10 (C) and (D) show the spontaneous activity (raw signal) of 300 s of a 3D cortical neuronal network grown onto glass microbeads recorded from one representative planar and 3D 100-µm-high microelectrode, respectively. It is possible to observe that both the bottom and the 100-µm-high layer of the 3D neuronal network structure exhibit the same spontaneous activity characteristics. This observation could be related to the fact that the 3D electrodes of the 3D chip can be seen as planar round-shaped electrodes raised to the 100-µm-high level.

Moreover, the extracted parameters from the analyzed spike data like mean firing rate, percentage of random spike, mean bursting rate, mean burst duration were used to further characterized the network dynamics (Figure 3.11 (A)-(H)). Here again, it can be noticed that the first-order statistics show similar values both at the bottom (level 0) and the 100-µm-high layer (level 1) of the 3D neuronal network structure. Especially, 3D cortical neuronal networks exhibit a level of firing rate of about 8 spikes/s and a percentage of random spikes of about 10% at both the bottom and the upper layer. Regarding the bursting activity at the single channel level, 3D networks present a frequency of bursts of about 10 burst/min and a duration of bursts of about 600 ms at both the planar and the 100-µm-high level.

Finally, by applying a cross-correlation algorithm recently developed and implemented in the software package SpiCodyn (Pastore et al. 2018), I estimated the functional connectivity to point out inter- and intra-level connections and thus actual functional interactions within and between the bottom (level 0) and the 100-µm-high layer (level 1) of the 3D neuronal network structure. From the adjacency matrix (i.e., connectivity), I discarded (thresholding procedure) the noisier and weaker connections and I quantified the inter- and intra-level connectivity links.

Figure 3.12 (A) shows the percentage of links intra- and inter-levels of one representative experiment. The 100-µm-high layer (level 1) of the 3D neuronal structure contains a larger number of electrodes than the bottom one (level 0). Thus, I expected a higher level of intra-connectivity (about 36 %) within the upper layer than the intra-connectivity within the bottom layer.

Moreover, it can be noticed that the inter-connectivity presents a level of about 37 %. Finally, in Figure 3.12 (B), I present the estimated connectivity map of one representative experiment to illustrate the intra- and inter-level connectivity links. For the sake of clarity, the planar and 3D electrodes are depicted in white and red color, respectively.

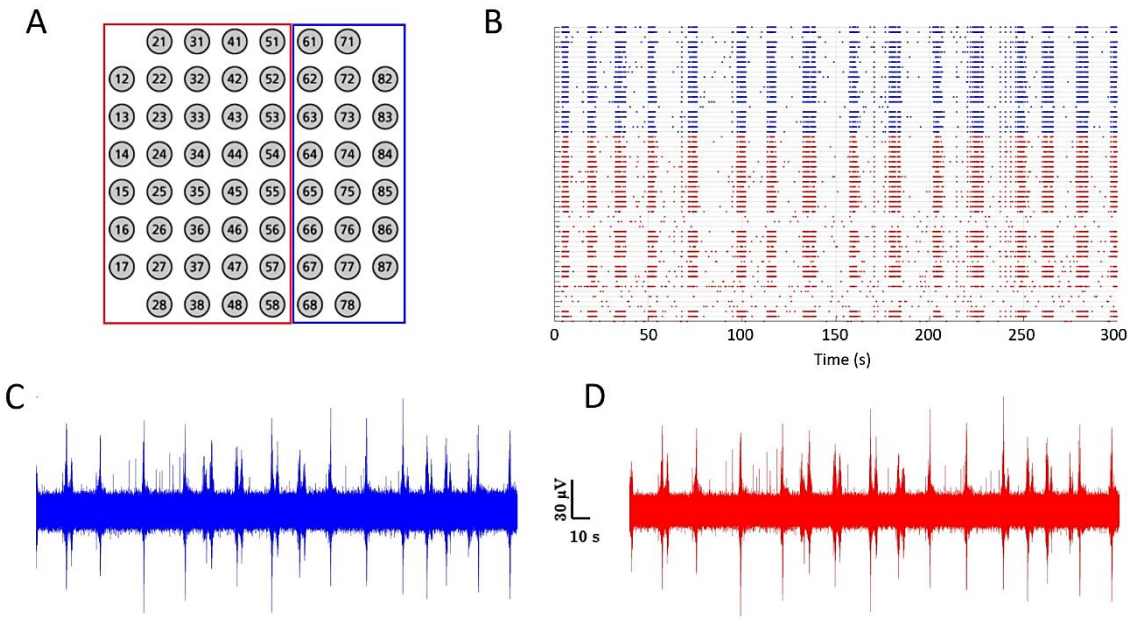

Figure 3.10. Spontaneous activity characterization of 3D neuronal networks coupled to 3D-MEAs. (A) 3D-MEA layout. Blue and red boxes include the planar and the 3D 100-µm-high electrodes respectively. (B) Raster plot showing 300 s of spontaneous activity of the bottom (blue dots) and upper (red dots) layer of a representative 3D cortical neuronal culture. (C) and (D) showing raw data of a representative channel of the planar (electrode 62) and upper (electrode 45) side of the 3D cortical neuronal network.

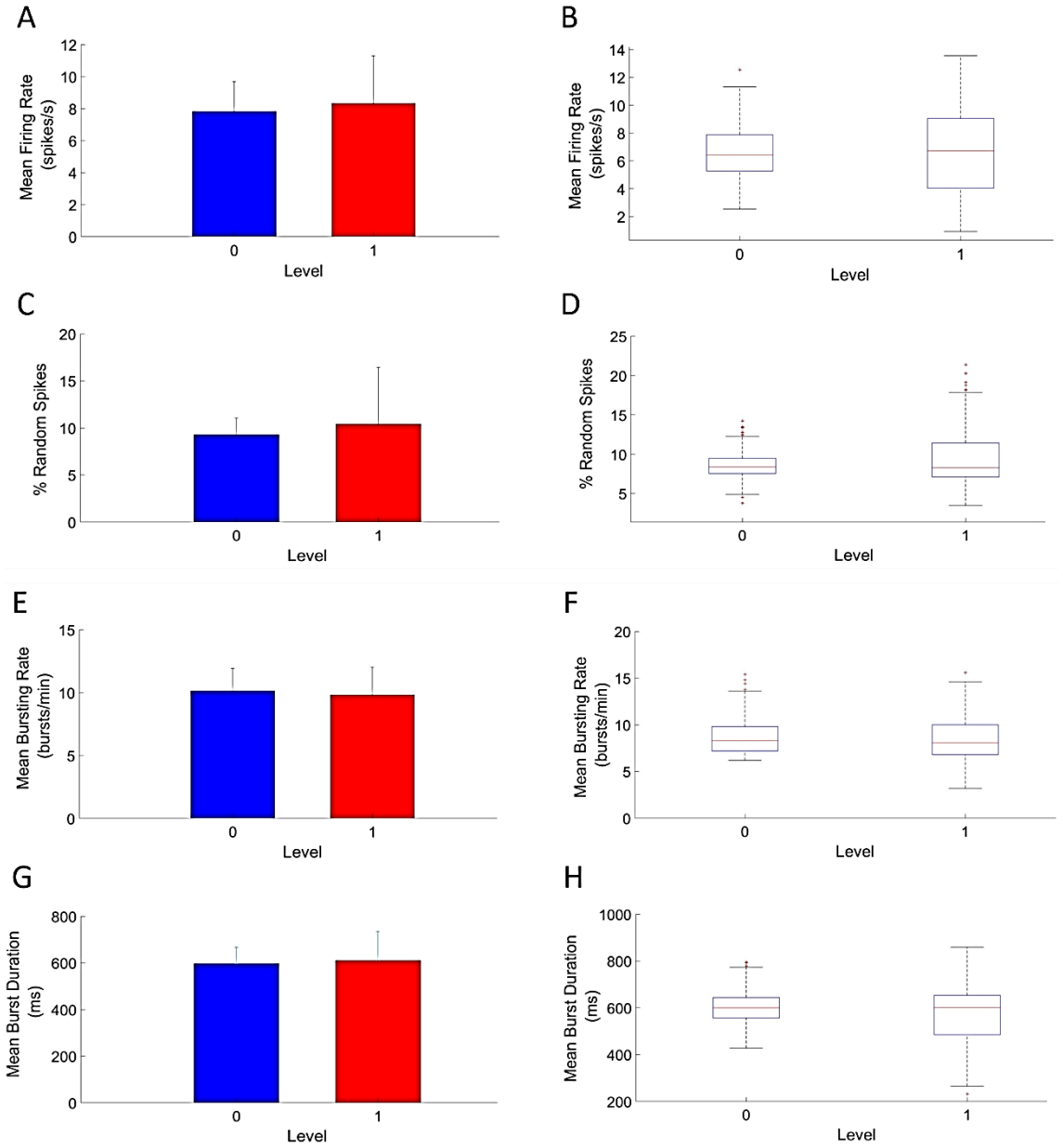

Figure 3.11. First-order statistics analysis. From (A) to (H), barplot and boxplot showing mean firing rate, percentage of random spikes, mean bursting rate and mean burst duration of the bottom layer (level 0) of a representative 3D cortical neuronal structure compared with the ones of the upper layer (level 1), respectively.

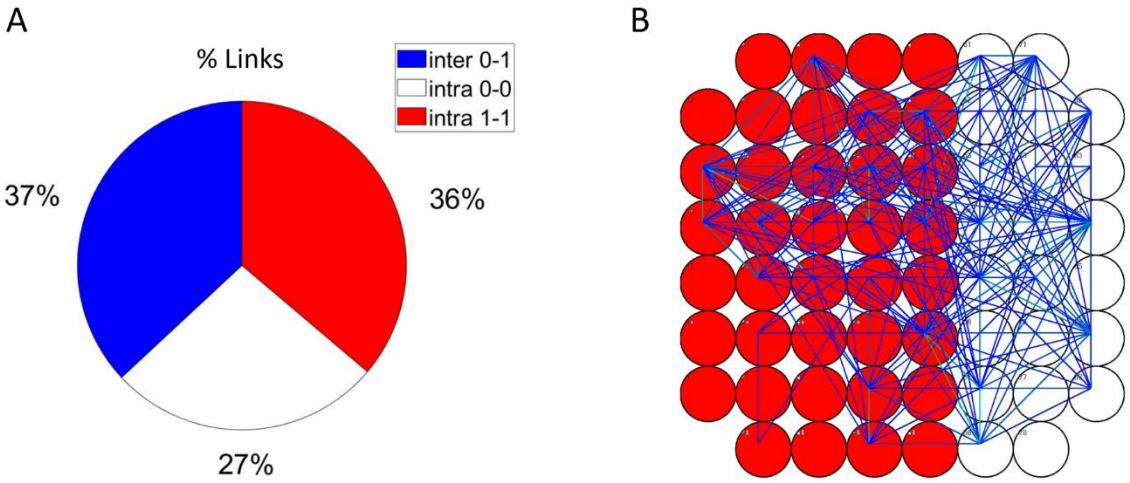

Figure 3.12. Functional connectivity of 3D neuronal networks. (A) Percentage of links intra- and inter-level of a 3D cortical neuronal culture evaluated during one representative experiment. Red and white slices represent the two different layer of the 3D neuronal network structure. (B) Connectivity map showing links intra- and inter-level of one experiment. Electrodes of the two levels are depicted in white (level 0) and red (level 1), respectively.

3.4.3.2 Electrophysiological Results from Mouse Acute Brain Slices

In this section, I successfully demonstrate the capability of the realized 3D-MEAs to record 4-AP-induced epileptiform-like and electrically-evoked activity in mouse acute brain slices. The potassium channel blocker 4-aminopyridine (4-AP) has been widely used as an *in-vitro* model of epilepsy for the last three decades (Avoli et al. 2002). This compound enhances neuronal activity and mimics the electroencephalographic activity recorded in patients affected by partial epilepsy. The bath application of 4-AP induces the progressive appearance of two major patterns of epileptiform activity, namely I-IC events and IC discharges (Boido et al. 2010, Gonzalez-Sulser et al. 2011, Ferrea et al. 2012, Medrihan et al. 2015, Chong et al. 2018). Standard interictal-like (I-IC) events are arbitrarily defined as discharges shorter than 1 s in duration. Typically, I-IC events are characterized by fast voltage oscillations (EPSPs/population spikes) followed by slow oscillations or negative shifts. Standard ictal-like (IC) events are identified as discharges with initially high-frequency voltage changes (tonic phase) followed by sporadic bursting activity (clonic phase). The duration of IC events usually ranges between 6 and 76 s.

Epileptiform discharges recorded in the 4-AP *in-vitro* epilepsy model are mediated by glutamatergic and GABAergic signalling. Both excitatory and inhibitory neurotransmissions modulate the frequencies and durations of these slow local field potentials (LFPs) discharges (Avoli et al. 2002). Especially, $GABA_A$ receptor signalling can be epileptogenic (Klaassen et al. 2006) and is required for the generation of interictal-like events in acute brain slices (Cohen et al. 2002). Indeed, in the 4-AP model, interictal-like events are blocked only when bicuculline, the competitive antagonist for $GABA_A$ receptors, is applied (Avoli et al. 2002). Thus, $GABA_A$ receptors play an important role in the 4-AP *in vitro* epilepsy model.

In this work, mouse acute brain slices were continuously perfused with ACSF-containing 4-AP (500 µM) throughout the all (n=3) experiments in order to induce such spontaneous epileptiform-like discharges.

I-IC and IC field potentials were successfully recorded by means of such 3D pillar-shaped gold MEAs. A comparison of the epileptiform-like activity recorded with both standard planar MEA (60 electrodes, 30 µm electrode diameter, 200 µm spaced) and the fabricated 3D pillar-shaped MEAs configurations was performed.

During the analysis, I-IC and IC events were identified according to the method described in the APPENDIX A.1. Then, the time course of the recorded epileptiform activity during a representative experiment has been depicted in a raster plot for all the three types of MEA technology taking into account (Figure 3.13 (A)).

Both I-IC and IC discharges were recorded with planar MEA and 3D-MEA all pillars (Figure 3.13 (B), (C), (D) and (E)). Instead, the 3D MEA half/half recordings only showed I-IC events with the absence of IC-like discharges (Figure 3.13 (F1) and (F2)). Interestingly, 3D pillar-shaped electrodes were able to record I-IC field potentials with amplitude higher than those obtained with 2D ones. As previously stated, such ability of the 3D pillar-shaped electrodes is mainly due to a better coupling between the tissue slice and the 3D pillar-shaped MEA chip. Noteworthy, 3D electrodes were also able to detect ictal-like discharges with amplitude and duration larger than the ones obtained with 2D counterparts.

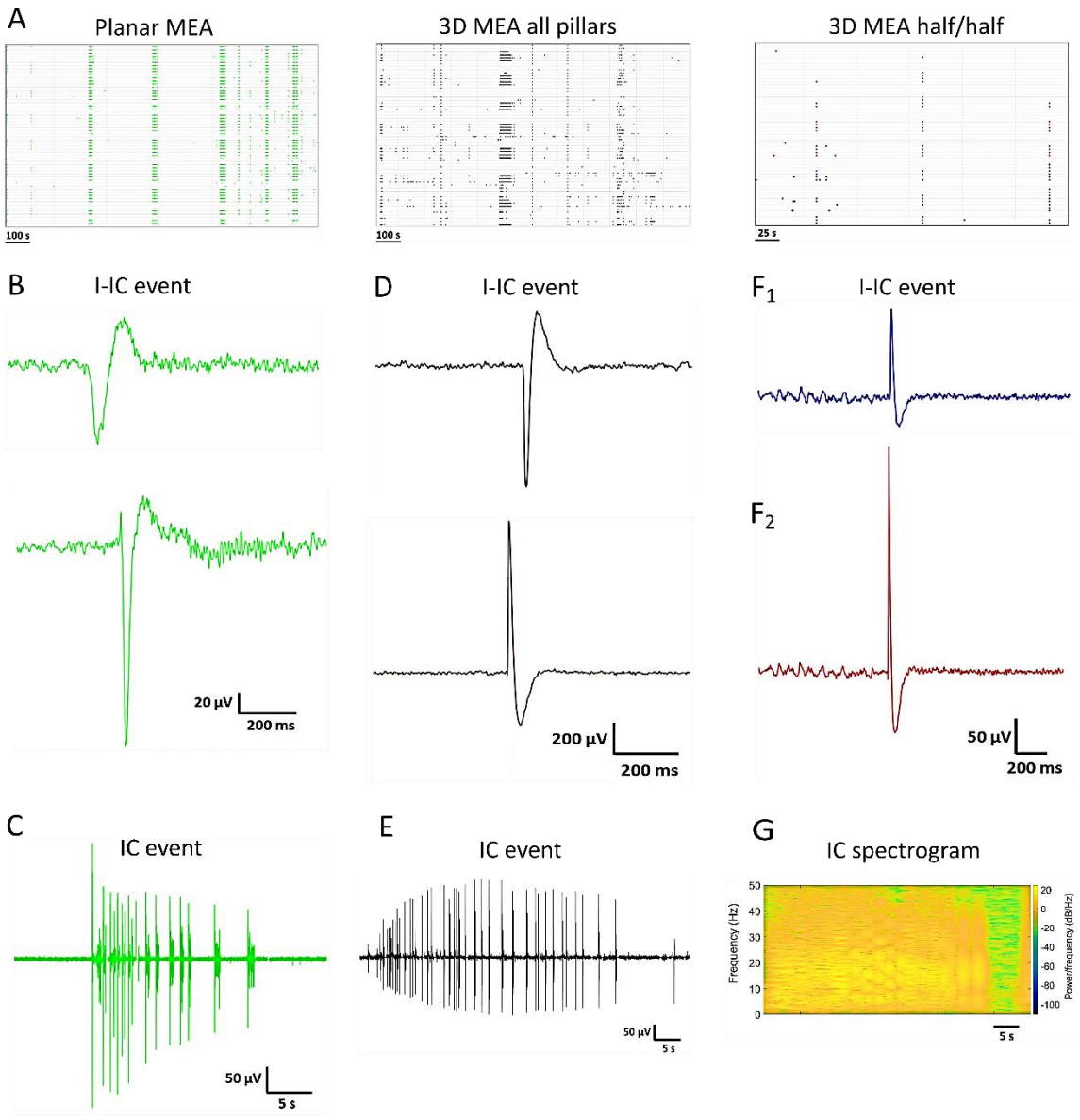

Figure 3.13. Characterization of 4-AP-induced epileptiform activity in mouse cortico-hippocampal brain slices. (A) Raster plot showing 4-AP-induced-epileptiform-like activity in mouse brain slices recorded by using planar MEA (left), 3D MEA all pillars (center) and 3D MEA half/half (right). (B) I-IC and (C) IC events recorded from one planar MEA representative channel. (D) I-IC and (E) IC events recorded from one 3D MEA all pillars representative channel. (F_1) and (F_2) represent an I-IC event recorded from one planar (blue trace) and 3D (red trace) representative channel of the 3D MEA half/half chip. (G) Spectrogram estimated from the IC trace reported in (E).

In the planar MEA recordings, the duration of ictal-like events typically ranged between 2 and 20 s. Instead, the IC discharges detected with 3D-MEA all pillars showed durations between 12 and 50 s.

Indeed, by looking at Figure 3.13 (E), it possible to observe an ictal-like event of about 50 seconds in duration recorded by using one 3D pillar-shaped electrode and the relative spectrogram, which highlights the high power content in the 1-50 Hz low-frequency band, is reported in Figure 3.13 (G).

To further characterize the epileptiform discharges recorded by using the fabricated 3D pillar-shaped MEAs in 4-AP *in-vitro* model, I performed spectral and amplitude analysis of such I-IC and IC events. Especially, to get insight the frequencies characterizing the recorded 4-AP-induced I-IC and IC activity, I analyzed the average power spectral density (PSD) of interictal- and ictal-like field potentials for both the 2D MEA and 3D-MEA all pillars configurations (Figure 3.14 (A) and (B)).

Mouse acute brain slices on 3D pillar-shaped electrodes exhibited both I-IC and IC events with higher power content in the 1-50 Hz band with respect to standard planar electrodes. In addition, I also estimated the mean power content of both I-IC and IC discharges in each brainwaves frequency band to further highlight the capability of the 3D pillar-shaped MEAs to record epileptiform-like events with larger power content than those obtained with 2D ones (Figure 3.14 (C) and (D)). The same evaluation approach was employed to characterize the epileptiform-like events recorded with the 3D MEA half/half chips. Figures 3.14 (G) and (H) represent the average PSD and power content estimation of I-ICs computed for both the 2D and 3D pillar-shaped electrodes of a 3D MEA half/half device, respectively. Here again, I found that slices on 3D electrodes showed I-ICs with higher power content than those arranged on 2D ones.

Such ability of the 3D pillar-shaped MEA devices to detect events with higher power content as compared to standard planar electrode arrays is mainly due to an enhanced coupling between the tissue slice and the top side of such pillar-shaped microelectrodes. As previously stated, such coupling between slice and 3D electrodes allow to improve recording and stimulation conditions in acute slices and thus, detecting of stronger signals with larger amplitudes.

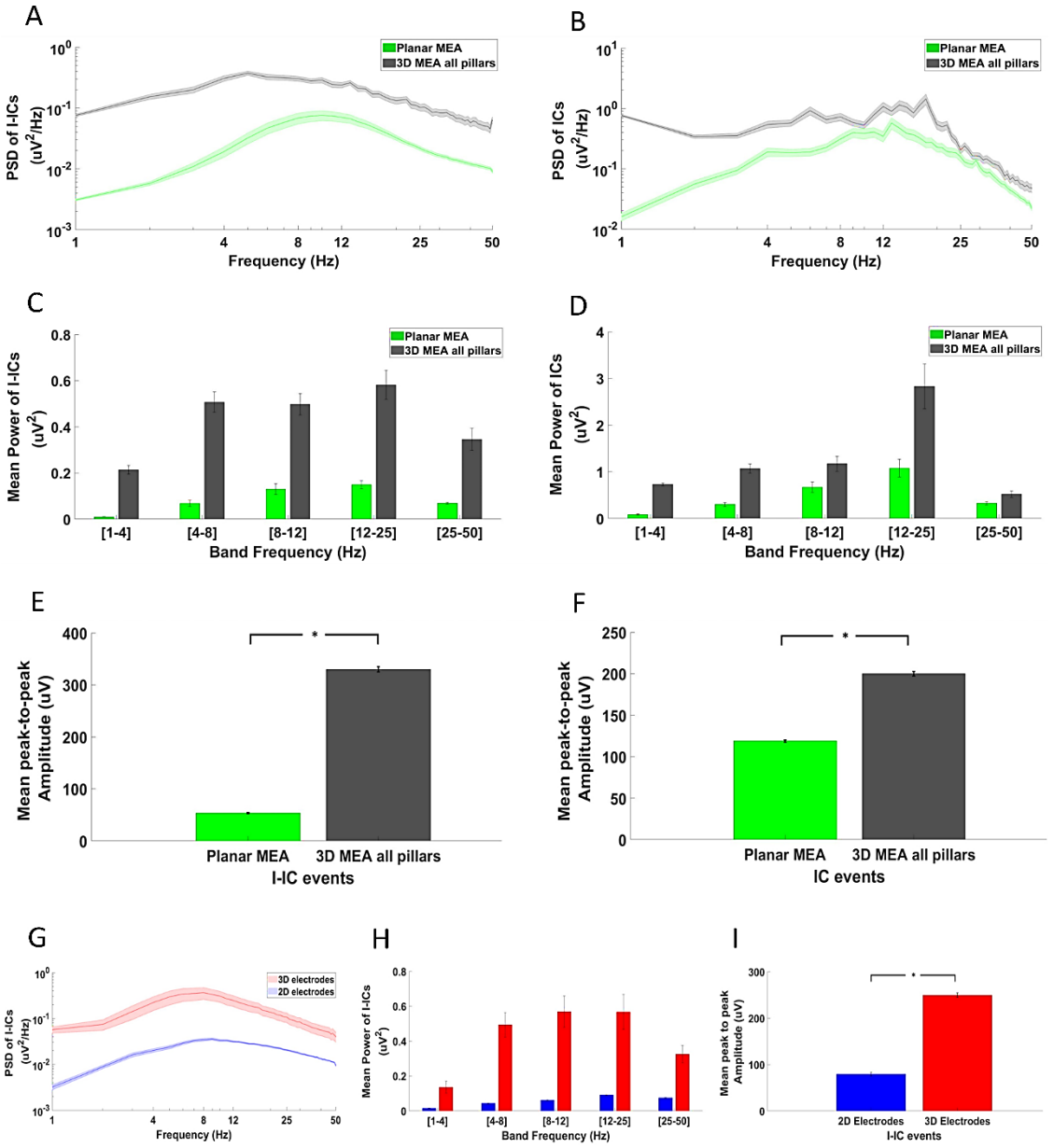

Figure 3.14. Spectral and Amplitude analysis of 4-AP-induced epileptiform activity in mouse cortico-hippocampal brain slices. (A)-(B) average power spectral density (PSD) estimated from the I-IC and IC events and evaluated for both planar MEA (green trace) and 3D MEA all pillars (dark trace) in the 1-50 Hz frequency band. (C)-(D) mean power content of I-IC and IC events estimated for both planar MEA (green bars) and 3D MEA all pillars (dark bars) and evaluated in each brainwave frequency band. (E)-(F) mean peak-to-peak amplitude of I-IC and IC events evaluated for both 2D MEA (green bar) and 3D MEA all pillars (dark bar). (G) average power spectral density (PSD) of I-IC traces evaluated for both planar (blue trace) and 3D electrodes (red trace) of a 3D MEA half/half. (H) mean power content of I-ICs evaluated for both 2D (blue bars) and 3D (red bars) electrodes of a 3D MEA half/half and estimated in each brainwave frequency band. (I) average peak-to-peak amplitude of I-ICs estimated for both 2D and 3D electrodes of a 3D MEA half/half. Asterisks above the plots indicate statistically significant differences. (*$P_{VALUE} < 10^{-3}$, Mann-Whitney U-test).

To further validate experimentally the developed 3D pillar-shaped MEA devices, I performed amplitude analysis of the epileptiform-like discharges induced by 4-AP in acute mouse brain slices. In Figures 3.14 (E) and (F) is reported the average peak-to-peak amplitude of interictal- and ictal-like discharges evaluated for both the planar MEA and 3D MEA all pillars configuration, respectively.

In both cases, I observed the capability of the 3D pillar-shaped electrodes to record epileptiform activities with higher amplitude than the one obtained with 2D counterparts. For the sake of clarity, the amplitude of an IC-like discharge has been calculated as mean of the peak-to-peak amplitudes of the all voltage oscillations included in the IC event under investigation.

In Figure 3.14 (I) is further stressed the ability of the 3D pillar-shaped electrodes to detect I-IC activity with larger amplitude as compared to planar electrodes in the case of 3D MEA half/half devices.

To further support the previously presented results and to ultimately demonstrate the capability of 3D pillar-shaped MEAs devices to record electrophysiological signals from acute brain slices, I performed experiments by delivering electrical stimulation on mouse (n=2) cortico-hippocampal brain slices. As previously reported in the section 3.3.5.1, stimulations were carried out with a frequency of 0.3 Hz for 5 min by using voltage biphasic pulses of ±1500 mV amplitudes and lasting 100 µs. Such voltage pulses were applied through one MEA electrode to locally stimulate the slice. The other electrodes were used for extracellular recording of the evoked activity in the slice. In Figure 3.15 (A, left) and (B, left) is shown a subset of the most responsive channels of a planar MEA and 3D MEA all pillars with the corresponding electrically-evoked activities that the slice exhibited in response to the applied stimulation, respectively.

The evoked response recorded from one representative 2D and 3D channel is reported in Figure 3.15 (A, right) and (B, right), respectively. The vertical red bar indicates the time from which the stimulation is delivered on the slice. Interestingly, in the case of stimulation delivered from 2D MEA, the slice response to the stimulus is similar for all the responding channels. Instead, when the stimulation is delivered from one electrode of the 3D MEA all pillars, the electrodes display a more pronounced variability.

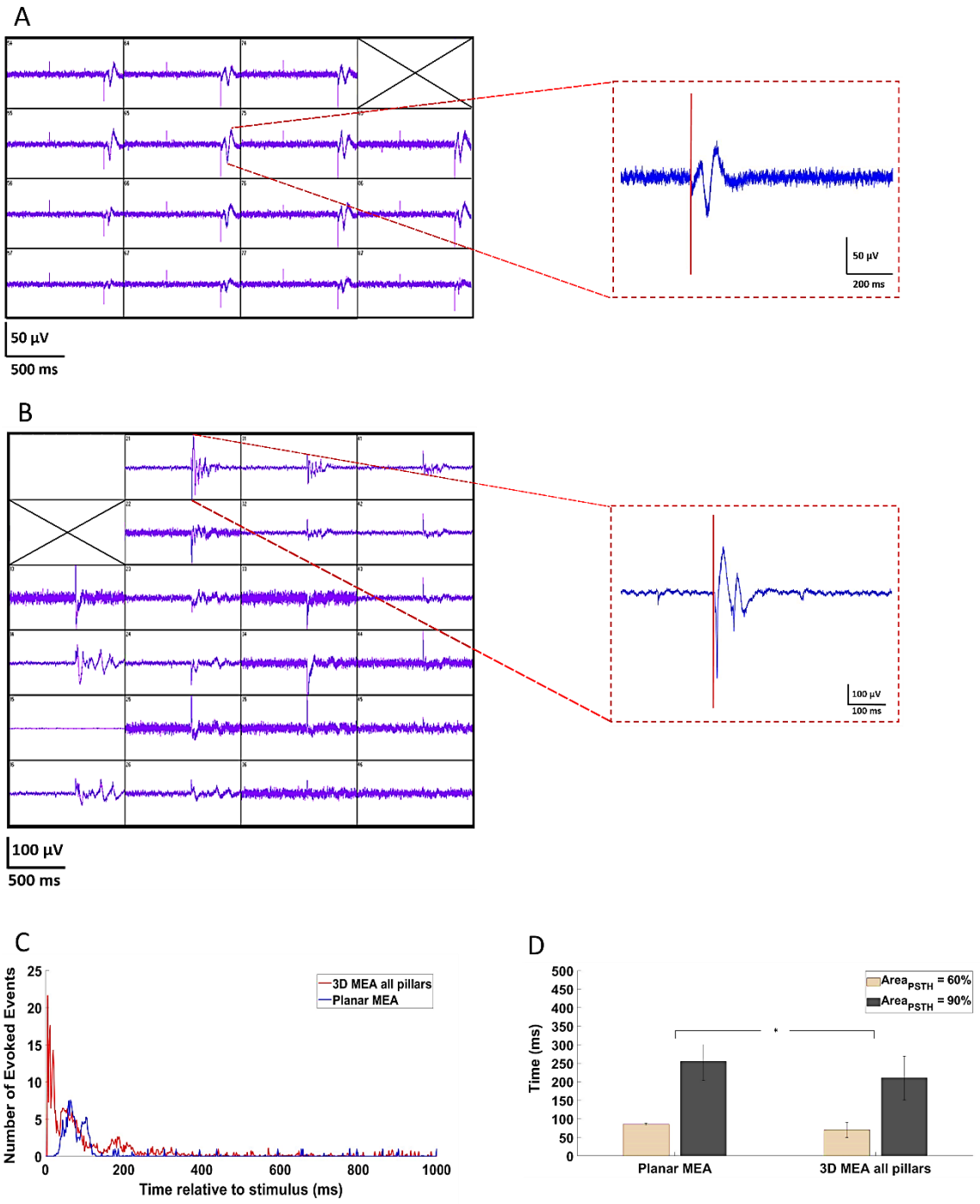

Figure 3.15. Mouse cortico-hippocampal brain slice response to electrical stimulation. (A) subset of the most responsive electrodes of planar MEA (left) and acute brain slice response to stimulation recorded from one representative 2D channel (right). (B) subset of the most responsive electrodes of 3D MEA all pillars (left) and acute brain slice response to stimulation recorded from one representative 3D channel (right). The cross indicates the electrode position from which the stimulus is delivered. (C) Mean PSTH profiles evaluated over all the most responsive channels of planar (blue) and 3D (red) MEA. (D) Time occurring to generate 60% and 90% of the response to stimulation for 2D and 3D MEA. Asterisks above the plots indicate statistically significant differences. (*$P_{VALUE} < 10^{-3}$, Mann-Whitney U-test).

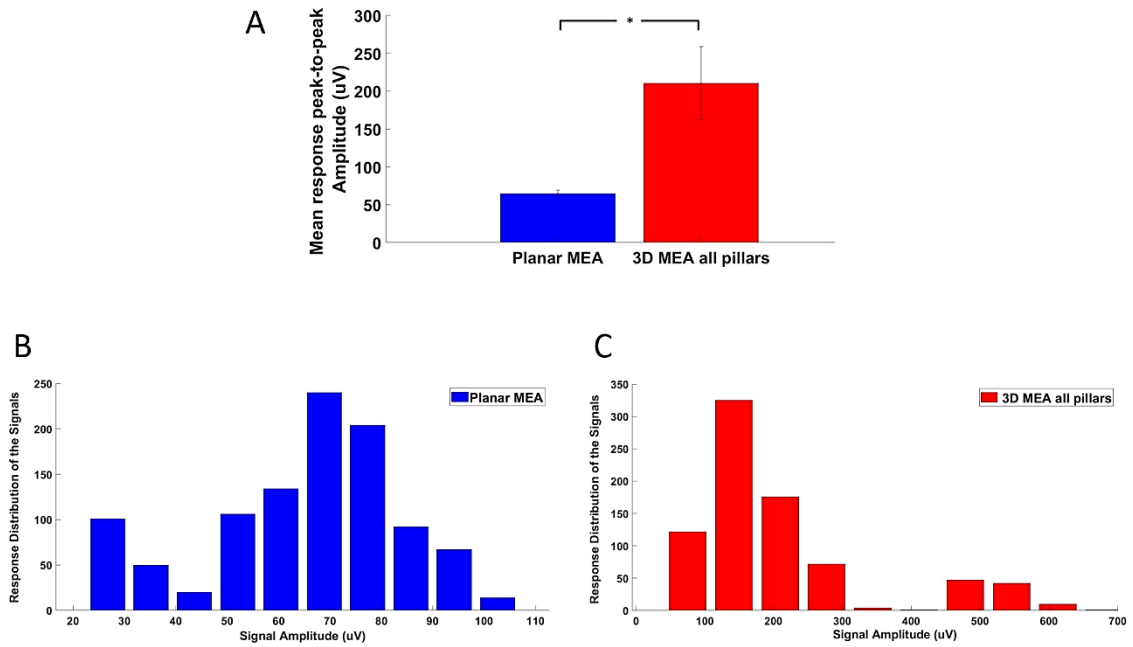

Figure 3.16. Mouse acute brain slice response to electrical stimulation. (A) Mean Peak-to-peak amplitude of the electrically-evoked responses to stimulation for 2D (blue) and 3D (red) MEA. (B) and (C) represent the response peak-to-peak amplitudes distribution of planar and 3D MEA, respectively. Asterisks above the plots indicate statistically significant differences. (*$P_{VALUE} < 10^{-3}$, Mann-Whitney U-test).

To quantify and examine the different response modes of the slice when the stimulation is delivered from one electrode of the planar MEA and 3D MEA all pillars, I evaluated the Post Stimulus Time Histogram (PSTH) averaged over all the most responsive channels of both the MEA configurations (Figure 3.15 (C)).

In the case of stimulation delivered from 3D electrode, the slice response is faster and closer to the stimulation time with respect to the planar electrode stimulation case. Moreover, the highest response peak (i.e. the maximum of the evoked response) was detected immediately after the stimulation in about 6 ms. Then, the number of evoked events exhibited a decreasing trend that goes to zero in about 400 ms. Instead, when the slice is stimulated from 2D electrodes, the evoked response is slower and more delayed than the one recorded with 3D electrodes and reaches the peak in about 70 ms.

To further stress the ability of 3D pillar-shaped electrodes to detect electrically-evoked responses faster than those obtained with 2D ones, I evaluated and compared the t_{60} and t_{90} (time delay to have the 60% and 90% of the response to stimulation, respectively) value averaged over all the most responding channels (Figure 3.15 (D)).

These time values are reported for slices stimulated from both the planar MEA and 3D MEA all pillars. I observed that slices stimulated from 2D electrodes exhibited t_{60} and t_{90} values higher than those obtained with stimulation delivered from 3D electrodes. Furthermore, I performed a peak-to-peak amplitude analysis of the evoked responses evaluated over all the most responding channels for both planar MEA and 3D MEA all pillars configurations. As previously demonstrated, here again, I found that 3D pillar-shaped electrodes were able to record electrically-evoked signals with amplitude higher than the one obtained with the 2D counterparts (Figure 3.16 (A)).

In Figures 3.16 (B) and (C), I also reported the peak-to-peak amplitudes distribution of the evoked responses for both planar and 3D MEA all pillars, respectively. It can be noticed that signals obtained with 3D pillar-shaped electrodes show a shift to the right, i.e. to larger response amplitudes.

In this way, I further demonstrate and point out the capability and ability of 3D pillar-shaped MEAs to successfully record stronger and larger extracellular signals from mouse acute brain slices allowing better recording and stimulation conditions without slice penetration and damage and/or laceration of the tissue slice with respect to previously reported 3D tip-shaped electrode arrays.

3.5 Discussion and Conclusion

Microelectrode arrays represent an important tool to study *in-vitro* neuronal cultures and acute brain slices. *In-vitro* models of neuronal cultures have become popular in physiology and pharmacology as they show better performance metrics compared with their *in-vivo* counterparts. The research standard for MEAs are planar MEAs but these suffer from rapid data attenuation in the z-direction when stimulating/recording from 3D dissociated neuronal networks or tissue slices. Thus, three-dimensional MEAs are required for interfacing with these types of 3D *in-vitro* neuronal systems.

In this chapter, I have successfully demonstrated an innovative microfabrication process simple, flexible and easy to be implemented. It allows to realize layout of 3D pillar-shaped microelectrodes with different heights by exploiting the electrodeposition through the holes realized in a pre-selected thick photoresist placed on the top side of a standard planar MEA.

In this way, it is possible to obtain arrays of 3D pillar-shaped microstructures with a height of 100 µm, 150 µm or more than 200 µm by changing the thickness of the photoresist. In this work, an array of 60 pillar-shaped gold microelectrodes of height 105 ± 5 µm and a simple gradient structure composed of planar and 3D 100-µm-high pillar-shaped gold microelectrodes have been developed to perform preliminary electrophysiological characterization of such 3D devices from 3D engineered *in-vitro* neuronal networks and acute brain slices.

I have further successfully demonstrated electrical characterization of such 3D-MEA chips by using an electrochemical impedance spectroscopy experimental setup to carry out impedance measurements of the electrodes.

Advantages of these new 3D pillar-shaped gold MEAs with respect to standard planar MEAs and previously reported 3D-MEA technologies for use with acute brain slices have been showed and explained in details.

Moreover, I have validated experimentally the fabricated 3D-MEAs by performing *in-vitro* tests with 3D engineered neuronal cultures and mouse acute brain slices.
I have successfully demonstrated the capability and ability of these 3D pillar-shaped gold MEAs to record electrophysiological spontaneous activity from 3D neuronal networks and both 4-AP-induced epileptiform-like and electrically-evoked activity from mouse acute brain slices.

Results showed that stronger signals with larger amplitudes and higher power content can be obtained by using such 3D pillar-shaped electrode devices with respect to 2D counterparts. Such ability of the developed 3D-MEAs chips is mainly due to an enhanced tissue slice coupling to the planar round-shaped top surface area of the fabricated 3D electrodes.

I believe this new 3D-MEA technology can represent a good and alternative non-invasive tool able to perform electrophysiological measurements from 3D *in-vitro* neuronal structures like 3D neuronal networks and acute brain slices, allowing better recording and stimulation performances as compared to planar electrode arrays and previously developed invasive 3D-MEA technologies.

References

Avoli M., D'Antuono M., Louvel J., Köhling R., Biagini G., Pumain R., D'Arcangelo G., Tancredi V. (2002). Network and pharmacological mechanisms leading to epileptiform synchronization in the limbic system in vitro. *Prog Neurobiol,* 68:167–207.

Bischofberger J., Engel D., Li L., Geiger J.R., Jonas P. (2006). Patch-clamp recording from mossy fiber terminals in hippocampal slices. *Nat Protoc,* vol. 1, no. 4, pp. 2075-81.

Boido D., Farisello P., Cesca F., Ferrea E., Valtorta F., Benfenati F., Baldelli P. (2010). Cortico-hippocampal hyperexcitability in synapsin I/II/III knockout mice: Age-dependency and response to the antiepileptic drug levetiracetam. *Neuroscience,* 171(1):268-83.

Cohen I., Navarro V., Clemenceau S., Baulac M., Miles R. (2002). On the origin of interictal activity in human temporal lobe epilepsy in vitro. *Science,* vol. 298, pp. 1418-1421.

Chong S.-Ah., Balosso S., Vandenplas Ca., Szczesny G.. Hanon E., Claes K., Van Damme X., Danis B., Van Eyll J., Wolff C., Vezzani A., Kaminski R. M., and Niespodziany I. (2018). Intrinsic Inflammation Is a Potential Anti-Epileptogenic Target in the Organotypic Hippocampal Slice Model. *Neurotherapeutics,* vol. 15, no. 2, pp. 470-488.

Dragas J., Viswam V., Shadmani A., Chen Y., Bounik R., Stettler A., Radivojevic M., Geissler S., Obien M., Müller J., and Hierlemann A. (2017). A Multi-Functional Microelectrode Array Featuring 59760 Electrodes, 2048 Electrophysiology Channels, Stimulation, Impedance Measurement and Neurotransmitter Detection Channels. *IEEE J Solid-State Circuits,* vol. 52, pp. 1576–1590.

Franks W., Schenker I., Schmutz P., and Hierlemann A. (2005). Impedance characterization and modeling of electrodes for biomedical applications. *IEEE Trans. Biomed. Eng.,* vol. 52, no. 7, pp. 1295–1302.

Ferrea E., Maccione A., Medrihan L., Nieus T., Ghezzi D., Baldelli P., Benfenati F., and Berdondini L. (2012). Large-scale, high-resolution electrophysiological imaging of field potentials in brain slices with microelectronic multielectrode arrays. *Frontiers in neuronal circuits,* vol. 6 80.

Farisello P., Boido D., Nieus T., Medrihan L., Cesca F., Valtorta F., Baldelli P., Benfenati F. (2012). Synaptic and extrasynaptic origin of the excitation/inhibition imbalance in the hippocampus of synapsin I/II/III knockout mice. *Cereb Cortex,* vol. 23, no. 3, pp. 581-93.

Frega M., Tedesco M., Massobrio P., Pesce M., and Martinoia S. (2014). Network dynamics of 3D engineered neuronal cultures: a new experimental model for in-vitro electrophysiology. *Scientific Reports 4,* Article number: 5489.

Gonzalez-Sulser A., Wang J., Motamedi G.K., Avoli M., Vicini S., Dzakpasu R. (2011). The 4-aminopyridine in vitro epilepsy model analyzed with a perforated multi-electrode array. *Neuropharmacology,* 60(7-8):1142-53.

Gu J. and McFarlane N. (2015). A Low Power Multi-Frequency Current Mode Lock-in Amplifier for Impedance Sensing. *IEEE International Instrumentation and Measurement Technology Conference (I2MTC) Proceedings.*

Heuschkel M.O., Fejtl M., Raggenbass M., Bertrand D., and Renaud P. (2002). A three-dimensional multi-electrode array for multi-site stimulation and recording in acute brain slices. *Journal of Neuroscience Methods,* vol. 114, no. 2, pp. 135-148.

Klaassen A., Glykys J., Maguire J. (2006). Seizures and enhanced cortical GABAergic inhibition in two mouse models of human autosomal dominant nocturnal frontal lobe epilepsy. *Proc. Natl. Acad. Sc.,* vol. 103, pp. 19152-19157.

Merrill D. R. and Tresco P. A. (2005). Impedance Characterization of Microarray Recording Electrodes in Vitro. *IEEE Trans. Biomed. Eng.,* vol. 52, no. 11.

Medrihan L., Ferrea E., Greco B., Baldelli P., and Benfenati F. (2015). Asynchronous GABA Release Is a Key Determinant of Tonic Inhibition and Controls Neuronal Excitability: A Study in the Synapsin II−/− Mouse". *Cerebral Cortex October,* vol. 25, pp. 3356-3368.

Puia T. S., Chena Y., Wonga C. C., Nadipalli R., Weerasekera R., Arya S. K., Yu H., Rahman A. R.A. (2013). High density CMOS electrode array for high-throughput and automated cell Counting. *Sensors and Actuators B Chemical.*

Park S., Lee Y. J. (2015). Precision Electrical Measurement Experiment Using a Lock-in Amplifier that is Suitable for Science and Engineering Undergraduates. *New Physics: Sae Mulli,* vol. 65, no. 4, pp. 328-332.

Pastore V.P., Godjoski A., Martinoia S., Massobrio P. (2018). SPICODYN: A Toolbox for the Analysis of Neuronal Network Dynamics and Connectivity from Multi-Site Spike Signal Recordings. *Neuroinformatics,* vol. 16, no. 1, pp. 15-30.

Rajaraman S., Choi S.-O., McClain M. A., Ross J. D., LaPlaca M. C., and Allen M. G. (2011). Metal-Transfer-Micromolded Three-Dimensional Microelectrode Arrays for *in-vitro* Brain-Slice Recordings. *Journal of microelectromechanical systems,* vol. 20, no. 2.

Rocha P. R. F., Schlett P., Kintzel U., Mailänder V., Vandamme L. K. J., Zeck G., Gomes H. L., Biscarini F., and De Leeuw D. M. (2016). Electrochemical noise and impedance of Au electrode/electrolyte interfaces enabling extracellular detection of glioma cell populations. *Scientific Reports,* vol. 6, a. n. 34843.

Tedesco M.T., Di Lisa D., Massobrio P., Colistra N., Pesce M., Catelani T., Dellacasa E., Raiteri R., Martinoia S., Pastorino L. (2018). Soft chitosan microbeads scaffold for 3D functional neuronal networks. Biomaterials, vol. 156, pp. 159-171.

Viswa V., Bounik R., Shadmani A., Dragas J., Jan M., Chen Y.,b, and Hierlemann A. (2016). 32-Channel Integrated Electrical Impedance Sensors on a Multifunctional Neural Microelectrode Array Platform. *Procedia Engineering,* vol. 168, pp. 510 – 513.

Xu J., Meynants G., Merken P. (2009). Low-power lock-in amplifier for complex impedance measurement. *3rd International Workshop on Advances in sensors and Interfaces.*

Chapter 4

CONCLUSIONS

4.1 Summary of this Research

In this dissertation, I presented a new three-dimensional microelectrode array (3D-MEA) for *in-vitro* electrophysiological applications.

The main goal of this work was the design, development, and characterization of innovative and truly 3D pillar-shaped gold MEAs for interfacing with 3D *in-vitro* neuronal structures. Associated goals of this research included the study and characterization of new *in-vitro* experimental models constituted of 3D engineered neuronal networks coupled to both 2D- and 3D-MEAs.

Chapter 1 outlined the goals of this dissertation and concluded with an overview of this work.

Chapter 2 provided a detailed description of the MEA technology for *in-vitro* neuronal interfacing. Firstly, an overview of the state-of-the-art of various planar or 2D-MEA technologies developed by various researchers around the world in the last 35 years is provided. Secondly, the *in-vitro* applications of such 2D-MEAs are reported. A brief introduction of 2D *in-vitro* neuronal models is first shown. Then, an overview of the main works dealing with 3D engineered *in-vitro* neuronal models developed in the last ten years is presented. Subsequently, the study and characterization of a new experimental paradigm composed of 3D chitosan engineered neuronal network coupled to planar MEA are reported. In a first work, an innovative approach for designing 3D engineered *in-vitro* neuronal cultures based on the assembly of chitosan microbeads is presented. Specifically, 3D neuronal constructs were developed and implemented by using two types of chitosan microparticles: neutralized chitosan and cross-linked chitosan with tripolyphosphate (TPP). Then, a detailed network dynamics characterization of such new 3D *in-vitro* neuronal models is provided. In a second reported work, the use of chitosan microbeads has been further explored and exploited to actively support 3D functional neuronal cultures coupled to planar MEAs. Chitosan microbeads based scaffolds were specifically optimized and adapted in order to be integrated onto planar MEAs to study and better understand the functional properties of biomimetic 3D hippocampal networks. In the last section of chapter 2, the state-of-art of integrated microfabrication approaches used for the development of *in-vitro* 3D-MEAs is presented. Finally, a detailed study and characterization of a complete 3D-3D *in-vitro* neuronal model composed of 3D engineered neuronal networks coupled to innovative 3D-MEA devices is provided. Such novel 3D-MEAs constituted by 3D gold ball-shaped microstructures positioned at different heights (i.e. gradient structure composed of planar, 50-µm-, 100-µm- and 150-µm-high gold ball-shaped microelectrodes) are used to study and analyze the dynamics and functional connectivity of 3D *in-vitro* hippocampal neuronal networks grown onto glass microbeads based-scaffold.

Chapter 3 presented a novel three-dimensional microelectrode array (3D-MEA) designed and developed in this dissertation – pillar-shaped gold 3D-MEA. The design of such 3D-MEA included 60 pillar-shaped gold microelectrodes of height 105 ± 5 µm and a diameter of about 60 µm and 45 µm at the top and bottom side, respectively.

Specifically, it was first realized a standard 60-channel planar MEA (60 µm in diameter, 200 µm inter-electrode distances) on borosilicate glass substrate. Then, 3D pillar-shaped gold microstructures were developed onto the top of such planar MEA by means of standard photolithography and gold electroplating processes. The top side of such pillar-shaped microelectrodes represented the only conductive area of the chip exposed to the direct contact of the active cells. The other parts (tracks, sidewalls of the pillars) of the fabricated 3D chips were completely passivated by using an oxide bi-layer (SiO_2 and TiO_2). Moreover, 3D-MEA devices with a simple gradient structure composed of both planar and 3D 100-µm-high pillar-shaped gold microelectrodes were realized.

Then, electrical characterization based on an electrochemical impedance spectroscopy experimental setup was performed to carry out impedance measurements of the electrodes of the developed 3D-MEAs.

Advantages of these new 3D pillar-shaped gold MEAs with respect to standard planar MEAs and previously reported 3D-MEA technologies for use with *in-vitro* acute brain slices were also showed and explained in details.

In addition, *in-vitro* tests with 3D engineered neuronal cultures and mouse acute brain slices were performed to experimentally validate the fabricated 3D-MEA devices. Preliminary electrophysiological characterization of such 3D pillar-shaped gold MEAs with 3D engineered *in-vitro* cortical neuronal networks was successfully carried out. Moreover, the capability and ability of these new 3D-MEAs to record both 4-AP-induced epileptiform-like and electrically-evoked activity from mouse acute brain slices were successfully demonstrated.

4.2 Recommendations for Future Research

The work presented in this dissertation mainly focuses on the design, microfabrication, and characterization of a new 3D pillar-shaped gold MEA and applications of this technology in the *in-vitro* environment.

Future directions of this research could take several forms. Firstly, the microfabrication process of the fabricated 3D-MEA devices needs to be optimized and further improved. The use of SU-8 negative-tone photoresist as a passivation layer to insulate the surface of the conductive tracks of such 3D chips from the direct contact of the active cells showed several drawbacks while interfacing with 3D *in-vitro* neuronal cultures (see APPENDIX

B for details).

Under incubator conditions, it has been observed an adhesion leak of SU-8 and a stripping of such a material from the underlying glass substrate. To this aim, new materials (e.g. humidity-resistant and/or long-term resistant materials) as passivation layers of the tracks should be tested and further explored. In addition, the compatibility of such materials with the underlying glass substrate should be verified. On the other hand, new substrates (e.g. plastic materials), embedding the 3D-MEAs, should be further explored and tested.

Moreover, new challenges are addressed to the design and development of more complex gradient structure 3D-MEA devices to accommodate the current and future needs of the *in vitro* electrophysiological, neurophysiological, and pharmacological communities. Arrays of 3D electrodes with different heights are required for use with 3D *in-vitro* neuronal cultures. Gradient structures composed of both planar, 50-µm-, 100-µm-, 150-µm-high electrodes and more than 200 µm could be developed to record the electrophysiological activity of 3D neuronal networks from different locations in the 3D space and thus, study and better understand how the network dynamics changes in different layers of the 3D neuronal structure. In this way, a more complete 3D-3D *in-vitro* neuronal model can be obtained. Moreover, such a system could be considered a more physiological model of a real brain structure and it could be further engineered to constitute bio-hybrid microsystems towards the development of brain-on-a-chip for neurophysiological investigations. Furthermore, it could be used as an operational platform to study brain pathologies or pharmacological treatments.

APPENDIX A

DATA ANALYSIS

A.1 Mouse Acute Brain Slices activity Analysis

All the analysis algorithms used to study the recorded activity from mouse acute brain slices were developed as MATLAB scripts (The Mathworks, Natick, MA, USA). Especially, the acquired raw signals were first band-pass filtered from 1-200 Hz with a 2nd order Butterworth filter and a notch filter was designed to remove 50 Hz noise from the signals. Filtered data were then down-sampled to 1000 Hz sampling rate. In addition, a specific algorithm was implemented to remove all the voltage artifacts from the filtered and down-sampled data. 4-AP-induced epileptiform-like discharges (I-IC and IC events) were detected from the obtained data without artifacts by using the MATLAB findpeaks function. Especially, the threshold used for the I-IC and IC events detection procedure was computed by means of a custom software package named SpyCode

(Bologna et al. 2010) developed in MATLAB. Moreover, the refractory period was carefully set to detect each slow local field potential as unique event.

Then, spectral and peak-to-peak amplitude analysis of the I-IC and IC events were performed. Amplitude analysis was also performed in the case of stimulation from the mouse acute brain slices. Data were expressed as mean ± standard error of the mean. Statistical analysis was performed to determine significant differences between each sample pairs by using MATLAB. Since data did not follow a normal distribution (evaluated by the Kolmogorov-Smirnov normality test), I performed a non-parametric Mann-Whitney U-test.

A.2 3D Neuronal Networks activity Analysis

Regarding the analysis of the recorded activity from 3D *in-vitro* neuronal cultures, I used a custom software package named SpyCode (Bologna et al. 2010), developed in MATLAB (The Mathworks, Natick, MA, USA). Spike detection was performed by using the Precise Timing Spike Detection (PTSD) algorithm (Maccione et al. 2009). The algorithm requires three parameters: a different threshold set to 8 times the standard deviation of the baseline noise, a peak lifetime period (set at 2 ms) and a refractory period (set at 1ms). To analyze and characterize the electrophysiological activity of 3D neuronal networks, some first-order statistics were extracted. In particular, the mean firing rate (MFR), i.e. the number of spikes per second of each channel and the percentage of random spikes, i.e. the fraction of spikes outside bursts were evaluated. Moreover, burst detection was performed according to the method described by Pasquale et al. (Pasquale et al. 2010). A burst is a sequence of spikes having an ISI (inter-spike interval, i.e., time intervals between consecutive spikes) smaller than a reference value (set at 100 ms in the experiments), and containing at least a minimum number of consecutive spikes (set at 5 spikes). The parameters extracted from this analysis were the mean bursting rate (MBR) and the mean burst duration (MBD), which are the frequency and the duration of the bursts at the single channel level respectively. The same approach used for the detection of bursts was applied for the detection of quasi-synchronous events at network level called network bursts (Bologna et al. 2010). The extracted parameters were the network bursting rate (NBR) and the network burst

duration (NBD). NBR computes the number of network bursts per minute, while NBD is the temporal extension of these events. Data were expressed as mean ± standard error of the mean. Statistical analysis was performed to determine significant differences between each sample pairs by using MATLAB. Since data did not follow a normal distribution (evaluated by the Kolmogorov-Smirnov normality test), I performed a non-parametric Mann-Whitney U-test.

APPENDIX B

SU-8 stripping from glass substrate

Many MEMS (Micro Electro Mechanical Systems) devices require processing of thick photoresist for the development of new microstructures with high aspect ratios.
SU-8 is a popular material in the MEMS field with single and multi-layer fabrication technologies reported by various researchers to achieve complex MEMS structures. Such a material has been widely used for many MEMS applications including microfluidics, mechanical structures like micro-gears, rigid molds for micromolding, etc. SU-8 is a resist consists of a polymeric epoxy resin by dissolving in an organic solvent and adding a photo-acid generator. Thanks to its high sensitivity, high transparency, excellent chemical resistance, good compatibility with electroplating, highly uniform coating, vertical sidewalls, low edge bead, SU-8 appears to be an ideal photoresist for MEMS fabrication.

In this dissertation, such a material has been employed as passivation layer to insulate the surface of the conductive tracks of the fabricated 3D-MEA devices from the direct contact of the active cells.

However, despite these clear and evident advantages, SU-8 showed several drawbacks while interfacing with 3D *in-vitro* neuronal cultures.

It has been noticed that SU-8 does not sustain the incubator conditions at 37 °C, 5% CO_2, 95% humidity after about two weeks. This step is mandatory to maintain cells alive and to guarantee their growth and differentiation for at least three weeks (at this age cells typically reach a stable maturation and are ready for recordings).

Specifically, under such incubator conditions, it has been observed that a lot of strengths appear inside the SU-8 photoresist, which create cracks on the surface or even delamination of the layer. These phenomena resulted in an adhesion leak and thus a stripping of the SU-8 layer from the underlying glass substrate.

In Figure B.1 (A) is showed how the Neurobasal medium (violet color), used for long-term maintenance of neuronal cell population, flows through the SU-8 cracks reaching the device boundaries. As previously stated, this phenomenon is mainly due to the adhesion leak of SU-8 from the galls substrate, which causes an SU-8 stripping under incubator conditions.

This is further highlighted in Figure B.1 (B), where the black arrow indicates the SU-8 stripping from the underlying glass substrate. Moreover, Figure B.1 (C) represents an enlargement of the previous Figure B.1 (B), where black arrows indicate fragments of SU-8 stripped away. In Figure B.1 (D), it is stressed the step before the SU-8 stripping which occur under incubator conditions.

These problems made impossible to perform good recordings and analysis. Possible solutions to overcome such drawbacks could be changing the passivation layer of the signal lines (e.g. humidity-resistant and/or long-term resistant materials) or changing the underlying glass substrate of the 3D chips (e.g. plastic materials).

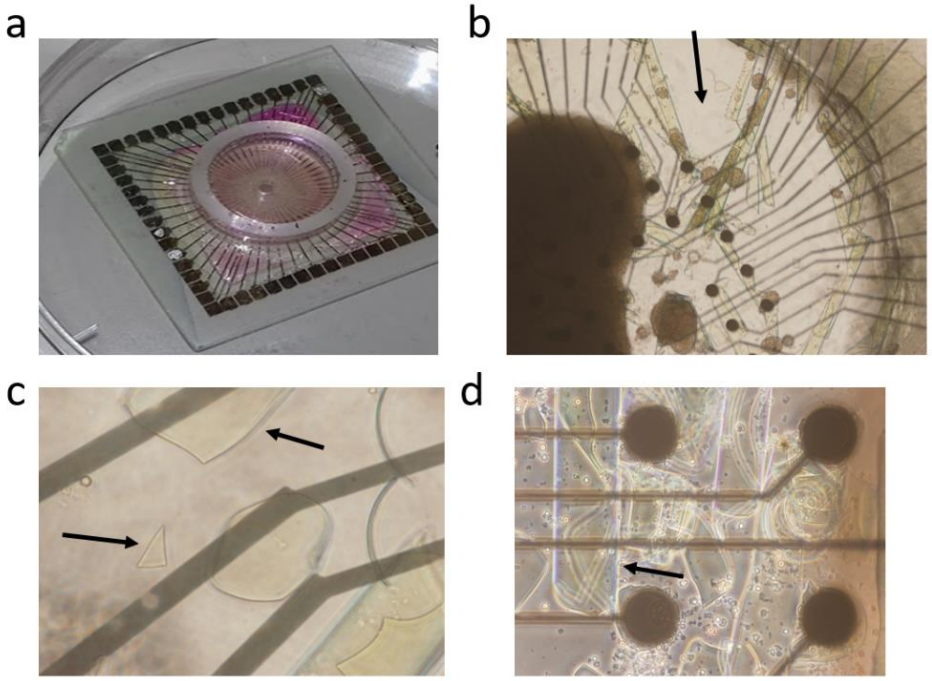

Figure B.1. (a), (b), (c) and (d) showing problems related to SU-8 stripping from the underlying glass substrate.

References

Bologna L. L., Pasquale V., Garofalo M., Gandolfo M., Baljon P. L., Maccione A., Martinoia S., and Chiappalone M. (2010). Investigating neuronal activity by SPYCODE multi-channel data analyzer, *Neural Netw,* vol. 23, pp. 685-97.

Maccione A., Gandolfo M., Massobrio P., Novellino A., Martinoia S., and Chiappalone M. (2009). A novel algorithm for precise identification of spikes in extracellularly recorded neuronal signals. *Journal of Neuroscience Methods,* vol. 177, pp. 241-249.

Pasquale V., Martinoia S., Chiappalone M. (2010). A self-adapting approach for the detection of bursts and network bursts in neuronal cultures. *J. Comput. Neurosci*, vol. 29, no. 1, pp. 213-229.